DISSERTATION

submitted to the

COMBINED FACULTIES OF THE NATURAL SCIENCES AND

MATHEMATICS

OF THE RUPERTO-CAROLA-UNIVERSITY OF HEIDELBERG,

GERMANY

FOR THE DEGREE OF

DOCTOR OF NATURAL SCIENCES

PUT FORWARD BY

MASTER PHYS. ANTON VASYUNIN

BORN IN: YEKATERINBURG (RUSSIA)

ORAL EXAMINATION: DECEMBER 2nd, 2009

Chemistry in the ISM and disks
on the verge of planet formation

REFEREES: PROF. DR. THOMAS HENNING
PROF. DR. RALF KLESSEN

Zusammenfassung

Der Schwerpunkt dieser Doktorarbeit liegt in der Verbesserung astrochemischer Modelle im Zeitalter von ALMA. Diese Epoche ist geprägt durch eine detaillierte Erforschung protoplanetarer Scheiben und der Suche nach außerirdischem Leben.

Zuerst untersuchen wir wie Unsicherheiten in den Reaktionskoeffizienten chemischer Reaktionen die Isotopenhäufigkeit und Säulendichte von Schlüsselmolekülen protoplanetarischer Scheiben beeinflussen. Wir isolieren eine Gruppe von Schlüsselspecies mit Säulendichten, die robust gegenüber Unsicherheiten des Reaktionskoeffizienten sind. Das macht diese zu guten potentiellen Indikatoren für die physische Beschaffenheit der Scheibe. Wir finden rund hundert Reaktionen mit sehr problematischen Reaktionskoeffizienten, welche genauer bestimmt werden müssen, um die Zuverlässigkeit astrochemischer Modelle zu verbessern.

Als nächstes konstruieren wir ein realistisches astrochemisches Modell unter der Benutzung eines Monte-Carlo-Ansatzes für alle chemischen Prozesse, was bisher in dieser Form noch umgesetz wurde. Dieses Modell versetzt uns die Lage, die stochastische Natur von chemischen Reaktionen auf der Oberfläche von Staubkörnern genau zu berücksichtigen. Diese Reaktionen sind eine wichtige Grundlage für das Entstehen von organischen Molekülen, die der Ausgangsstoff für Leben, wie wir es kennen, sind. Es wird gezeigt, daß der neueste Ansatz der modifizierten Geschwindigkeitsgleichung nach Garrod et al. (2008) die genaueste beschleunigte Methode ist, um stochastische Effekte in Astrochemie zu modellieren.

Zum Abschluß verwenden wir unser Modell für die Untersuchung der chemischen Zusammensetzung einer sich in der Entwicklung befindlichen Scheibe mit Staubkoagulation, um die chemischen Indikatoren für diesen Prozeß zu ermitteln. Erstmalig wurde ein modernes astrochemisches Modell mit einem detaillierten Ansatz von Staubkoagulation und Sedimentation verbunden.

Abstract

The general purpose of the thesis work is to improve astrochemical models in the era of ALMA. This era is characterized by the active study of protoplanetary disks and the search for extraterrestrial life.

First, we study how uncertainties in the rate coefficients of chemical reactions affect the abundances and column densities of key molecules in protoplanetary disks. We isolate a group of key species which have column densities that are not very sensitive to the rate uncertainties, making them good potential tracers of physical conditions in disks. We identify about a hundred reactions with the most problematic rate coefficients, which need to be determined more accurately in order to improve the reliability of modern astrochemical models.

Second, we build a realistic astrochemical model using a Monte Carlo approach to all chemical processes, which is the first time this has been done. This allows us to properly take into account the stochastic nature of grain surface chemical reactions, which are of essential importance for the formation of organic molecules – i.e., the precursors of life as we know it. The recent modified rate approach (MRE) of Garrod et al. (2008) is shown to be the most accurate fast approach of accounting for stochastic effects in astrochemical modeling.

Finally, we apply our model to the study of the chemical composition of an evolving protoplanetary disk with grain growth, in order to reveal chemical tracers of this process. For the first time, a state-of-the-art astrochemical model is coupled with a detailed model of grain growth and sedimentation.

To Olga and Tatiana.

Acknowledgements

Contents

CONTENTS

List of Figures

List of Tables

LIST OF TABLES

Publications

Part of the results presented in the thesis have been published in the following papers

1. *A Unified Monte Carlo Treatment of Gas-Grain Chemistry for Large Reaction Networks. I. Testing Validity of Rate Equations in Molecular Clouds*, A.I. Vasyunin, D.A. Semenov, D.S. Wiebe, Th. Henning, 2009, The Astrophysical Journal, vol. 691 issue 2, pp. 1459-1469.

2. *Chemistry in Protoplanetary Disks: A Sensitivity Analysis*, A.I. Vasyunin, D.A. Semenov, Th. Henning, V. Wakelam, E. Herbst, A.M. Sobolev, 2008, The Astrophysical Journal, vol. 672 issue 1, pp. 629-641.

3. *A new modified-rate approach for gas-grain chemistry: Comparison with a unified large-scale Monte Carlo simulation*, R.T. Garrod, A.I. Vasyunin, D.A. Semenov, D.S. Wiebe, Th. Henning, The Astrophysical Journal Letters, Volume 700, Issue 1, pp. L43-L46 (2009).

4. *Chemistry in protoplanetary disks: analysis of uncertainties*, A.I. Vasyunin, D.A. Semenov, Th. Henning, V. Wakelam, E. Herbst, A.M. Sobolev, 2007, Molecules in Space and Laboratory, meeting held in Paris, France, May 14-18, 2007. Editors: J.L. Lemaire, F. Combes, pp. 112-113.

1

Introduction

The origin of life in the Universe is the fundamental question exciting the human mind since the dawn of a mankind. It is an interdisciplinary problem that requires the combined effort of scientists from many different branches of scientific schools of thought, from philosophy to chemistry, physics and mathematics. Astronomy plays a particular role here, as it studies the cycle of matter in the Universe. From the formation of atoms to the genesis of prebiotic molecules in space, from the emergence of the first stars to the formation of planetary systems and planets – all these questions are crucial for the understanding of the origin of life.

Since the first discovery by Mayor and Queloz (1995a), 374 extrasolar planets have been discovered around 295 stars to date[1]. These planets exhibit a large diversity in mass (ranging from 1.9 M_{earth} for Gl 581 e (Mayor et al., 2009) to 11.79 Jupiter masses for XO-3b (Johns-Krull et al., 2008)) and orbital distance (from less than 0.02 AU for COROT-7b (Leger et al., 2009) to 40 AU for 2M1207b (Mohanty et al., 2007)) from their central stars.

The process of planet formation is ubiquitous, and represents the final stage in a large-scale process of star formation. It is commonly accepted that stars are formed from molecular clouds through the process of gradual turbulent fragmentation and collapse (Mac Low and Klessen, 2004; McKee and Ostriker, 2007). Schematically, the process of low-mass star formation can be divided into four parts (Andre et al., 2000): (1) a region of a molecular cloud becomes dense enough to overcome gas and magnetic pressure and starts to collapse from the inside out (Class 0 object); (2) after 10^4 - 10^5

---

[1]http://exoplanet.eu, The Extrasolar Planet Encyclopedia

1. INTRODUCTION

years of contraction, a protostar which is deeply embedded into the surrounding matter is formed with a flattened disk-like structure around it, along with outflows that remove angular momentum (Class I object); (3) after another $\sim 10^6$ years of further contraction the pre-main sequence star completes forming and becomes visible, as most of the remaining surrounding material has been accumulated in the circumstellar disk, with a mass on the order of a few percent of the stellar mass (Class II object); (4) after 10^7 years of evolution the circumstellar disk becomes a "debris," disk with little dust in it and only a small amount of gas. Planetary systems may form during stages (3) – (4) by means of the process of dust coagulation (e.g., Natta et al., 2007a; Setiawan et al., 2008).

The early stages of planet formation are hard to study observationally, since Class I objects are still deeply embedded sources, while the Class II protoplanetary disks are relatively compact ($\leq 1\,000$ AU) and opaque at wavelengths shortward of $\sim 100\mu$m (e.g., van Dishoeck and Blake, 1998). The bulk of the disk density and thermal structure can be resolved with radio-interferometers in low- and high-lying transitions of distinct molecular tracers, e.g. CO, CN, HCN etc. (e.g., van Dishoeck and Blake, 1998). Unfortunately, molecular hydrogen is not observable until it is hot (~ 300 K), and cannot be used as a tracer of the disk mass (Carmona et al., 2008). Using ground-based and space-borne infrared telescopes (e.g., VLT, Spitzer, Herschel, Keck, etc.), the physical conditions and chemical composition of inner disk regions can now be studied (e.g., Carr et al., 1993; Lahuis et al., 2006; Salyk et al., 2007). In order to extract complete information about the disk structure from spectral maps of molecular lines, one has to combine physico-chemical modeling (e.g., Aikawa et al., 2001, 2002; Bergin and Langer, 1997; Herbst and Klemperer, 1973; Pavlyuchenkov et al., 2006; Semenov et al., 2005) with line radiative transfer simulations (e.g., Hogerheijde and van der Tak, 2000; van Zadelhoff et al., 2003a).

The process of grain evolution in protoplanetary disks has been observationally confirmed (see e.g., Natta et al., 2007b; Rodmann et al., 2006; Sicilia-Aguilar et al., 2006; van Boekel et al., 2004, 2005), and numerous detailed models of grain growth have been developed (e.g., Brauer et al., 2008a, 2007; Dullemond and Dominik, 2004; Nakagawa et al., 1981). Dust evolution is an important factor for astrochemistry because it affects both the efficiency of UV penetration into the disk, as well as the rates of gas-grain interactions and surface processes. Dust grain surfaces serve as a catalyst for important

reactions, from the formation of molecular hydrogen to complex (organic) molecules (Garrod and Herbst, 2006; Garrod et al., 2008; Gould and Salpeter, 1963; Hasegawa et al., 1992). Understanding grain surface chemistry is a challenge, since observations of grain mantle composition are difficult, and modeling requires detailed lab data on surface processes as well as rigorous mathematical approaches capable of accounting for the stochastic nature of the processes involved (e.g., Caselli et al., 1998; Herbst and Shematovich, 2003; Tielens and Hagen, 1982).

Rapid progress in observational techniques has lead to dramatic improvements in spectral and angular resolution. 21st-century facilities such as Herschel, ALMA, eVLA, SKA are expected to revolutionize the quality of observational data available for researchers (e.g., Herbst, 2008). Newer, more detailed, models with a combined treatment of radiative transfer, physical and chemical processes, and grain evolution will be needed in order to interpret these new data. In my thesis, I focus primarily on astrochemical modeling, as it is a very interesting and actively-developing interdisciplinary field, which stands on the edge of chemistry, astrophysics and the science of surface processes. The results of astrochemical modeling are of great importance for the interpretation of radio observations, the modeling of the physics and dynamics of astrophysical objects (molecular abundances, ionization degree and the cooling of the gas). The formation of complex pre-biotic molecules on the surfaces of interstellar dust grains is another topic of considerable interest in astrochemistry.

The following problems are studied in my thesis: (1) the influence of uncertainties in the rates of chemical reactions on the results of astrochemical modeling; (2) the development of a stochastic approach to grain surface chemistry, which is suitable for large chemical networks and the wide range of physical conditions typical of protostellar objects and protoplanetary disks; (3) the modeling of the chemical structure of evolving protoplanetary disks, where grain evolution and possible stochastic effects have been taken into account.

1.1   Structure of the dissertation

The tasks which are stated above are investigated in four chapters of this thesis.

Chapter 2 is devoted to the study of the influence of uncertainties in chemical reaction rates on the results of astrochemical modeling of protoplanetary disks. First, we

estimate the dispersion of modeled abundances of chemical species due to inaccuracies in reaction rates using random variations of rates within their intervals of uncertainties. Then, the resulting inaccuracies in observable column densities of several important species are estimated. Finally, we develop simple correlation technique to single out chemical reactions responsible for most of the uncertainties in modeled species abundances. Using this technique, we isolate a small set of 56 chemical reactions that are responsible for most of uncertainties in abundances of several important species. These reactions are proposed as a subject for further lab studies.

In chapter 3, a stochastic model of the chemical evolution of the interstellar medium is developed. A time-dependent gas-grain chemical model is presented, consisting of about 600 species and 6000 reactions, with a stochastic description of grain surface chemistry. For the first time, both the gas phase and grain surface reactions are simulated with a unified Monte Carlo approach. This unified model is used to test the validity of rate equations and the modified rate equations (MRE) of Caselli et al. (1998) for a set of physical conditions relevant to translucent clouds, dark dense cores, and infrared dark clouds. It is shown that neither the classical rate equations, nor their modified versions, are able to properly account for stochastic effects in the case where a high mobility of surface species is assumed.

In chapter 4, we extend the comparison started in the previous chapter to a newly proposed modification of the rate equations (Garrod, 2008). We show that in contrast to previous attempts, this version of modified rate equations exhibits very good agreement with the Monte Carlo results over the entire range of physical conditions considered. Using this version of MRE, we study the importance of stochastic effects in protoplanetary disks.

Chapter 5 is devoted to the study of the chemistry of evolving protoplanetary disks with grain growth. We study how the processes of grain growth and sedimentation affect the chemical composition of disks, with an emphasis on the abundances of key observational tracers. For the first time, a detailed model of grain growth and sedimentation in the disk is coupled with a state-of-the-art astrochemical model. Our results imply that grain growth affects chemistry mostly in the inner parts of disks (closer than 100 AU) and may be observed via molecular line observations of chemical tracers such as HCN and N_2H^+.

The chapters with scientific results listed above are precluded with an introductory part and concluding remarks about future prospects for the presented work.

1. INTRODUCTION

2

Chemistry in Protoplanetary Disks: A Sensitivity Analysis

2.1 Introduction

More than 140 organic and inorganic molecular species consisting of up to 13 atoms have been identified in space so far[1], including such complex species as dimethyl ether (CH_3OCH_3; Snyder et al., 1974) and acetamide (CH_3CONH_2; Hollis et al., 2006). The rich variety of the observed molecules implies that many more relevant yet undiscovered species must be involved in the processes of their formation and destruction. Still, only a tiny fraction of these species have been firmly detected in several protoplanetary disks, including CO (and its isotopes), CN, HCN, HNC, H_2CO, C_2H, CS, HCO^+, $H^{13}CO^+$, DCO^+, and N_2H^+ (Dutrey et al., 1997; Kastner et al., 1997; Qi et al., 2003; Thi et al., 2004; van Zadelhoff et al., 2001). Multi-molecule, multi-transition observations of emission lines with (sub-)millimeter interferometers and single-dish antennas provide a wealth of information about planet-forming disks resembling the young Solar Nebula (Aikawa et al., 2003; Dutrey et al., 2007b; Pety et al., 2006; Qi et al., 2005; Simon et al., 2000).

---

[1] http://astrochemistry.net

2. CHEMISTRY IN PROTOPLANETARY DISKS: A SENSITIVITY ANALYSIS

An ultimate goal of disk studies is the reconstruction of the evolutionary history and spatial abundance distribution of various species, which requires sophisticated chemical models (Aikawa and Nomura, 2006; Ilgner et al., 2004; Markwick et al., 2002; Semenov et al., 2005; Tscharnuter and Gail, 2007; van Zadelhoff et al., 2003a; Willacy and Langer, 2000). The analysis and modeling of observational data acquired with limited spatial and spectral resolution is not complete without taking all possible uncertainties into account such as instrumental errors, uncertainties in the distance to source, orientation, etc. Whereas these uncertainties can in general be reduced either by using better observational data provided by current interferometers (PdBI, SMA) equipped with a new generation of receivers or in the future with the advent of more powerful instruments like ALMA, EVLA, and Herschel, there is an *intrinsic* source of ambiguity in all the chemical models – our limited knowledge of the reaction rate coefficients.

Modern astrochemical databases include up to about $4\,500$ gas-phase reactions and ~ 450 species (Le Teuff et al., 2000; Millar et al., 1997; Smith et al., 2004; Woodall et al., 2007), but many of these reactions have poorly estimated rate coefficients with uncertainties of about a factor of 2 and larger. For example, radiative association reactions lead to the formation of new complex species out of smaller ones through the photon relaxation of an excited collisional molecular complex. Under low-density space conditions where three-body processes are unlikely, these reactions may have rate coefficients as high as $\sim 10^{-9}\,\mathrm{cm^3\,s^{-1}}$ and as low as $\sim 10^{-17}\,\mathrm{cm^3\,s^{-1}}$, depending on the density of vibrational states of the complex. The radiative association rates are usually difficult to measure in the laboratory as well as to predict theoretically, especially for bigger species (Bates, 1951; Herbst, 1980; Williams, 1972).

In contrast, dissociative recombination of molecular ions almost always proceeds very rapidly, in particular at low temperature, with rate coefficients that can be accurately obtained (Florescu-Mitchell and Mitchell, 2006). However, the products and their relative branching fractions branching channels of many dissociative recombination reactions are not known precisely, particularly at low temperatures (see though Ishii et al., 2006; Öjekull et al., 2006; Semaniak et al., 2001), which may spoil theoretical predictions (see, e.g. Geppert et al., 2005a; Millar et al., 1988).

Recently, Vasyunin et al. (2004, Paper I hereafter) investigated the influence of uncertainties in rate coefficients on molecular abundances in dense and diffuse clouds,

using the gas-phase UMIST 95 database. They found that the abundance uncertainties of simple species are limited to within about an order of magnitude and increase substantially with the number of atoms in the molecule, though the uncertainties still do not exceed the observational errors for simple molecules. They proposed a sensitivity analysis to identify those reactions that introduce the largest errors in the computed concentrations. Wakelam et al. (2005, hereafter Paper II) studied uncertainties in the gas-phase chemistry of hot cores and demonstrated that at late times, $\geq 10^4$ yr, modeled abundances of important molecules can suffer from large uncertainties due to poorly known rate coefficients. Wakelam et al. (2006a) focused on dense cloud chemistry and took uncertainties in the physical parameters into account, as well as comparing the osu.2003 and UMIST 99 chemistries. These authors came to conclusions that grain-surface reactions should be considered in order to achieve better consistency with the observational data, even though there is a large degree of ambiguity in simple cloud models based on static physical and chemical structures. Finally, Wakelam et al. (2006b) expanded this study by using their uncertainty analysis to show that there is a bistability in the abundances of many species that are hyper-sensitive to the adopted value of the ratio of the cosmic ray ionization rate of helium to that of hydrogen (see also Boger and Sternberg, 2006; Pineau des Forets et al., 1992; Shalabiea and Greenberg, 1995). Furthermore, Izzard et al. (2007) recently studied the effect of proton-capture reaction rate uncertainties in the NeNa and MgAl chains on the abundances of the Ne, Na, Mg and Al isotopes produced in intermediate-mass AGB stars.

Despite previous work in rate uncertainties, to the best of our knowledge, there have been no attempts in the literature to study how these reaction uncertainties, which are unlikely to be eliminated in the near future, affect the results of astrochemical modeling in the wide range of physical conditions typical of protoplanetary disks. In this chapter, we extend the previous analyses by Vasyunin et al. (2004, Paper I) and Wakelam et al. (2005, Paper II) to the conditions of a low-mass protoplanetary disk surrounding a young T Tauri star. The aims of our study are several. First, we analyze how large the abundance and column density scatter for key species are due to uncertainties in rate coefficients. Second, we investigate how these uncertainties vary with disk location. Third, we isolate the reactions whose rate uncertainties contribute most to the abundance scatter and which are therefore worth studying in detail. Last, we

predict how the overall consistency of theoretical models will be improved after these reaction rates are better constrained.

The organization of this chapter is the following. The adopted disk physical structure and time-dependent gas-grain chemical model are presented in Sect. 2.2.1. The Monte Carlo method used to introduce the uncertainties in the RATE 06 reaction rates is described in Sect. 2.2.2. In Section 2.3 we report computed distributions of the mean molecular abundances and column densities and their errors in the whole disk, and analyze the influence of the rate coefficient uncertainties on these quantities. A correlation method that allows determination of the role of various reactions in the abundance uncertainties as a function of time and disk location is outlined, and results for several key species are presented in Sect. 2.4.1. Particular attention is paid to the identification of the most uncertain reactions for the chemical evolution of key species in the entire disk. In Sect. 2.4.2 we predict to what extent the abundance scatter due to the rate uncertainties will be lowered when accurate rate values of several dozens most problematic reactions are available. The remainder of Section 2.4 is concerned with problems in different classes of reactions. Final conclusions are drawn in Sect 2.5.

2.2 Disk model and uncertainty approach

2.2.1 Physical structure and chemical model of the disk

In our simulations, we adopted the 1+1D steady-state irradiated disk model with vertical temperature gradient that represents the low-mass Class II protoplanetary disk surrounding the young T Tauri star DM Tau (D'Alessio et al., 1999a). The disk has a radius of 800 AU, an accretion rate $\dot{M} = 10^{-8}\,M_\odot\,\mathrm{yr}^{-1}$, a viscosity parameter $\alpha = 0.01$, and a mass $M \simeq 0.07\,M_\odot$ (Dutrey et al., 1997; Piétu et al., 2007). The thermal and density structure of the disk is shown in Fig. 2.1. As a disk age we used a value of ~ 5 Myr, which has been derived by Simon et al. (2000) based on evolutionary track modeling of the central star. In chemical simulations an outer disk region beyond the distance of 50 AU from the central star is considered. This is the only routinely accessible disk region with existing (sub-)millimeter interferometers.

We assumed that the disk is illuminated by UV radiation from the central star with an intensity $G = 410\,G_0$ at $r = 100$ AU ($G(r) \propto r^{-0.5}$) and by interstellar UV radiation with intensity G_0 in plane-parallel geometry (Bergin et al., 2003; Draine, 1978; Dutrey

Figure 2.1 Temperature (K) and density (cm^{-3}) structure of the adopted disk model. The total scale height of the disk Z_{max} increases with the radius such that at $r = 100$ AU it has a value of 90 AU, whereas $Z_{max} \approx 1\,300$ AU at $r = 800$ AU.

et al., 2007b; van Dishoeck, 1988). The dust grains are assumed to be uniform $0.1\,\mu$m spherical particles made of amorphous silicates with olivine stoichiometry (Semenov et al., 2003), with a dust-to-gas mass ratio of 1%. The self-and mutual-shielding of CO and H$_2$ against UV photodissociation is computed using the pre-calculated factors from Tables 10 and 11 in Lee et al. (1996).

Three other high-energy sources in the model that drive chemistry either through dissociation, ionization, or desorption are cosmic rays, decay of short-lived radionuclides, and stellar X-rays. The X-ray ionization rate in a given disk region is computed according to the results of Glassgold et al. (1997a,b) with parameters for their high-metal depletion case. In this model, the thermal ~ 5 keV X-ray photons are generated at ~ 0.1 AU above the central star, with a total X-ray luminosity of $\approx 10^{30}$ erg cm^{-2} s^{-1} (Glassgold et al., 2005). The cosmic-ray ionization rate is assumed to be 1.3×10^{-17} s^{-1}. The ionization rate caused by radionuclide decay (primarily ^{26}Al and ^{60}Fe) is 6.5×10^{-19} s^{-1} (Finocchi and Gail, 1997). We adding the X-ray and radionuclide ionization rates to those involving cosmic ray particles (CRP) and CRP-induced UV photons.

A modified static gas-grain chemical model that includes gas-grain interactions without surface reactions and turbulent mixing has been utilized (Semenov et al., 2005). We allow only surface formation of molecular hydrogen using the approach of Hollenbach and McKee (1979). This modification significantly decreases the numerical demands of our chemical code and makes it computationally tractable while allows us to include all necessary physical processes. The gas-phase reaction rates and their uncertainties are taken from the recent RATE 06 database, in which the effects of dipole-enhanced

ion-neutral rates are included (Woodall et al., 2007). To calculate photoreaction rates through the disk, we adopt pre-computed fits of van Dishoeck (1988) instead of integrating the wavelength-dependent cross sections over the local UV spectrum (see van Zadelhoff et al., 2003a).

Gas-grain interactions include the accretion of neutral molecules onto dust surfaces with a sticking efficiency of 100%, dissociative recombination of ions on charged dust grains, and grain re-charging, as well as UV-, CRP-induced and thermal desorption of surface species. Desorption energies E_{des} are mostly taken from the recent osu.2007[1] database (Garrod and Herbst, 2006) or roughly estimated by analogy for about 20 molecules.

Overall, our network consists of positively and negatively as well as neutral dust grains, 420 gas-phase and 157 surface species made of 13 elements, and 5773 reactions. Among these 5773 reactions are 4517 gas-phase reactions, 2 charge exchange reactions for dust grains, 940 dissociative recombination reactions of ions on charged and neutral grains, and 314 accretion/desorption processes.

As initial abundances, we have adopted the so-called "low metal" set of Lee et al. (1998) as listed in Table 2.1 and assumed that all hydrogen is mostly locked in its molecular form. In these initial abundances, the standard solar elemental composition is depleted in heavy elements by, e.g., 200 times for S up to more than 10^4 for Fe, Cl, P, and F. The mostly atomic initial abundances are chosen instead of those from a molecular cloud model because this choice allows the abundance uncertainties to accumulate in a long sequence of chemical reactions with imprecise rates, starting from basic processes that reach steady-state at early times during the disk evolution. Willacy et al. (1998) have shown that most of the molecular abundances are hardly affected by the choice of input abundances. Note also that the resulting abundance uncertainties can be sensitive to the initial elemental concentrations (Wakelam et al., 2006b). However, we do not allow the elemental concentrations to vary in order to keep the computations in reasonable limits.

2.2.2 Method to model rate uncertainties

Each reaction rate coefficient in the RATE 06 database is given in the standard Arrhenius form and thus relies on 3 parameters: α (the absolute value at room temperature),

---

[1] `https://www.physics.ohio-state.edu/~eric/research.html`

Table 2.1. Initial abundances

Species	n(X)/n(H)
He	9.75(-2)[a]
H_2	4.99(-1)
H	2.00(-3)
C	7.86(-5)
N	2.47(-5)
O	1.80(-4)
S	9.14(-8)
Si	9.74(-9)
Na	2.25(-9)
Mg	1.09(-8)
Fe	2.74(-9)
P	2.16(-10)
Cl	1.00(-9)
F	1.00(-10)

[a] A(-B) means $A \times 10^{-B}$

2. CHEMISTRY IN PROTOPLANETARY DISKS: A SENSITIVITY ANALYSIS

β (the index for the power law dependence of the rate on temperature), and γ (the activation energy barrier in K). A specific expression for the reaction rate coefficient depends on the type of chemical process: bimolecular reaction, direct cosmic-ray ionization reaction, photodissociation, etc. Note that in all cases the rate coefficient scales linearly with the parameter α.

In addition to these three parameters, the RATE 06 reaction rates are characterized by an accuracy estimate (A, B, C, and D), where the uncertainties are smaller than 25%, 50%, within a factor of 2, and within an order of magnitude. Almost all reactions with measured rates belong to the first group ($\sim 1\,400$ reactions), while those reactions with rates that were "guessed" or derived by analogy are assigned to the third group ($\sim 2\,800$ reactions), which contains most of the ion-neutral reaction rates. The second group includes about 300 mostly neutral-neutral and photodissociation reactions, whereas the fourth group consists of only 4 photodissociation reactions (Woodall et al., 2007).

In accord with the latest osu.2007 network, we adopted a rate uncertainty of one order of magnitude for radiative association reactions. Such a large uncertainty factor is justified by the difficulty in calculating or measuring these rate coefficients (e.g., Herbst, 1985). The uncertainty factors vary widely for the photoreaction rates since the corresponding frequency-dependent cross-sections have limited accuracy and have been obtained only for a fraction of molecules in the UMIST database (van Dishoeck, 1988; van Dishoeck et al., 2006a).

Our method to model abundance uncertainties is based on the computation of a large set of chemical models, using identical physical and initial conditions and the same chemical network, but with randomly varied rate coefficients within their uncertainty limits. We utilized the same method to introduce uncertainties in the rate coefficient values as described in Dobrijevic and Parisot (1998), Dobrijevic et al. (2003), and Wakelam et al. (2005). The rate coefficient for each gas-phase reaction i is randomly chosen over a log-normal distribution with median α_i and dispersion F_i. Consequently, the rate coefficient of the i-th reaction spans an interval between α_i/F_i and $\alpha_i \times F_i$ with a probability of 68% (1σ). We generated a sequence of these log-normally distributed rates for all gas-phase reactions in our chemical network using the following expression:

$$\alpha_i^l = \alpha_i \times (F_i)^\epsilon, \qquad (2.1)$$

where α_i^l is the l-th realization of the i-th reaction rate, α_i is the standard RATE 06 rate value for the i-th reaction, F_i is the dispersion, or the uncertainty factor, for this rate, and ϵ is randomly distributed from -1 to 1 with an uniform distribution law.

Using this approach, we allowed the rates of only 4517 gas-phase reactions to vary in our network. The rates of all other processes (gas-grain interactions, dissociative recombination of molecular ions on grains, and recharging of dust grains) were kept constant. Not did we account for possible variations among the parameters of the disk physical model. Such an idealization allowed us to focus solely on an investigation of how uncertainties in gas-phase reactions affect the results of the disk chemical modeling.

Using 8 000 realizations of the RATE 06 network, we simulated 5 Myr of chemical evolution in the outer, $r \geq 50$ AU, disk of DM Tau. The disk grid consists of 5 radial (50, 100, 200, 380, and 760 AU) and 10 equidistant vertical points (with step sizes of 3.2, 7.6, 18, 41.7, and 96 AU for the considered radii). Such a huge number of utilized chemical models with randomly varied rates leads to low values of statistical noise in the distributions of the abundance scatters at any particular disk location, assuring the correctness of the sensitivity analysis. Moreover, a large number of varied reaction rates allows an analysis of all reactions in the chemical network, in contrast to models with limited chemistry included in previous works (e.g., Wakelam et al., 2005). Still, even with the modest 5×10 spatial resolution of the adopted disk model and without surface reactions, the overall computational time needed to calculate the chemistry with these 8 000 networks was about 3 days on a 4-CPU PC machine (3.0 GHz Xeon, 8 Gb RAM).

2.3 Results

2.3.1 Abundance distribution profiles

Before we perform a detailed analysis of the influence of the rate uncertainties on the modeled molecular abundances, we investigate the abundance distribution profiles. Because we utilized a log-normal distribution for the rate coefficients, one might expect that for each molecule the abundance distribution should show a normal (Gaussian) profile in logarithmic scale. If this hypothesis is correct, one can use the dispersion – a measure of the scatter of randomly varied values that have a Gaussian distribution – as a convenient quantity characterizing the abundance and column density uncertainties.

2. CHEMISTRY IN PROTOPLANETARY DISKS: A SENSITIVITY ANALYSIS

As shown in Paper II, this assumption may not be fullfiled for certain species and certain time steps. For example, when molecular abundances of a particular species show a steep decline or increase with time then at that moment the corresponding histogram of the abundance distribution can have several peaks and thus be far from a Gaussian shape because of sampling effects. Bimodal distributions can also be obtained if the system is highly sensitive to a small variation of specific parameter. Wakelam et al. (2006b) showed that dense cloud chemistry hypersensitive, and even bistable, to the ratio between He and H_2 cosmic-ray ionization rates in particular conditions. In this case our uncertainty method would tend to overestimate the dispersion of the modeled abundances. The disk chemistry is very rich in a sense that it proceeds vastly differently in various disk regions and at different times, so it is natural to expect that the abundance distributions of some species can sometime deviate from a normal distribution.

We carefully studied this problem and found that such a situation happens rarely at late times, ≥ 1 Myr, for which our analysis will be performed. In Fig. 2.2 we show several representative histograms of the abundance distributions at 5 Myr, using HCO^+ and CO as an example. For an inner disk region, at $r \approx 97.5$ AU, $z \approx 30$ AU, a strong deviation from the Gaussian shape is clearly visible, with 2 distinct peaks and a gap in between (Fig. 2.2, top panels). Note that this is one of the few exceptional cases that is discussed in detail below. Everywhere else through the disk the HCO^+ and CO abundances have nearly Gaussian-like profiles (Fig. 2.2, bottom panels). This condition holds for other key species as well, implying that the averaged abundances in the disk should not differ from the values computed with the standard RATE 06 network. Moreover, in Paper I we found that the Gaussian shape of the abundance distribution is also preserved for the uniform distribution of the rate uncertainties in linear scale.

In the rest of this chapter, we will refer to one standard deviation (1σ) in the modeled abundance distribution as the "abundance uncertainty". In our notation "abundance scatter" represents twice the abundance uncertainty in logarithmic scale ($2 \log \sigma$). It is the abundance uncertainties that have to be taken into account when interpreting the observational data with a chemical model.
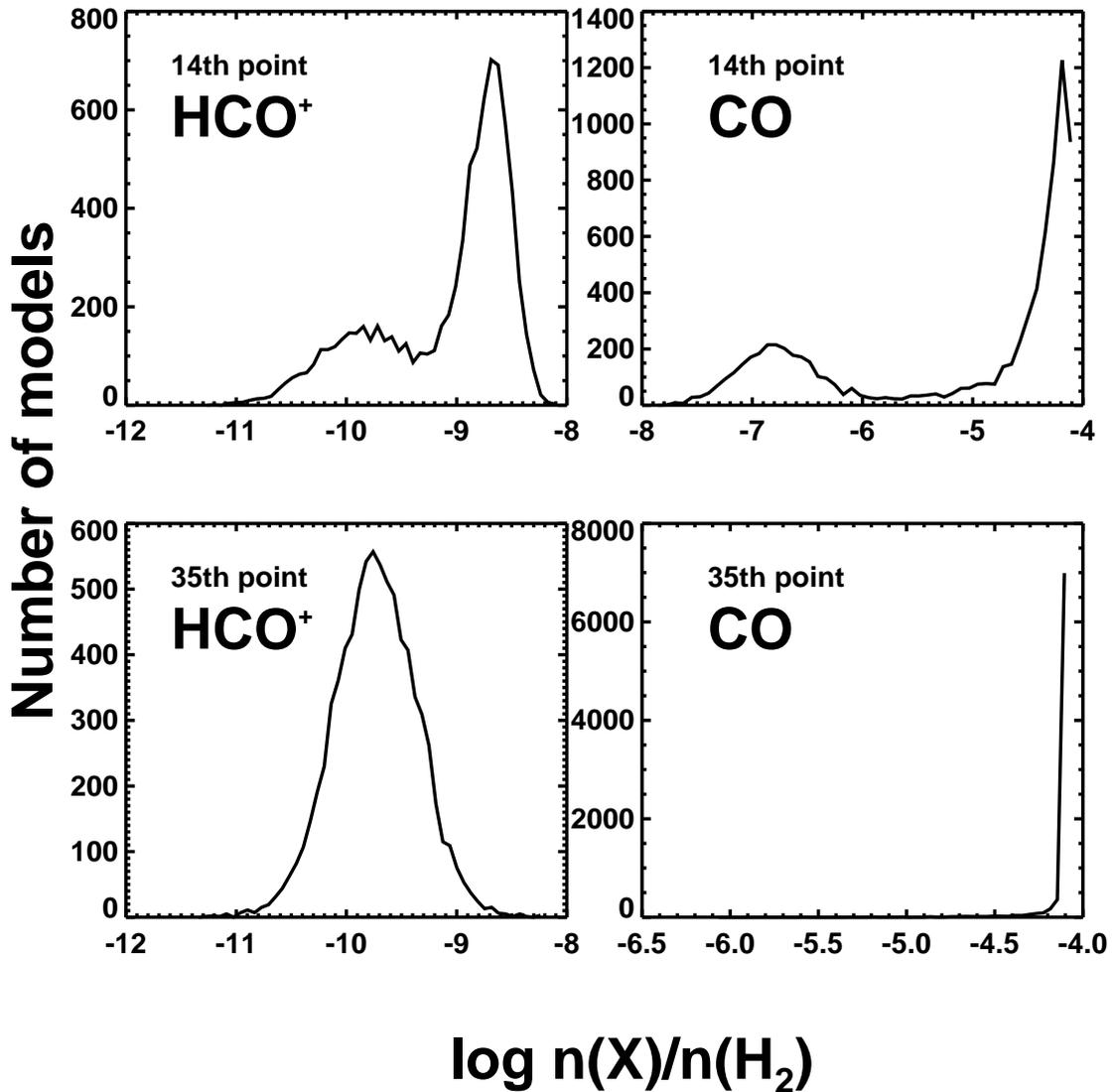
Figure 2.2 Histograms of the abundance distributions show the number of chemical models in which a given molecular abundance is reached at 5 Myr. (Top) Non-Gaussian, double-peak distributions are shown for HCO^+ (left) and CO (right) in the inner disk region ($r \approx 97.5$ AU, $z \approx 30$ AU). (Bottom) Nearly Gaussian distributions are shown for the same species but located farther out from the central star ($r \approx 382$ AU, $z \approx 205$ AU). The point numbers in the boxes refer to the disk cells for which these calculations were performed.

2. CHEMISTRY IN PROTOPLANETARY DISKS: A SENSITIVITY ANALYSIS

2.3.2 Distribution of the mean abundances in the disk

Although the evolution of all species was calculated in 8 000 realizations of the chemical model, in what follows we focus on several key molecules that are used as tracers of disk physical structure and chemical composition. Our list of important species includes molecules that are widely used for kinematic studies and determination of the density and temperature (CO, CS, H_2CO, NH_3, and HCN) as well as for probing such major parameters as ionization degree (HCO^+), radiation fields (CN, HCN), and the yet-to-be detected C^+ as a dominant ion in the disk surface (Aikawa et al., 2003; Dutrey et al., 1997, 2007b; Kastner et al., 1997).

We use time-dependent abundances to analyze the chemical evolution of these species in detail. The analysis is based on the calculation of the relative importance of each reaction in the chemical network for the abundance change of a molecule under investigation at a given time (Wiebe et al., 2003). This allows us to weight all reactions in the model and isolate a few most important pathways for chemical evolution of one or several species under specific physical conditions. In the case of protoplanetary disks, such an analysis has to be performed for several tens of representative cells.

In Fig. 2.3 we show the mean abundances of these molecules in the disk at 5 Myr, which are obtained by averaging the results of the chemical network. The vertical extension of the disk is scaled by one hydrostatic scale height, $H(r) = \sqrt{2}C_s/\Omega$, where C_s is the midplane sound speed and Ω is the Keplerian frequency (Dartois et al., 2003). The unity pressure scale height is about 25 and 320 AU at distances of 100 and 800 AU, respectively.

The "sandwich"-like chemical structure of the disk is clearly seen in Fig. 2.3. In the "dark", cold, and dense midplane at $\leq 0.5 - 1$ pressure scale height, the molecules freeze out onto dust grains within $100 - 100\,000$ yr and low steady-state fractional abundances of $\sim 10^{-14} - 10^{-10}$ are reached. The abundances of the gas-phase species in the midplane at late times are sustained by the CRP-induced desorption of the mantle materials. The midplane abundance of CO $\sim 10^{-8}$, is higher because this molecule is very abundant ($\approx 10^{-4}$) in the gas phase initially, and since CO ice is rather volatile because of its low CO desorption barrier of $\sim 930\,K$ (Bisschop et al., 2006). Overall, the gas-phase abundances in the midplane tend to slightly increase with radius as the disk surface density and thus the density in midplane decrease and gas-grain interactions
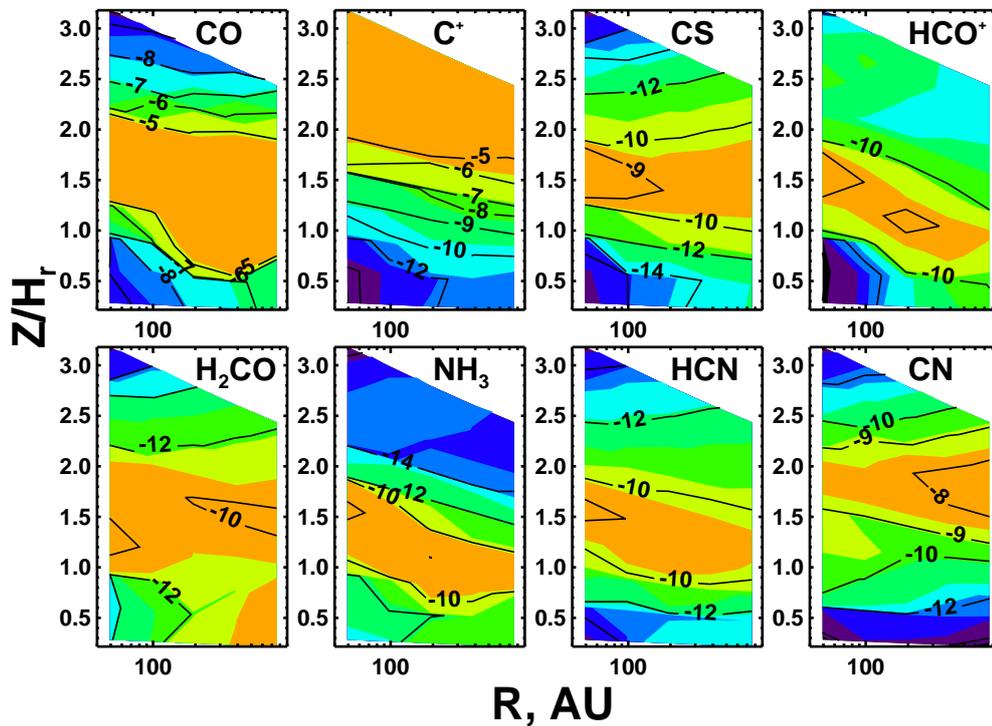
Figure 2.3 Distribution of mean molecular abundances relative to the total amount of hydrogen nuclei for several observationally important species in the disk at 5 Myr. The distributions are obtained by averaging the 8 000 model results calculated with randomly varied reaction rates. Results are shown for CO, C^+, CS, HCO^+ (top row, from left to right) and H_2CO, NH_3, HCN, and CN (bottom row) at $r \geq 50$ AU. The disk vertical axis is given in units of the pressure scale height.

2. CHEMISTRY IN PROTOPLANETARY DISKS: A SENSITIVITY ANALYSIS

become less intense, which slows down the freeze-out of gas-phase molecules onto dust grain surfaces.

The surface layer of the disk ($Z/H(r) \geq 2$) is deficient in molecules due to strong irradiation by high-energy stellar and interstellar photons. Even CO, which is self-shielded and mutually-shielded by H_2 against UV photodissociation cannot survive. Among the considered species, only C^+ reaches its maximal concentration and becomes the most abundant ion in the surface layer, with an abundance of $\sim 10^{-4}$. The thickness of this highly ionized layer (~ 1 pressure scale height down from the disk surface) stays nearly constant with radius for all key species but highly reactive radicals CS and CN, whose abundances are already high ($\sim 10^{-9}$) at scale pressure heights as high as $Z/H(r) \approx 2$ at all radii (Fig. 2.3).

In contrast, polyatomic species tend to concentrate in the warm, chemically rich intermediate layer ($\leq 1 - 2$ pressure scale height, depending on the radius). The model-averaged abundances for the considered species, $\sim 10^{-10} - 10^{-4}$, are close to the values computed with the standard RATE 06 network and those found in previous work (Aikawa and Herbst, 1999; Aikawa et al., 2002; Dutrey et al., 2007b; Willacy et al., 2006; Willacy and Langer, 2000).

Now let us consider the chemical processes that form and destroy the considered species in the intermediate layer. In contrast to dense cloud models, for many species in this disk zone steady-state is reached by $\sim 10^3 - 10^5$ yr. This is due to the higher densities encountered in the warm layer ($\geq 10^6 - 10^8$ cm^{-3}) than in the cloud cores ($\sim 10^4 - 10^6$ cm^{-3}) and a non-negligible flux of the UV radiation. Impinging interstellar UV photons allow many surface species to desorb back into the gas phase (Garrod and Herbst, 2006; Hasegawa and Herbst, 1993), thus reducing their surface abundances and overall importance of gas-grain interactions for disk chemical evolution at late times, $t \geq 10\,000$ yr.

The evolution of CO and HCO$^+$ in the intermediate layer is governed by a small set of reactions at all radii. The CO molecules are formed via reactions of atomic oxygen with CH, CH$_2$, and C$_2$ at $t \leq 1\,000$ yr, and partly through the dissociative recombination of HCO$^+$ afterwards (at this stage steady-state has been reached and there is a loop between CO and its protonated form). The light hydrocarbons that are precursors of CO are themselves rapidly created within a few years via the radiative association of C with H and H$_2$, and CH with H$_2$. The CO is mainly removed from the

22

gas phase by accretion onto the dust grain surfaces in outer, cold regions and by reactive collisions with helium ions in the inner, X-ray ionized part of the intermediate layer. In the upper part of this layer, CO is also photodissociated. The ion HCO^+ initially forms via reactions of O with CH and ionized light hydrocarbons, CH_n^+ (n=1–3), and the ion-neutral reaction between CO and CH_5^+ (also producing methane). At a later time of $\geq 1\,000$ yr, HCO^+ becomes the most abundant ion in the intermediate layer and the dominant molecular ion in the disk, with a fractional abundance of $\sim 10^{-9}$. At this steady-state stage, HCO^+ is mainly produced via reactive collisions between CO and H_3^+ and destroyed by dissociative recombination with electrons and negatively charged grains.

The chemically related H_2CO molecule is produced through reaction of CH_3 with oxygen atoms. At a later time of $\sim 10^5$ yr H_2CO is involved in a simple formation-destruction cycle. It starts with protonation of formaldehyde by HCO^+, H_3O^+, and H_3^+, which is followed by dissociative recombination into H_2CO (33%), CO (33%), or HCO (33%). Apart from photodissociation and freeze out, another direct destruction channel for H_2CO in the upper, more ionized part of the intermediate layer is the ion-neutral reaction with C^+, which produces either CO and CH_2^+, HCO^+ and CH, or H_2CO^+ and C. The chemical evolution of formaldehyde typically reaches steady-state at about 10^5 yr with a gas-phase abundance of $\leq 3 \times 10^{-10}$. Note that in the same disk chemical model as discussed above but with a set of surface reactions taken from Garrod and Herbst (2006) the overall (gas-phase and surface) abundance of formaldehyde is decreased by a factor of several as it is converted to methanol by hydrogenation on grain surfaces.

The photostable radical CN is abundant (10^{-8}) at an upper, less molecularly rich disk layer ($Z/H(r) \approx 1.8$, Fig. 2.3). The initial formation channel for the cyanogen radical is the radiative association between C and N, followed by the neutral-neutral reaction of N and CH, and dissociative recombination of $HCNH^+$ at later times ($t \geq 10^4$ yr). Other, less important formation pathways for CN at this stage are neutral-neutral reactions between C and NO producing CN and O as well as between C and OCN leading to CN and CO. The destruction of CN mostly proceeds through photodissociation and neutral-neutral reaction with N forming highly photostable nitrogen molecules and C.

In turn, $HCNH^+$ is produced by ion-neutral reactions between H_2 and HCN^+ and between N and $C_nH_2^+$ ($n = 3, 4$) at early times ($t \leq 10^3$ yr). Later the steady-state

2. CHEMISTRY IN PROTOPLANETARY DISKS: A SENSITIVITY ANALYSIS

recycling of $HCNH^+$ is reached, which involves dissociative recombination of $HCNH^+$ into either HCN (33%), HNC (33%), or CN (33%), followed by re-production of $HCNH^+$ via protonation of HCN and HNC by either H_3^+, H_3O^+, or HCO^+ as well as via the ion-neutral reaction of CN with H_3^+.

The chemistry of HCN is tightly related to the evolution of CN and $HCNH^+$. HCN is mainly produced by neutral-neutral reactions involving nitrogen and methylene or methyl at early evolutionary stages, $t \leq 10^4$ yr. Later the evolution of HCN proceeds as a part of the $HCNH^+$ formation-destruction loop. The major destruction routes for gas-phase HCN include freeze-out onto dust grains and the ion-neutral reaction with C^+, which forms CNC^+ and H. Another important destruction channel for HCN in the upper disk layers at $\sim 1.5 - 2$ scale heights is photodissociation. Steady-state for HCN is typically reached within $\geq 10^4$ yr, with an abundance of about a few $\times 10^{-10}$.

The layer where abundant ammonia exists is located somewhat deeper toward the disk midplane compared with HCN and especially CN because NH_3 can be photodissociated by UV photons shortward of $\approx 1\,950$ Å(van Dishoeck, 1988). The main formation route for ammonia is dissociative recombination of NH_4^+, which itself is formed through a sequence of hydrogen insertion reactions starting with the production of the NH^+ ions from N^+ reacting with H_2. Upon formation, NH^+ repeatedly reacts with molecular hydrogen and gains an addition hydrogen atom until NH_4^+ is formed. The destruction of ammonia proceeds mainly via ion-neutral reactions with C^+ and S^+ in the upper intermediate layer as well as H_3^+, H_3O^+, and HCO^+ in a deeper region, which leads again to NH_4^+ and either H_2, H_2O, or CO. For all radii, the abundance of ammonia reaches a steady-state value of $\leq 3 \times 10^{-10} - 10^{-9}$ at very late times of $\geq 10^5 - 10^6$ yr.

The chemical evolution of CS is governed by neutral-neutral reactions between sulphur atoms and either CH, CH_2, or C_2 initially, and later, at $t \geq 10^3$ yr, by an extended formation-destruction cycle of H_nCS^+ (n=1–3) and HC_2S^+. At this evolutionary stage these complex ions are produced by ion-neutral reactions of protonated water, H_3^+, and HCO^+ with H_nCS (n=0–2). The initial routes to form the HCS^+ ion are the reactions between CH_3^+ and S or CS^+ and H_2, whereas HC_2S^+ forms predominantly via reaction of CH_3 and S^+. The H_3CS^+ ion is mostly produced in reactive collisions of methane with sulphur ions. Upon formation, HCS^+ dissociatively recombines into CS ($\sim 10\%$) or CH ($\sim 90\%$), while HC_2S^+ breaks up equally into C_2S or CS. The H_2CS^+ and

H_3CS^+ ions recombine with equal probabilities into CS and either HCS or H_2CS. Finally, the major destruction channels for CS are photodissociation and the ion-neutral reaction with C^+. The steady-state abundance for CS, $\sim 10^{-9}$, is usually attained at about $10^3 - 10^5$ yr in our model.

2.3.3   Distribution of the abundance and column density uncertainties

For each key molecule, we derived the distribution of abundance uncertainties (dispersion) in the disk. The results are shown in Fig. 2.4. These uncertainties are quite different in different disk regions. Note that the overall abundance uncertainties are not much larger for the more complex (heavy) species among considered, in comparison to those with fewer atoms (e.g., compare C^+, CO, HCO^+, and H_2CO). However, if we would focus on even more complex species (e.g., consisting of > 7 atoms), the abundance uncertainties will in general increase with the number of atoms in the molecule, as shown by Vasyunin et al. (2004) and Wakelam et al. (2006a).
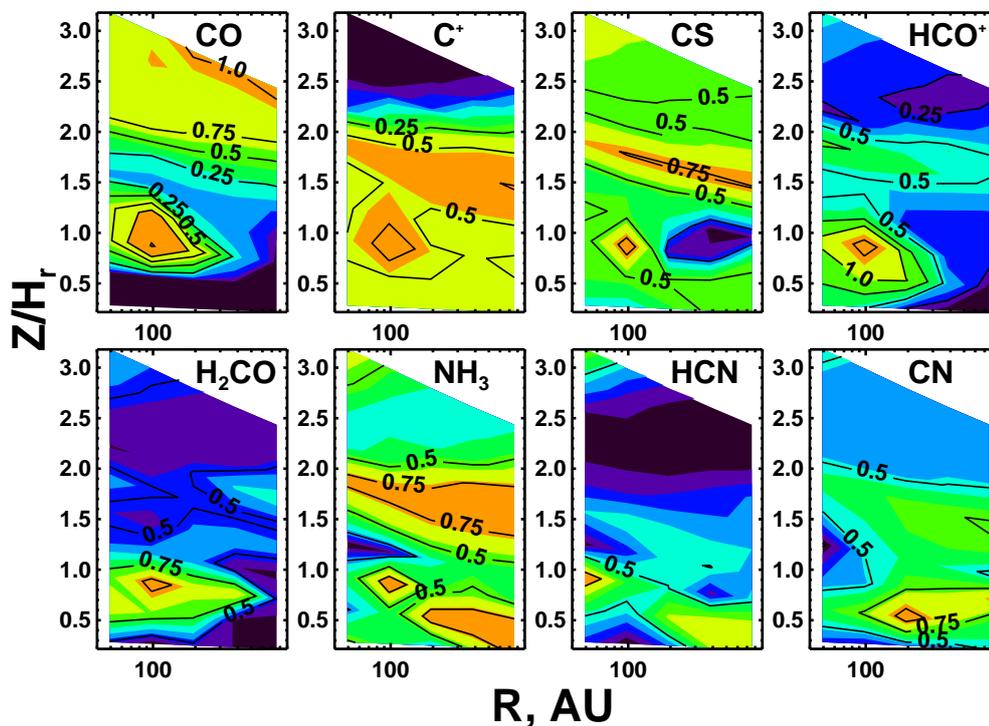
Figure 2.4 The same as in Fig. 2.3 but for abundance uncertainties (logarithmic units).

Among the key reactions, the rates of photodissociation and photoionization pro-

25

2. CHEMISTRY IN PROTOPLANETARY DISKS: A SENSITIVITY ANALYSIS

cesses can be uncertain by factors of 2 and larger. Moreover, their absolute values depend on the details of the UV radiative transfer modeling (van Zadelhoff et al., 2003a). Thus, it is not surprising that in the disk atmosphere at $Z/H(r) \geq 1.5 - 2$ large abundance uncertainties with a factor of $\leq 10 - 30$ are reached for most of the species, in particular across the interface between the intermediate layer and the disk atmosphere. A notable exception is ionized carbon, because it contains essentially all of the element carbon in the disk atmosphere and thus maintains a high steady-state abundance that is not affected by chemistry. This effect leads to relatively low values of the C^+ abundance uncertainties, in particular a factor of ≤ 3. The same is true for CO, which locks up all carbon in the disk midplane and intermediate layer at ≤ 2 pressure scale height and here has its lowest abundance uncertainty, a factor of ≤ 2 (Fig. 2.4).

There is a disk region adjacent to the midplane at $r \sim 100$ AU, $Z/H(r) \sim 1$, where the abundance uncertainties of the considered carbon-bearing species including CO show an increase of up to one order of magnitude (see HCO^+, Fig. 2.4). There, the chemistry of CO and hence all chemically related species (e.g., HCO^+, H_2CO, etc.) are prone to the hypersensitivity at $\geq 10^6$ yr caused by the rate uncertainty of the X-ray ionization of helium atoms, as discussed in Wakelam et al. (2006b). This region is moderately warm, with a temperature $T \sim 25 - 40$ K, and well shielded from the UV radiation from the central star and the interstellar UV radiation ($A_V \leq 2 - 5$ mag). The thermal bremsstrahlung X-ray photons (~ 5 keV) generated at ~ 0.1 AU above the star, however, are able to penetrate into this region (Glassgold et al., 1997a), with a total ionization rate of $\sim 10^{-16}$ s^{-1}. These X-ray photons produce helium ions that rapidly react and destroy the CO molecules (forming O and C^+). In turn, these C^+ ions are used to reform CO but also to slowly produce carbon chain molecules (e.g., C_2H_2) and cyanopolyynes (e.g., HC_3N), which are removed from the gas phase by freeze out onto the dust surfaces. These heavy surface molecules lock up most of the elemental carbon at $t \geq 1$ Myr such that the gas-phase abundance of CO is reduced to $\sim 10^{-9} - 10^{-7}$. The overall efficiency of the carbon chain formation and the decline of the CO abundance at late times sensitively depend on the He ionization rate. Consequently, the CO histogram of the abundance distribution at 5 Myr has a double-peaked, non-Gaussian shape, as shown in Fig. 2.2.

The abundances of nitrogen-bearing species such as CN, HCN, and NH_3 in the region around the midplane at $r > 200$ AU (Fig. 2.4) possesses a high sensitivity to the rate of the CRP ionization of He. The histograms of CN, HCN, and NH_3 are not fully Gaussian at 5 Myr in this region, and our method tends to overestimate the resulting abundance uncertainties. This region is so cold that at late times, $t \geq 3 \times 10^5$ yr, most molecules are removed from the gas phase by freeze-out. At this evolutionary stage, H_3^+ and later H^+ become the most abundant charged species. The primal formation pathway for H^+ is the slow ion-neutral reaction between He^+ and H_2. The rise of the H^+ abundance at ~ 5 Myr($\leq 10^{-8}$) occurs in part because of the slowness of the radiative recombination of ionized hydrogen atoms in the molecular-deficient gas. The total electron concentration increases in tandem with H^+, and leads to more rapid dissociative recombination of $HCNH^+$ and NH_4^+ (precursor ions for CN, HCN, and NH_3). Consequently, the previously low gas-phase abundances of these nitrogen-bearing molecules increase at $t \sim 5$ Myr by factors of several. The steepness and evolutionary pattern for these abundance gradients depend sensitively on the abundance of helium ions.

In the rest of the intermediate layer, the chemical evolution of the gas-phase species is initiated by radiative association reactions with high uncertainties but governed later by ion-neutral and neutral-neutral reactions with many accurately estimated rates. The situation in the disk midplane is similar, though at later times the chemical evolution of many gas-phase species is governed by the steady-state accretion-desorption life-cycle, which has no uncertainties in our model. This effect leads to lower abundance uncertainties of a factor of ~ 3 than occur in the upper disk region (see Fig. 2.4).

It is interesting to note that for CO, C^+, and NH_3 the uncertainty peak does not coincide with the maximal relative abundance in the disk. One might expect that the scatter in their column densities could be smaller than for other considered species (CS, CN, HCN, HCO^+, and H_2CO), for which uncertainty peaks and maximum abundances tend to coincide.

In Fig. 2.5, the radial distributions of the column densities at 5 Myr are plotted for the considered species (dotted lines). In addition, in Table 2.2 we compile typical intrinsic uncertainties of the column densities of a larger set of key molecules in protoplanetary disks at 100 AU. Indeed, the overall uncertainty in the column densities of CO, C^+, and NH_3 as well as H_3^+, H_2O, N_2H^+, and $HCNH^+$ is less than a factor
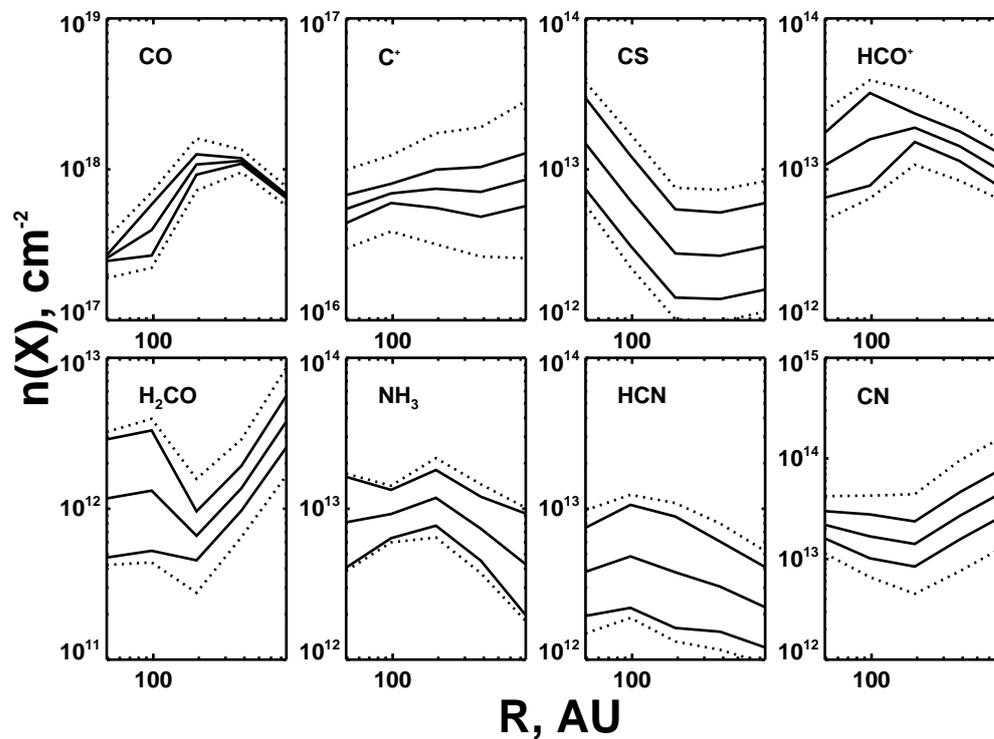
Figure 2.5 The same as in Fig. 2.4 but for radial distributions of the column densities. The central solid line represents the model-averaged column densities. The corresponding column density scatters computed with the standard model are depicted with dotted lines. The column density scatters calculated with the chemical model where the rates of the 56 most problematic reactions are varied by small factors of 1.25–2 only are shown with solid lines.

Table 2.2. Typical column density uncertainties

Species	Standard model	Improved model
H_3^+	factor $\sim$2	$\sim$1.5
C^+	factor $\sim$2	$\sim$1.5
CO	factor $\sim$1.25	1.1
CO_2	factor $\sim$3.5	$\sim$2.5
CS	factor 3	2.5
HCO^+	factor $\sim$ 3	$\sim$1.5
H_2CO	factor 3	$\sim$1.5
CN	factor 4	2
HCN	factor $\sim$ 3	2.5
HNC	factor 3	$\sim$ 2.5
N_2H^+	factor 2.5	2
NH_3	factor 2.5	2.5
$HCNH^+$	factor 2.5	2.5
H_2O	factor 1.7	1.4
C_2H	factor 4	$\sim$ 3

of about 2. Using this uncertainty value as a criterion, we assign these species to the so-called first uncertainty group. On the other hand, the column densities of CS, CN, HCN, HCO$^+$, and H$_2$CO as well as CO$_2$, C$_2$H, and HNC have larger error bars up to a factor of 4. These species belong to the second uncertainty group. It is likely that the species from the first sensitivity group are more reliable observational tracers than the species from the second one.

Note that the column density uncertainties do not exceed a factor of about 4 even for formaldehyde and are comparable with observational uncertainties. However, for heavier species (e.g., HC$_9$N), which are not included in our study, the uncertainties are likely larger, as shown in Paper I and Paper II. In our model, these uncertainties slowly increase with time and typically reach steady-state at $\geq 10^5$ yr. The column density uncertainties can be used as error bars of the theoretically predicted quantities when comparing with observational data. Moreover, one can envisage a situation when, for an object with a well-studied structure, high-resolution observations followed by advanced modeling will allow putting such tight constraints on molecular abundances or column densities that it may help to determine the rate coefficients of some key reactions *observationally*.

2.4   Discussion

In the previous section, we demonstrated how and to what extent the uncertainties of the rate coefficients affect the computed abundances and column densities of several key species in the disk. In this section, we discuss the relative contributions of individual reactions to the uncertainties of these key molecules.

2.4.1   Sensitivity analysis method

The chemical evolution of even a simple molecule usually involves a large number of reactions in the adopted chemical network. The non-linearity of the equations of chemical kinetics often makes it a challenge to find a direct link between the rate value of a certain reaction and the molecular abundances. Thus an efficient numerical method is required (see, e.g., Turanyi, 1997).

Using a sensitivity analysis based on a simple correlation method, we have shown in Paper I that under the physical conditions of dark and diffuse clouds the rate un-
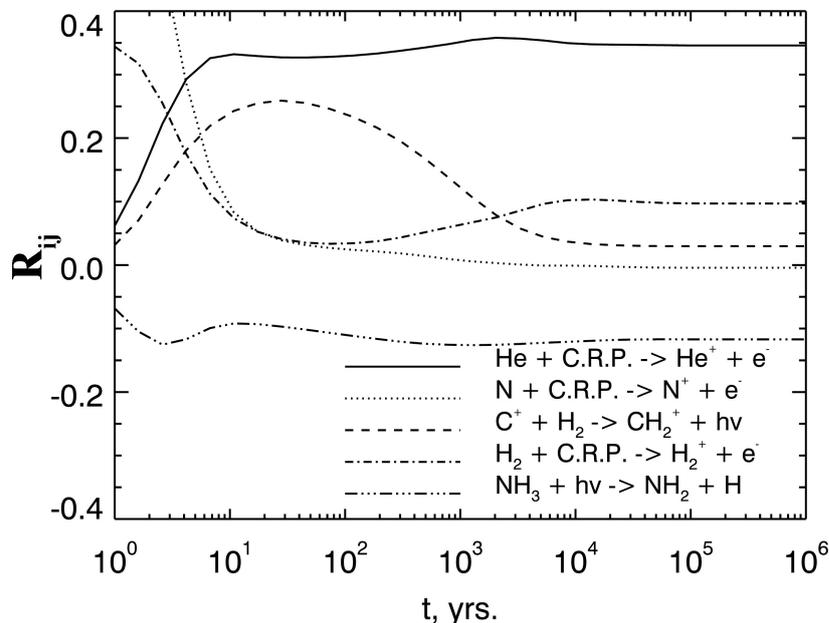
Figure 2.6 The largest correlation coefficients of relevant reactions for the evolution of NH_3 as a function of time in the disk intermediate layer ($r = 97$ AU, $z = 30$ AU).

certainties of only a handful of chemical reactions affect the accuracy of the resulting abundances to the highest extent. For the disk chemistry studied in this chapter a modified, two-stage sensitivity analysis was performed.

First, for each selected molecule, we calculated time-dependent linear correlation coefficients between the abundances and rate coefficients for all 8 000 realizations of the RATE 06 network, and 19 logarithmically taken time steps over the 5 Myr of disk evolution at each disk cell. The coefficients $R_{ij}(t)$ are given by the expression

$$R_{ij}(r,z,t) = \frac{\sum_l \left(x_i^l(r,z,t) - \overline{x_i(r,z,t)}\right)(\alpha_j^l - \overline{\alpha_j})}{\sqrt{\sum_l \left(x_i^l(r,z,t) - \overline{x_i(r,z,t)}\right)^2 \sum_l \left(\alpha_j^l - \overline{\alpha_j}\right)^2}}, \qquad (2.2)$$

where $x_i^l(r,z,t)$ is the molecular abundance of the i-th species computed with the l-th realization of the UMIST network, $\overline{x_i(r,z,t)}$ is the standard (mean) abundance of this species, α_j^l is the j-th reaction rate coefficient for the l-th realization of the RATE 06 network, and $\overline{\alpha^j}$ is the standard rate coefficient of the j-th reaction.

This is in contrast to Paper I where the analysis of statistically significant reactions was performed for only the final time step. Since at various evolutionary stages the

chemistry of a molecule is typically governed by a restricted number of chemical processes, at any particular time step the abundance correlation will be high only for some of the key reactions, as shown in Fig. 2.6 for the case of ammonia. The obvious drawback of such a "single-time" approach is that it does not account for the cumulative character of the abundance uncertainties. Therefore, we integrated the absolute values of time-dependent correlation coefficients over the entire evolutionary time of 5 Myr. These quantities are called "cumulative correlation coefficients".

With this cumulative criterion, one can identify those reactions whose rate uncertainties are the most important for the abundance scatter of one molecule in one specific disk region. As a general criterion for the entire disk, we utilized the cumulative correlation summed up over all 50 disk grid cells, followed by summation over the 8 considered species (CO, C^+, CS, HCO^+, H_2CO, CN, HCN, NH_3). One should bear in mind that the results of our analysis rely on the inherent assumption that the absolute values of the rate coefficients and their uncertainties in RATE 06 are accurately determined. This assumption may not be fullfiled for all important reactions in the RATE 06 database as we will show below. Such reactions will not be treated correctly by our sensitivity analysis.

2.4.2 Identification of the most problematic reactions

We calculated disk-averaged cumulative correlations for all 5773 reactions in our chemical network and for 8 key species: CO, C^+, CS, HCO^+, H_2CO, CN, HCN, and NH_3. The corresponding cumulative correlations, normalized in descending order, steadily decline with the number of reaction. The 56 most "problematic" reactions and their weights for these 8 molecules are listed in Table 2.3. We term by "weight" the corresponding cumulative correlations summed over the all 50 disk cells and renormalized to the maximum value of 1148.1, which is achieved for the RA reaction between H_2 and C.

These 56 reactions correspond to 1% of the total number of reactions in our chemical model. Moreover, such an apparently small number of reactions is chosen to stimulate experimental and theoretical studies of the rate coefficients of the reactions with high astrochemical importance. Note also that some of the most "problematic" reactions in Table 2.3 have been carefully studied as their rates have small uncertainties of only factors of 1.25–1.5.

Table 2.3. Most problematic reactions in astrochemical model of protoplanetary disk

Reaction			Uncertainty	Weight	Type
$H_2 + C$	$\rightarrow$	**$CH_2 + h\nu$**	**factor 10**	1.0	**RA**
$H_2 + C^+$	$\rightarrow$	**$CH_2^+ + h\nu$**	**factor 10**	4.2(-1)	**RA**
$H_2 + CH$	$\rightarrow$	$CH_3 + h\nu$	factor 10	1.6(-2)	RA
$H_2 + CH_3^+$	$\rightarrow$	$CH_5^+ + h\nu$	factor 10	7.6(-2)	RA
$C + H$	$\rightarrow$	$CH + h\nu$	factor 10	2.3(-2)	RA
$C + N$	$\rightarrow$	$CN + h\nu$	factor 10	2.2(-2)	RA
$C^+ + e^-$	$\rightarrow$	$C + h\nu$	factor 10	1.2(-2)	RR
$CH_3^+ + e^-$	$\rightarrow$	$CH_3 + h\nu$	factor 10	1.2(-2)	RR
$H_2 + C.R.P.$	$\rightarrow$	**$H_2^+ + e^-$**	**factor** 2^*	1.4(-1)	**CRI**
$H_2 + C.R.P.$	$\rightarrow$	$H^+ + H + e^-$	factor 2	1.0(-2)	CRI
$He + C.R.P.$	$\rightarrow$	$He^+ + e^-$	factor 2	2.3(-1)	CRI
$N + C.R.P.$	$\rightarrow$	$N^+ + e^-$	factor 2	9.7(-2)	CRI
$C + h\nu$	$\rightarrow$	$C^+ + e^-$	factor 2	3.8(-1)	PI
$C + C.R.P.h\nu$	$\rightarrow$	$C^+ + e^-$	factor 2	6.7(-2)	PI
$CO + h\nu$	$\rightarrow$	$O + C$	factor 10	5.6(-2)	PD
$CH + h\nu$	$\rightarrow$	$C + H$	factor 2	2.3(-2)	PD
$CH_2 + h\nu$	$\rightarrow$	$CH + H$	factor 2	6.8(-3)	PD
$CN + h\nu$	$\rightarrow$	$N + C$	factor 2	3.2(-2)	PD
$CS + h\nu$	$\rightarrow$	$S + C$	factor 2	2.6(-2)	PD
$NH_3 + h\nu$	$\rightarrow$	$NH_2 + H$	factor 1.5	8.2(-3)	PD
$HCN + h\nu$	$\rightarrow$	$CN + H$	factor 1.5	1.5(-2)	PD
$OH + h\nu$	$\rightarrow$	$O + H$	factor 1.5	7.8(-3)	PD
$He^+ + CO$	$\rightarrow$	$O + C^+ + He$	factor 1.25	9.6(-3)	IN
$He^+ + N_2$	$\rightarrow$	$N + N^+ + He$	factor 1.25	7.4(-3)	IN
$H_3^+ + C$	$\rightarrow$	$CH^+ + H_2$	factor 2	3.3(-2)	IN
$H_3^+ + O$	$\rightarrow$	$OH^+ + H_2$	factor 1.5	1.0(-2)	IN
$H_3^+ + CO$	$\rightarrow$	$HCO^+ + H_2$	factor 1.25	7.3(-3)	IN
$H_2^+ + N$	$\rightarrow$	$NH^+ + H$	factor 2	4.3(-2)	IN
$H_2 + He^+$	$\rightarrow$	$He + H^+ + H$	factor 2	2.0(-2)	IN
$H_2 + He^+$	$\rightarrow$	$He + H_2^+$	factor 2	2.1(-2)	IN
$H_2 + NH_3^+$	$\rightarrow$	$NH_4^+ + H$	factor 1.5	4.4(-2)	IN
$H^+ + O$	$\rightarrow$	$O^+ + H$	factor 1.5	8.4(-3)	CT
$C^+ + CH$	$\rightarrow$	$C_2^+ + H$	factor 2	1.3(-2)	IN
$C^+ + OH$	$\rightarrow$	$CO^+ + H$	factor 2	3.1(-2)	IN

Table 2.3 (cont'd)

Reaction			Uncertainty	Weight	Type	
$C^+ + NH$	$\rightarrow$	$CN^+ + H$	factor 2	1.1(-2)	IN	
$C^+ + HCN$	$\rightarrow$	$CNC^+ + H$	factor 1.25	7.9(-3)	IN	
$C + HCO^+$	$\rightarrow$	$CO + CH^+$	factor 2	2.7(-2)	IN	
$CH + S^+$	$\rightarrow$	$CS^+ + H$	factor 2	2.6(-2)	IN	
$CH_2^+ + O$	$\rightarrow$	$HCO^+ + H$	factor 2	7.2(-3)	IN	
$NH_3^+ + Mg$	$\rightarrow$	$NH_3 + Mg^+$	factor 2	1.1(-2)	CT	
$C + CH_2$	$\rightarrow$	$C_2H + H$	factor 2	3.6(-2)	NN	
$C + C_2H$	$\rightarrow$	$C_3 + H$	factor 2	8.3(-3)	NN	
$N + CH_2$	$\rightarrow$	$HCN + H$	factor 1.5	8.5(-2)	NN	
$N + CN$	$\rightarrow$	$N_2 + C$	factor 2	4.6(-2)	NN	*
$N + HCO$	$\rightarrow$	$HCN + O$	factor 2	2.9(-2)	NN	
$H + CH_2$	$\rightarrow$	$CH + H_2$	factor 1.25	1.9(-2)	NN	
$H + CH$	$\rightarrow$	$C + H_2$	factor 1.5	1.1(-2)	NN	
$CH + O$	$\rightarrow$	$HCO^+ + e^-$	factor 1.5	4.0(-2)	NN	
$CH + O$	$\rightarrow$	$CO + H$	factor 1.25	8.3(-3)	NN	
$CH + N$	$\rightarrow$	$CN + H$	factor 1.25	2.3(-2)	NN	
$CH + S$	$\rightarrow$	$CS + H$	factor 2	1.6(-2)	NN	
$CH_2 + S$	$\rightarrow$	$CS + H_2$	factor 2	6.3(-2)	NN	
$CH_2 + O$	$\rightarrow$	$CO + H + H$	factor 1.25	1.0(-2)	NN	
$CH_3 + O$	$\rightarrow$	$H_2CO + H$	factor 1.25	1.4(-2)	NN	
$HCO^+ + e^-$	$\rightarrow$	$CO + H$	factor 1.25	3.1(-2)	DR	
$NH_4^+ + e^-$	$\rightarrow$	$NH_3 + H$	factor 1.25	8.1(-3)	DR	

*These rates are partly uncertain due to uncertainties in physical parameters.

Note. — (CRI) Cosmic ray ionization; (CT) Charge transfer; (DR) Dissociative recombination; (IN) ion-neutral reaction; (NN) Neutral-neutral reaction; (PD) Photodissociation; (PI) Photoionization; (RA) Radiative association; (RR) Radiative recombination. Three most important reactions for the disk chemistry as identified by the sensitivity analysis are written in boldface.

In order to demonstrate that these 56 reactions are indeed important and their rate uncertainties strongly affect the abundances, we re-calculated the disk chemical evolution but allowed the rates of these 56 reactions to vary by only a factor of 1.25 (and 2 for radiative association). Such idealization is thought to mimic the situation when all of these 56 rates will be accurately measured in the laboratory or derived theoretically.

The resulting uncertainties in the molecular column densities are shown in Fig. 2.5 (solid lines) and reported in Table 2.3 (last column). Compared with the initial column density uncertainties, the refined chemical model leads to smaller error bars for most of the considered molecules, in particular for CO, HCO^+, H_2CO, CN, and H_2O. However, the improvement is not so obvious for nitrogen-bearing species (HCN, HNC, NH_3, $HCNH^+$) as well as CO_2, CS, and C_2H. Their chemical evolution is governed by a large set of key reactions that are only partly included in the list of the 56 most problematic reactions (Table 2.2)[1].

The fact that the uncertainties in column densities decrease not only for the 8 key species, but also for some other molecules in Table 2.2 clearly indicates that some of the reactions from Table 2.3 are relevant for their chemical evolution. For H_3^+ these are the ionization of H_2 and reactions of H_3^+ with C, O, and CO. As we have shown in Sect. 2.3.1, reactions with H_3^+ are an essential ingredient of disk chemistry. The decrease in the abundance error bars for H_3^+ in the model with refined rate uncertainties leads to smaller abundance uncertainties in the related species: HCO^+, H_2CO, H_2O, HCN, HNC, $HCNH^+$, and CS. Table 2.3 contains a number of reactions important for the evolution of CO and CO_2; e.g., formation of light hydrocarbons, neutral-neutral reactions of these hydrocarbons with oxygen, and CO photodissociation. The former reactions affect the evolution of C_2H, while photodissociation is an important process for CN.

Below we discuss the contributions of each reaction type in detail.

2.4.2.1 Radiative association

The most problematic reactions in the disk are radiative association (RA) reactions. Radiative association leads to the formation of a larger molecule from two smaller species upon their collision, and requires the emission of excess energy in the form

---

[1]An extended version of this table is freely available from the authors upon request.

2. CHEMISTRY IN PROTOPLANETARY DISKS: A SENSITIVITY ANALYSIS

of a photon. RA reactions allow the formation of new bonds and more chemically "advanced" species (van Dishoeck and Blake, 1998). The corresponding rate values are often so low for small species that they are difficult to obtain with high accuracy (Bates and Herbst, 1988; Herbst, 1980; Smith, 1989; Williams, 1972). Nonetheless, assigned uncertainties for many of these reactions in RATE 06 are only a factor of 2 and less. Since we assume that the rate coefficients of such reactions may vary by an order of magnitude, in accord with the recent OSU database, it is not surprising that some RA reactions are identified as among the most problematic reactions for disk chemistry. Its importance is also rise due to the fact that we start calculation from the atomic initial abundances and use time-integrated correlation coefficients. It means that at early evolutionary time chemistry is dominated by RA reactions and, therefore, its time-integrated correlation coefficients increase greatly at early times.

Two RA reactions are particularly important for the chemical evolution and accumulation of the abundance uncertainties. First is the reaction between H_2 and C, which produces CH_2 everywhere through the disk at all times. The rate coefficient of this reaction is not well known, with with an estimated value of 10^{-17} cm^3 s^{-1} at $T = 10 - 300$ K (Prasad and Huntress, 1980; Woodall et al., 2007). This reaction is relevant for the evolution of CO, HCO^+, H_2CO, CS, and HCN. Second, the reaction between H_2 and C^+ leads to the formation of CH_2^+ (important for C^+, HCO^+, CS, NH_3, and CN), with an estimated rate coefficient of $\approx 4 \times 10^{-17}$ cm^3 s^{-1} (Herbst, 1985). These two reactions initiate processes of C and H addition in the chemical model and thus should be relevant for nearly all species containing carbon and hydrogen.

The next most important RA reaction (8th place out of 56) is the formation of protonated methane from molecular hydrogen and CH_3^+ ($\alpha = 1.3 \times 10^{-14}$ cm^3 s^{-1}, $\beta = -1$; Smith, 1989), which is an important molecular ion for CO destruction. More recently the rate of this reaction has been measured at low temperature of 10 K by Gerlich (1995), $1.1 \pm 0.1 \times 10^{-13}$ cm^3 s^{-1} for para-H_2.

Much less important (27th and 28th place) are two slow reactions between C and H or N producing CH or CN radicals. It is interesting to note that the latter reaction has different rate coefficients in the OSU and RATE 06 databases (Smith et al., 2004; Woodall et al., 2007). While in osu.2007 this reaction rate has no temperature dependence and no activation barrier ($\alpha = 10^{-17}$ cm^3 s^{-1}; Prasad and Huntress, 1980), in RATE 06 the corresponding rate is low, 7.9×10^{-19} cm^3 s^{-1}, and possesses a small

barrier of 96 K (relevant temperature range is between 300 and 2 700 K; Singh and Andreazza, 2000). Thus the RATE 06 and osu.2007 rate coefficients for the RA reaction between C and N differ by an order of magnitude in a wide temperature range.

The situation is similar for the RA reaction between molecular hydrogen and CH that forms CH_3 – an important radical for the evolution of formaldehyde. The corresponding osu.2007 rate at 10 K is 2.5×10^{-16} $cm^3 s^{-1}$ ($\alpha = 3.25 \times 10^{-17}$ $cm^3 s^{-1}$, $\beta = -0.6$). In contrast, in RATE 06 this reaction has a small barrier of 11.6 K and the 10 K rate value is lower by an order of magnitude, 1.8×10^{-17} $cm^3 s^{-1}$ ($\alpha = 5.09 \times 10^{-18}$ $cm^3 s^{-1}$, $\beta = -0.71$, and $\gamma = 11.6$ K; Brownsword et al., 1997).

In addition to radiative association, we list radiative recombination reactions of C^+ and CH_3^+ in the same group in Table 2.3. The radiative recombination of ionized carbon is a key reaction for the evolution of C^+. Its rate coefficient at room temperature is 4.67×10^{-12} $cm^3 s^{-1}$ with an inverse temperature exponent of 0.6 (Woodall et al., 2007). The assumed uncertainty of this rate (the factor of 10) in osu.2007 is in contrast to the results of Nahar and Pradhan (1997), who have theoretically predicted this rate value and found that the corresponding uncertainty is only $\sim 10\%$. In the RATE 06 database the uncertainty of this rate constant is set to 50%.

Finally, the radiative recombination of CH_3^+ is the least probable channel in the reactive collisions between methyl ions and electrons. The rate of this process is estimated to be much higher than for other recombination reactions involving atomic species, particularly in cold regions, and might be accurately determined in laboratory ($\alpha = 1.1 \times 10^{-10}$ $cm^3 s^{-1}$, $\beta = -0.5$; Le Teuff et al., 2000; Millar et al., 1997; Woodall et al., 2007). In the osu.2007 database, this rate has a steeper dependence on temperature, $\beta = -0.7$ (Smith et al., 2004).

We conclude that RA reactions require a particular attention because their rate uncertainties are often large and not well known so that the modeling results can be heavily affected.

2.4.2.2 Cosmic ray ionization

The next most important reactions that contribute strongly to the resulting abundance scatter of many molecules are the cosmic ray ionization of molecular hydrogen and helium atoms. The cosmic ray particles able to penetrate deeply into the disk are mostly high-energy protons ($E \geq 100$ Mev) and heavy nuclei (e.g. iron, $E \sim 1$ Gev)

2. CHEMISTRY IN PROTOPLANETARY DISKS: A SENSITIVITY ANALYSIS

(Dalgarno and McCray, 1972; Dolginov and Stepinski, 1994; Leger et al., 1985). Direct ionization initiate chemical evolution in dark and cold regions where cosmic ray particles remain the main ionization source (Herbst and Klemperer, 1973). In the disk this is the outer midplane at $r \geq 30$ AU and the lower part of the intermediate layer (Gammie, 1996; Semenov et al., 2004). Moreover, since we added the X-ray ionization rate to the CRP rate value in an attempt to crudely treat the effect of high-energy stellar radiation, it is not surprising that high correlation coefficients for some CRP-ionization reactions are reached in the disk atmosphere and intermediate layer at $r \leq 100$ AU for several key species such as CO (see Fig. 2.4). A more accurate approach to model X-ray chemistry in disks is required (Lepp and Dalgarno, 1996; Maloney et al., 1996; Neufeld et al., 1994; Stäuber et al., 2005).

It is natural that because the cosmic ray ionization of H_2 and He is the primal chemical process, it is also the key factor for the accumulation of abundance scatters. In the RATE 06 database the corresponding rate coefficients are estimated to be accurate within a factor of 2 (Woodall et al., 2007). However, this rate uncertainty has two origins.

First, there is the *physical* uncertainty that is related to our limited knowledge of the absolute CRP flux and its penetrating ability, which may vary in different astrophysical objects (Caselli et al., 1998; Dolginov and Stepinski, 1994; Spitzer and Tomasko, 1968). While the direct ionization process driven by CRPs is well studied and the corresponding cross sections and rates are well known (Solomon and Werner, 1971), the second *chemical* uncertainty resides in the treatment of the ionization by energetic secondary electrons (Glassgold and Langer, 1973). Here the elemental composition of the gas plays a decisive role (Ilgner and Nelson, 2006).

The CRP-induced ionization rate of H_2 currently used in all UMIST and OSU databases was taken from the PhD thesis of Black (1975). It was computed for a mixture of atomic and molecular hydrogen but new calculations for a mixture of hydrogen and helium would be required in order to have a more consistent rate value (see discussion in Wakelam et al., 2006b). Other CRP-ionization reactions listed in Table 2.3 do not have a reference in the RATE 06 database so it is hard to judge how accurate their rates are.

Apparently, the rate uncertainty of the CRP-driven reactions can be partially eliminated by more accurate modeling of the full cascade of ionizing events, but the physical

uncertainty will still remain, which needs more efforts from observers. Wakelam et al. (2006b) have demonstrated how crucial this may be for the results of pure gas-phase chemical models of static molecular clouds.

2.4.2.3   Photoreactions

Another set of chemical processes with problematic rates are photodissociation (PD) and photoionization (PI) reactions, as listed in Table 2.3. These reactions are important in those regions where UV photons are either able to penetrate (the disk atmosphere and intermediate layer) or are induced by cosmic ray particles (disk midplane; Prasad and Tarafdar, 1983). High-energy UV photons destroy or ionize gas-phase molecules and allow surface species to desorb back into the gas phase.

While both the PD and PI cross sections for many species can be measured or calculated with a rather good accuracy of $\leq 50\%$ (van Dishoeck, 1988; van Dishoeck et al., 2006a), the major difficulty in obtaining accurate photorates is our limited knowledge of the UV radiation field inside protoplanetary disks. Bergin et al. (2003) and van Dishoeck et al. (2006a) have shown that many T Tauri stars emit strong, non-blackbody UV radiation. Their spectra resemble that of the interstellar (IS) UV radiation field, with a large fraction of the UV flux emitted in the Lyα line. van Zadelhoff et al. (2003a) have demonstrated the importance of scattering for the UV penetration deep into the disk interior. Furthermore, for the two most abundant molecules, H_2 and CO, that effectively dissociate through partly overlapping lines shortward of about $1\,120$ Å, the optical thickness in these lines can become so high that self- and mutual-shielding have to be taken into account (Dalgarno and Stephens, 1970; Jonkheid et al., 2006a; Lee et al., 1996; van Dishoeck, 1988).

In the UMIST and OSU databases, the photorates have mostly been adopted from the compilation of van Dishoeck (1988) and Roberge et al. (1991), where they have been computed using a simple plane-parallel approach and the IS (IS) UV radiation field of Draine (1978). The IS UV flux is characteristic of a diluted radiation field from an early B star ($T_{\mathrm{eff}} \sim 30\,000$ K) located at a distance of ~ 10 pc, with a cut-off at 912 Å due to absorption by interstellar atomic hydrogen (Spitzer, 1978; van Dishoeck, 1994). Obviously, it is not representative of the UV radiation from much cooler Herbig Ae and T Tauri stars surrounded by circumstellar disks. Recently, van Dishoeck et al.

(2006a) have recalculated the corresponding PD and PI rates, using more appropriate UV spectral distributions typical of Herbig Ae, T Tauri, and Sun-like stars.

The 10 problematic photodissociation and photoionization reactions found by the sensitivity analysis are involved in either the formation of key species (C^+ and CN), their destruction (CO, CN, CS, NH_3, and HCN), or the destruction of parental molecules (OH, CH, and CH_2). Their rates in the RATE 06 database are in general inaccurate by a factor of 2 with some exceptions. The photodissociation of CO proceeds indirectly, through predissociation, and depends on the amount of molecular hydrogen and CO molecules in the line of sight to the source of UV radiation (van Dishoeck, 1987), and thus has a rate uncertainty of a factor of 10 (see Table 2.3). In contrast, the rates of direct photodissociation of NH_3, OH, and HCN are inaccurate by the factor of 1.5 only (Roberge et al., 1991). Despite such small error bars, the latter three reactions were identified as problematic reactions for disk chemistry.

2.4.2.4 Ion-neutral and neutral-neutral reactions

Ion-neutral (IN) and neutral-neutral (NN) reactions form the largest fraction of the problematic reactions (32 out of 56) for disk chemistry, but their individual importance is not as significant as for CRI and RA reactions (Table 2.3).

Ion-neutral reactions are usually exothermic and rapid, and lead to the formation of new species by bond rearrangement. Their rate coefficients can often be obtained by simple Langevin theory, which relates the isotropic polarizability of the species and its reduced mass (Clary, 1988). For molecules that possess a large dipole moment, the rate values can be significantly enhanced at low temperature by the long-distance Coulomb attraction between the positive ion and negatively charged side of the molecule (Adams et al., 1985; Clary et al., 1985). Moreover, many neutral-neutral reactions with small barriers or without a barrier can also be fast under interstellar conditions. The rates of most radical-radical reactions and even some radical-stable neutral reactions are controlled by long-range attractive forces and thus do not get smaller at low temperatures (see, e.g., Canosa et al., 1997; Sims et al., 1993, 1994b; Smith, 1988). The typical rate coefficient for these reactions is about an order of magnitude lower than for ion-neutral processes. The rates of some of the fast neutral-neutral reactions at low temperatures have been measured in the laboratory and predicted theoretically (e.g., Chastaing et al., 2001; Clary et al., 1994; Sims et al., 1994a; Smith et al., 2004).

In RATE 06, most of the IN and NN rate coefficients are uncertain by a factor of 2 and less, up to the accuracy of 25% (Table 2.3). However, a major ambiguity that resides in the IN rate constants is the treatment of their temperature dependence. In two versions of the RATE 06 database the rate value for the reaction involving a polar molecule and a molecular ion can have a negative dependence on temperature ($\beta = -0.5$; adopted in this work) or no temperature dependence ($\beta = 0$), while its rate coefficient fits the value at room temperature. In contrast, in the OSU network the corresponding IN rates based on low temperature theoretical estimations to be most accurate at ~ 10 K even though the listed reaction rate coefficients are scaled with respect to 300 K with $\beta \sim -0.5$. Two problematic reactions involving a polar molecule and an ion with significantly different rates in RATE 06 and osu.2007 are those between C^+ and NH, forming CN^+ and H ($\alpha_{\mathrm{osu.2007}} = 4.6 \times 10^{-9}$ cm^3 s^{-1} vs. $\alpha_{\mathrm{RATE 06}} = 7.8 \times 10^{-10}$ cm^3 s^{-1}) and between S^+ and CH, producing CS^+ and H ($\alpha_{\mathrm{osu.2007}} = 4.4 \times 10^{-9}$ cm^3 s^{-1} vs $\alpha_{\mathrm{RATE 06}} = 6.2 \times 10^{-10}$ cm^3 s^{-1}).

Other IN reactions with different rates in the RATE 06 and osu.2007 databases are reactions involving an atom and a molecular ion. The break up of molecular hydrogen upon collision with helium ion involves a small barrier of 35 K and $\alpha = 3.7 \times 10^{-14}$ cm^3 s^{-1} in RATE 06 (the relevant temperature range is between 10K and 300K; Woodall et al., 2007), while in osu.2007 the same rate coefficient is about 5 times smaller and has no barrier (Smith et al., 2004). However, this results in difference of the osu.2007 and RATE 06 rate values of an order of magnitude at most.

Similarly, the OSU reaction between molecular hydrogen and ionized ammonia produces hydrogen atom and protonated ammonia with a rate coefficient of 1.5×10^{-14} cm^3 s^{-1} and a steep temperature dependence ($\beta = -1.5$). In RATE 06 this reaction has a non-Langevin rate with $\beta = 0$. At temperatures below 20 K its rate coefficient is twice as large, $\alpha = 3.36 \times 10^{-14}$ cm^3 s^{-1}, and a negative activation barrier of -35.7 K exists (Adams and Smith, 1984). At temperatures between 20 and 300 K this reaction has no barrier and $\alpha = 2 \times 10^{-13}$ cm^3 s^{-1}. For temperatures above 300 K the rate coefficient is 1.7×10^{-11} cm^3 s^{-1} and a barrier is about $1\,000$ K (Fehsenfeld et al., 1975). Consequently, the osu.2007 and RATE 06 rate values can differ by up to one order of magnitude.

Finally, the IN reaction between H_3^+ and O produces only OH^+ and H_2 in OSU, but in RATE 06 a second, less probable alternative channel that leads to the production of

2. CHEMISTRY IN PROTOPLANETARY DISKS: A SENSITIVITY ANALYSIS

ionized water and atomic hydrogen is given (Milligan and McEwan, 2000).

Note that the 4 IN reactions with the smallest rate uncertainty of 25% are still problematic for disk chemistry. Such high sensitivity of the disk modeling results to the rates of these reactions is caused by their importance for the evolution of CO, HCO^+, and HCN. The most important one is the IN reaction between helium ions and CO, which leads to the hypersensitivity of the final abundances of many carbon-bearing species in the inner part of the disk intermediate layer (see Fig. 2.2). The other reactions include the primal route to the formation of HCO^+ and destruction of CO: $H_3^+ + CO \rightarrow HCO^+ + H_2$ ($\alpha = 1.7 \times 10^{-9}$ cm^3 s^{-1}; Kim et al., 1975) as well as the destruction of molecular nitrogen by ionized helium ($\alpha = 6.4 \times 10^{-10}$ cm^3 s^{-1}; Woodall et al., 2007) and destruction of HCN by ionized carbon ($\alpha = 3.1 \times 10^{-9}$ cm^3 s^{-1}, $\beta = -0.5$; Clary et al., 1985).

All of the 15 problematic neutral-neutral reactions for disk chemistry are reactions involving atoms (O, N, C, H, S) and either light hydrocarbons (C_nH_m, n=1,2, m=1–3) or CN, HCO, and H_2CO. In contrast to the IN reactions, the NN reactions are mainly important for the chemical evolution of the key species in warm disk regions, in particular reaction with atomic oxygen (Tscharnuter and Gail, 2007). Though their rates are rather accurate, with uncertainties that are typically not higher than 50%, some of the NN rates are still different in RATE 06 and osu.2007 databases.

The NN reaction between N and HCO produces only OCN and H in osu.2007, with a rate coefficient of 10^{-10} cm^3 s^{-1} (Smith et al., 2004). In RATE 06 this reaction has in addition 2 other channels that form either HCN and O ($\alpha = 1.7 \times 10^{-10}$ cm^3 s^{-1}) or CO and NH ($\alpha = 5.7 \times 10^{-12}$ cm^3 s^{-1}, $\beta = 0.5$, and $\gamma = 1\,000$ K; Woodall et al., 2007).

Another reaction in the list is H + CH, which leads to C and H_2. In osu.2007, the rate coefficient has a weak dependence on temperature and no barrier ($\alpha = 2.7 \times 10^{-11}$ cm^3 s^{-1}, $\beta = 0.38$; Le Teuff et al., 2000), while in RATE 06 this rate has $\beta = 0$ and an 80 K barrier ($\alpha = 1.3 \times 10^{-10}$ cm^3 s^{-1}; Woodall et al., 2007).

Finally, the neutral-neutral reaction between H and CH_2, which forms CH and H_2, has the osu.2007 rate coefficient of 2.7×10^{-10} cm^3 s^{-1} taken from the UMIST 95 database, but this value is only 6.6×10^{-11} cm^3 s^{-1} in RATE 06.

We conclude that the reaction rates of many important ion-neutral and neutral-neutral reactions are not known accurately enough, as a major controversy in their

temperature dependence still persists. This is particularly true for the reactions involving an ion and a polar molecule, whose rates in RATE 06 can differ by a factor of ~ 5 at 10 K for the dipole/non-dipole versions of this ratefile. The ion-polar rates in osu.2007 can be larger than those in the dipole version of RATE06 by another factor of 4-5, especially for linear neutral reactants, in which allowance is made for sub-thermal rotational populations via the so-called "locked-dipole" approach.

2.4.2.5 Dissociative recombination

Molecular ions are efficiently converted into other, less complex molecules via dissociative recombination (DR) with electrons or charged grains. Similarly to IN reactions, these processes are especially fast at low temperatures with typical rate coefficients of about 10^{-6} cm^{-3} s^{-1} at 10 K due to the long-range Coulomb attraction. The DR rates can be measured rather accurately with afterglow and storage ring techniques (Florescu-Mitchell and Mitchell, 2006). However, the sensitivity of their branching ratios with respect to the temperature is mostly unexplored and may not be described by a simple power law at low T (Petrignani et al., 2005).

A strong influence of the DR rates and branching ratios on the results of chemical models of molecular clouds has been found (Geppert et al., 2005a; Millar et al., 1988; Semaniak et al., 2001). Our sensitivity method picked up two DR reactions that introduce significant uncertainties in computed abundances in protoplanetary disks. These include dissociative recombination of protonated ammonia into ammonia and hydrogen atoms (50th place out of 56), and a main destruction channel for HCO$^+$ (19th place, see Table 2.3). Note that their rates are supposed to be known within an uncertainty of 25%.

The DR of HCO$^+$ in RATE 06 has one dissociative channel to CO and H with the total rate coefficient of 2.4×10^{-7} cm^3 s^{-1} and $\beta = -0.69$ (Mitchell, 1990). In the osu.2007 database 2 additional channels are listed, which lead to the formation of either OH and C or CH and O but with a much smaller probability of $\sim 4\%$ each. The DR of NH$_4^+$ in both RATE 06 and osu.2007 involves 3 branching channels into NH$_2$ and either two hydrogen atoms (21%) or one molecular hydrogen (10%), or ammonia and atomic hydrogen (69%) with the total rate of 1.5×10^{-6} cm^3 s^{-1} and $\beta = -0.5$ (Vikor et al., 1999).

Still, more effort needs to be invested into the (re-)investigation of the DR branching ratios and their temperature-dependence, especially at low ~ 10–20 K temperatures.

2.5 Summary and conclusions

The influence of gas-phase reaction rate uncertainties on the results of disk chemical modeling has been studied by a Monte Carlo method. The rate coefficients in the RATE 06 network were varied 8 000 times within their uncertainty limits using a log-normal distribution. Sets of abundances, column densities, and their error bars were computed for a number of key species in protoplanetary disks. We found that typical uncertainties of the molecular column densities do not exceed a factor of 3–4 even for the largest of the key molecules, which is comparable with observational uncertainties. The column densities of CO, C^+, H_3^+, H_2O, NH_3, N_2H^+, and $HCNH^+$ have particularly small error bars. A straightforward correlation analysis between molecular abundances and reaction rates was performed for the entire evolutionary time, and the most problematic reactions involving CO, C^+, CS, HCO^+, H_2CO, CN, HCN, and NH_3 were identified. We showed that the rate coefficients of about a hundred chemical reactions constituting only a few percent of the entire RATE 06 database need to be determined more accurately in order to significantly decrease uncertainties in the modeled abundances and column densities of the key observable molecules. We argue that it is worthwhile to (re-)investigate, either experimentally or theoretically, the rate coefficients of basic radiative association and cosmic ray ionization reactions as well as the temperature-dependence of key ion-neutral and neutral-neutral reactions, and the branching ratios and products of dissociative recombination processes. The rate uncertainties of cosmic ray ionization and photoreactions are partly due to uncertain physical parameters such as the CRP flux and UV penetration, and thus can be decreased with better physical models and observational data.

In this chapter, we considered the first big issue in astrochemical modeling – the influence of uncertainties in rates of chemical reactions on modeling results. Using an estimation of the uncertainties obtained above, we perform a comparison of stochastic and deterministic techniques to model surface chemistry in the next chapter of the dissertation.

3

A unified Monte Carlo treatment of gas-grain chemistry for large reaction networks: molecular clouds

3.1   Introduction

Chemical processes are discrete in nature, and it has been realized long time ago that their microphysically correct theoretical treatment should rest upon stochastic methods (Gillespie, 1976). While in cellular biology Monte Carlo simulations of chemical processes in cells are widespread, most models in astrochemistry are based on deterministic rate equation (RE) approach, which has been proved to be inaccurate for chemical processes on "cell-like" objects like dust grains and PAHs (Caselli et al., 1998; Herbst and Shematovich, 2003; Lipshtat and Biham, 2003; Stantcheva and Herbst, 2004; Tielens and Hagen, 1982). The concept of mass-action kinetics, which lies behind rate equations, being adequate for gas-phase reactions, is not appropriate in the case of

3. A UNIFIED MONTE CARLO TREATMENT OF GAS-GRAIN CHEMISTRY FOR LARGE REACTION NETWORKS: MOLECULAR CLOUDS

small surface population (number of particles ≤ 1 per grain). This situation is often the case in grain surface catalysis. Rates of surface reactions obtained through this approach may be strongly incorrect, leading to an improper estimation of timescales of fundamental processes, like H_2 formation, and significant errors in abundances of other species.

Up to now, a number of attempts have been made to assess the significance of stochastic effects for astrochemical simulations and to develop suitable numerical methods. In the context of astrochemistry first attempt to treat grain surface chemistry stochastically has been made by Tielens and Hagen (1982). In this study, equilibrium abundances of gas-phase species were used to obtain accretion rates and to calculate time-dependent populations of surface species through Monte Carlo approach. All surface species but H_2 were assumed to remain on the grain surfaces.

Subsequent attempts to account for the discrete nature of surface reactions can be divided into two categories. The first category encompasses different modifications to the rate equations for grain surface chemistry (Caselli et al., 2002, 1998; Stantcheva et al., 2001). The main idea behind these modifications is to restrict rates of diffusive surface reactions by accretion or desorption rates of reactants. Thus, the so–called accretion-limited regime is taken into account, when the rate of a particular surface reaction is determined by the flux of reactants accreting on a grain and not by their diffusion over the surface. For simple reacting systems, results obtained with this semi-empirical approach were found, at least, to be in closer agreement with Monte Carlo (MC) computations than the treatment by rate equations alone. However, the applicability of the modified rate equations (MRE) to large chemical networks has not been tested so far. Moreover, it is impossible to investigate purely stochastic effects, like bistability, with this technique, still purely deterministic in its nature (Boger and Sternberg, 2006; Le Bourlot et al., 1993; Lee et al., 1998; Shalabiea and Greenberg, 1995).

In the second category of studies the master equation is solved with different methods. Because the chemical master equation describes probabilities of a chemically reacting system to be in all possible states of its phase space and the number of these states grows exponentially with the number of species, their direct integration is only possible for extremely simple systems, consisting of a very few different components. Biham et al. (2001), Green et al. (2001) and Lipshtat et al. (2004) have performed a direct

integration of the master equation to investigate H_2 formation. These studies demonstrated that in some cases this fundamental process cannot be adequately described with the rate equation approach. In Stantcheva et al. (2002), Caselli et al. (2002) and Stantcheva and Herbst (2003) direct integration of the master equation was applied to study the evolution of a simple H—O—CO surface chemical network and deuterium fractionation. Direct integration of the master equation in more complex networks of grain surface reactions is hampered by the lack of appropriate computing power. To the best of our knowledge, the only successful simulation of a more extended surface chemical network in astrochemistry, consisting of 19 reactions, with direct integration of the master equation was accomplished by Stantcheva and Herbst (2004).

A Monte Carlo approach based on continuous-time random-walk method has been developed by Chang et al. (2005) to model recombination of hydrogen atoms on interstellar grains. The advantage of this method is that it allows to model formation of H_2 and other molecules on surfaces of arbitrary roughness, which has later been demonstrated by Cuppen and Herbst (2007).

To relax computational requirements needed to solve the master equation, the moment equation approximation was suggested by Lipshtat and Biham (2003) and Barzel and Biham (2007). Currently, this is the most promising approach to efficient simulations of gas-grain systems with complex grain surface chemistry, because the moment equations can be easily combined with rate equations used to simulate gas-phase chemical processes. But, strictly speaking, the moment equations are an approximation and their validity should be verified by a comparison with exact methods.

The only feasible technique allowing us to obtain an exact solution to the master equation for complex chemically reacting systems is Monte Carlo method developed by Gillespie (1976). This approach is widely used in molecular biology for simulation of chemical processes in living cells and can also be applied to astrochemical problems. Gillespie's Stochastic Simulation Algorithm (SSA) was first used in complex astrochemical networks by Charnley (1998), where SSA was applied to gas-phase chemistry only. Later a simple grain surface H—O—CO chemical model, similar to the one considered in Caselli et al. (1998), was developed by Charnley (2001). In this model, gas-phase abundances of species were assumed to be constant and desorption was neglected. No coupled gas-grain chemical model was studied.

3. A UNIFIED MONTE CARLO TREATMENT OF GAS-GRAIN CHEMISTRY FOR LARGE REACTION NETWORKS: MOLECULAR CLOUDS

The chemical master equation is usually considered as a method to model surface reactions. However, due to its universality, it can be used to model the gas-phase chemistry as well. The reason why the rate equations are so popular as a tool to study gas-phase chemistry in astronomical environments is the fact that they are easier to implement and much more computationally effective. However, if one uses the rate equations to model gas-phase chemistry and some stochastic approach to model surface chemistry one has to find a way to match the two very different computational techniques. The first study in which a Monte Carlo treatment of grain surface chemistry was coupled to time-dependent gas-phase chemistry is Chang et al. (2007). In this chapter iterative technique is utilized to combine very different Monte Carlo and rate equations approaches. Calculations are performed for the time interval of $2 \cdot 10^5$ years and a relatively simple H—O—CO surface network consisting of 12 reactions is used.

Even though remarkable progress has been made to develop stochastic approaches to astrochemistry, up to now there are no studies in which a stochastic treatment of a complex grain surface chemical network is fully coupled to time-dependent gas-phase chemistry. The situation gets less complicated when the same method is used for both gas-phase and surface chemistry. In this chapter, for the first time, we present a "complete" time-dependent chemical gas-grain model, calculated with Monte Carlo approach. We solve the master equation with a Monte Carlo technique, using it as a single method to treat gas-phase reactions, surface reactions, and gas-grain exchange processes simultaneously. The gas-phase chemical network includes more than 6000 reactions while surface network consists of more than 200 reactions.This Monte Carlo model is used to test the validity of rate equations and modified rate equations for a range of physical conditions, typical of diffuse and dense clouds. So far, no comparison of RE and MRE techniques against rigorous stochastic approach over a wide range of physical conditions, typical for astrophysical objects, has been made.

There is clear observational evidence that interstellar grains have complex mineral composition and may have either amorphous or crystalline structure. In general, it is believed that interstellar dust particles are made of olivine-like silicates and some form of amorphous carbon or even graphite (Draine and Lee, 1984a). The location on a surface which may be occupied by an accreted molecule is commonly referred to as a surface site. The density of sites and binding energies for specific species strongly depend on the dust material and its structure. Binding energies E_b, that is, potential

barriers between adjacent sites, have been assumed by Hasegawa et al. (1992) to be roughly 0.3 of corresponding desorption energies E_D. In Pirronello et al. (1997a, 1999, 1997b), Katz et al. (1999) and Perets et al. (2005) experimental results on the H_2 formation, the ratio of diffusion energy to desorption energy, E_b/E_D, was found to be close to 0.77 for H atoms. This ratio determines the surface mobility of species and is of utter importance for estimating surface reaction rates.

Another factor defining rates of reactions involving H and H_2 (and their isotopologues) is related to the possibility of their tunneling. Non-thermal quantum tunneling of these species allows them to scan grain surface and find a reacting partner quickly. This mechanism has been suggested as an explanation of efficient H_2 formation in the ISM. Later analysis of the cited experimental results has lead Katz et al. (1999) to the conclusion that tunneling does not happen. The absence of tunneling implies lower mobility, so that surface processes are essentially reduced to accretion and desorption. However, this conclusion turned out to be not the final one. In other studies (e.g. Cazaux and Tielens, 2004) alternative explanations of these experiments have been proposed and some shortcomings of the theoretical analysis performed in Katz et al. (1999) have been found. So, up to now the question of presence or absence of tunneling effects on grain surfaces is not settled, and the E_b/E_D ratio is not well constrained. With this in mind, two different models of grain surface reactions are considered: (1) the surface mobility of all species is caused by thermal hopping only with high E_b/E_D ratio equal to 0.77, (2) temperature-independent quantum tunneling for H and H_2 is included in addition to thermal hopping with low E_b/E_D ratio equal to 0.3.

The organization of the chapter is as follows. In Section 2 we describe physical conditions adopted in simulations and chemical model used. Section 3 contains basics of stochastic reaction kinetics and detailed description of the Monte Carlo code used for simulations. In Section 4 the validity of rate equations and modified rate equations is checked against Monte Carlo method. First, global agreement between methods is investigated. Then, some interesting species are discussed separately. In Section 5 a discussion is presented. Section 6 contains the conclusions.

3.2 Modeling

3.2.1 Physical conditions

In the present study, we consider grain surface reactions under physical conditions typical of irradiated translucent clouds, cold dark cores and infrared dark clouds. We consider temperatures T between 10 and 50 K, densities $n(\mathrm{H})$ between 200 and $2 \cdot 10^4$ cm^{-3} (three values of $n(\mathrm{H})$ and five values of T), and visual extinctions of 0.2 mag at $n(\mathrm{H}) = 200$ cm^{-3}, 2.0 mag at $n(\mathrm{H}) = 2 \cdot 10^3$ cm^{-3} and 15 mag at $n(\mathrm{H}) = 2 \cdot 10^4$ cm^{-3} (e.g., Hassel et al., 2008; Snow and McCall, 2006). This A_v roughly corresponds to the distance of order of 0.4–0.5 pc from the cloud boundary (at constant density). The cloud is illuminated by the mean interstellar diffuse UV field. The dust temperature is assumed to be equal to gas temperature. We do not study the earliest stage of the molecular cloud evolution, which is essentially the stage when atomic hydrogen is converted into hydrogen molecules. The chemical evolution is simulated assuming static physical conditions. While it is still a matter of debate how long does it take for a typical isolated cloud core to become gravitationally unstable and to start collapsing, we assume a short timescale of 1 Myr which seems to be appropriate for the TMC1 cloud (see e.g. Roberts et al., 2004; Semenov et al., 2004).

3.2.2 Chemical model

The chemical model is the same as described in Vasyunin et al. (2008). The gas-phase reactions and their rates are taken from the RATE 06 database, in which the effects of dipole-enhanced ion-neutral rates are taken into account (Woodall et al., 2007). All reactions with large negative activation barriers are excluded. The rates of photodissociation and photoionization of molecular species by interstellar UV photons are taken from van Dishoeck et al. (2006b). The self- and mutual shielding of CO and H$_2$ against UV photodissociation are computed as described in van Zadelhoff et al. (2003b) using pre-calculated factors from Tables 10 and 11 from Lee et al. (1996). Ionization and dissociation by cosmic ray particles are also considered, with a cosmic-ray ionization rate of $1.3 \cdot 10^{-17}$ s^{-1} (Spitzer and Tomasko, 1968).

The gas-grain interactions include accretion of neutral species onto dust grains, thermal and photodesorption of mantle materials, dissociative recombination of ions on charged grains and grain re-charging processes. The dust grains are uniform $0.1 \, \mu$m

spherical particles made of amorphous silicates of olivine stoichiometry (Semenov et al., 2003), with a dust-to-gas mass ratio of 1%. The sticking probability is 100%. Desorption energies E_D and surface reaction list are taken from Garrod and Herbst (2006).

The grain surface is assumed to be compact, with surface density of $2 \cdot 10^{14}$ sites cm^{-2}, which gives $\approx 3 \cdot 10^5$ sites per grain (Biham et al., 2001). We employ two models to calculate the rates of surface reactions (Table 3.1). In Model T (T for tunneling) the tunneling timescale for a light atom to overcome the potential barrier and migrate to another potential well is computed using Eq. (10) from Hasegawa et al. (1992), with the barrier thickness of 1Å. In Model H (H for hopping) we do not allow H and H$_2$ to scan surface sites by tunneling. The diffusion timescale for a molecule is calculated as the timescale of thermal hopping multiplied by the total number of surface site and is given by Eq. (2) and Eq. (4) from Hasegawa et al. (1992). The hopping rates are sensitive to the adopted values of diffusion energy, which are not well constrained. Thus, we consider low and high diffusion energies which are calculated from adopted desorption energies by multiplying them by factors of 0.3 (like in Hasegawa et al., 1992) (Model T) and 0.77 (Katz et al., 1999) (Model H), respectively. For all considered models, the total rate of a surface reaction is calculated as a sum of diffusion or tunneling rates divided by the grain number density and multiplied by the probability of reactions (100% for processes without activation energy).

Overall, our network consists of 422 gas-phase and 157 surface species made of 13 elements, and 6002 reactions including 216 surface reactions. As initial abundances, we utilize the "low metallicity" set of Lee et al. (1998), where abundances of heavy elements in the gas are assumed to be severely depleted. All hydrogen is molecular initially. The chemical evolution for 1 Myr in the classical deterministic approaches is computed with the fast "ALCHEMIC" code[1] in which the modified rate equations are implemented according to Caselli et al. (1998). No further modification for reactions with activation energy barriers is used (see Caselli et al., 2002).

---

[1]Available upon request: semenov@mpia.de

3. A UNIFIED MONTE CARLO TREATMENT OF GAS-GRAIN CHEMISTRY FOR LARGE REACTION NETWORKS: MOLECULAR CLOUDS

Table 3.1 Adopted surface chemistry models

Model	Based on	Tunneling	$E_{\mathrm{b}}/E_{\mathrm{D}}$
T	Hasegawa et al. (1992)	Yes	0.3
H	Katz et al. (1999)	No	0.77

3.3 Stochastic reaction kinetics

3.3.1 Theoretical foundations

We consider a chemically reacting system which consists of N different types of species $\{S_1 \ldots S_N\}$ and M chemical reactions $\{R_1 \ldots R_M\}$ (Gillespie, 1976). All these species are contained in a constant volume Ω, in which local thermal equilibrium is reached, so that the system is well mixed. We denote the number of species of type i at time t as $X_i(t)$. The ultimate goal is to determine the state vector $\vec{X}(t) = \{X_1(t)...X_N(t)\}$ of the system at any given time $t > t_0$, assuming certain initial conditions $\vec{X}(t_0) = \vec{X}_0$.

Let us assume that each reaction R_j retains properties of a Markov chain and can be considered as a set of independent instantaneous events. Each chemical reaction is described by two quantities, the discrete state vector $\vec{\nu} = \{\nu_{1j}, ..., \nu_{Nj}\}$ and the propensity function a_j. The components of the state vector ν_{ij} represent the net change in populations of the ith species due to the jth reaction. By definition, the propensity function

$$a_j(\vec{X})dt \tag{3.1}$$

is the probability for a reaction R_j to occur in the volume Ω over the time interval dt. In analogy to the reaction rate in the rate equation approach, for a one-body reaction the propensity function a_j can be expressed through rate constants and numbers of reactants as

$$a_j(\vec{X}) = c_j x_1. \tag{3.2}$$

Here, c_j is the rate constant of the jth reaction and x_1 is the absolute population of reagent. For a two-body heterogeneous reaction this expression changes as follows:

$$a_j(\vec{X}) = c_j x_1 x_2, \tag{3.3}$$

where c_j is the reaction rate constant, x_1 and x_2 are the abundances of first and second reactants. If we deal with a two-body homogeneous reaction (like H + H → H_2), the

expression for its propensity function becomes somewhat more complicated:

$$a_j(\vec{X}) = \frac{c_j}{2}x_1(x_1 - 1) \tag{3.4}$$

This expression reflects the fact that the rate of a homogeneous two-body reaction is proportional to the number of all possible pairs of its reactants. The term $(x_1 - 1)$ is important for a proper calculation of the reaction rate in the stochastic regime when the average reagent population is close to unity and cannot be properly reproduced by the rate equation approach. Note that the abundances of species are always integer numbers in these expressions.

These definitions allow to characterize the microphysical nature of chemical processes and to establish a basis for stochastic chemical kinetics. A vector equation that describes the temporal evolution of a chemically reacting system by stochastic chemical kinetics is the chemical master equation. To derive this equation one has to introduce the probability of a system to be in the state $\vec{X}(t)$ at a time $t > t_0$:

$$P(\vec{X}, t \mid \vec{X}_0, t_0) \equiv Prob(\vec{X}(t) = \vec{X} \mid \vec{X}(t_0) = \vec{X}_0). \tag{3.5}$$

Here $P(\vec{X}, t \mid \vec{X}_0, t_0)$ is the conditional probability density function of the time-dependent value $\vec{X}$. Temporal changes of $\vec{X}$ are caused by chemical reactions with rates defined by Eq. (3.1). Therefore, the change of $P(\vec{X}, t \mid \vec{X}_0, t_0)$ over the time interval dt is the sum of probabilities of all possible transitions from the state $\vec{X}_0$ to the state $\vec{X}(t)$:

$$P\left(\vec{X}, t + dt \mid \vec{X}_0, t_0\right) =$$

$$P\left(\vec{X}, t \mid \vec{X}_0, t_0\right) \cdot \left[1 - \sum_{j=1}^{M}\left(a_j(\vec{X})dt\right)\right] +$$

$$\sum_{j=1}^{M} P(\vec{X} - \vec{\nu_j}, t \mid \vec{X}_0, t_0) \cdot \left(a_j(\vec{X} - \vec{\nu_j})dt\right)$$

The first term in this equation is derived from the fact that the system is already in the state $\vec{X}$ and describes the probability for the system to leave the state during the time interval dt. The second term defines the total probability for the system to reach the state $\vec{X}$ from states $\vec{X} - \vec{\nu_j}$ during the time interval dt due to a reaction R_j. Finally, we formulate the chemical master equation:

$$\frac{\partial P(\vec{X}, t \mid \vec{X}_0, t_0)}{\partial t} = \sum_{j=1}^{M}[a_j(\vec{X} - \vec{\nu_j})P(\vec{X} - \vec{\nu_j}, t \mid \vec{X}_0, t_0) - a_j(\vec{X})P(\vec{X}, t \mid \vec{X}_0, t_0)] \tag{3.6}$$

This vector equation looks similar to the conventional set of balance equations. However, it properly takes into account the discrete nature of chemical processes and, thus, has a much wider range of applicability. Unfortunately, an analytic integration of the chemical master equation is only possible in a very limited number of cases (several species and reactions, see e.g. Stantcheva and Herbst, 2004). Thus, one has to rely on various numerical techniques to solve this equation.

3.3.2 Implementation of the Monte Carlo algorithm

In principle, any normalization of abundances can be used in Eq. (3.6). In particular, if we take Ω to be a unit volume, we end up with the usual number densities, which are widely used in astrochemical models. When dealing with mixed gas-dust chemistry, one has to be more careful with the normalization. As surface reactions can only proceed when both reactants reside on a surface of the same grain, we define Ω as the volume of the interstellar medium that contains exactly one dust grain,

$$\Omega_{\mathrm{MC}} = \frac{\frac{4}{3}\pi\rho_{\mathrm{dust}}r^3}{\rho_{\mathrm{gas}}\gamma},\tag{3.7}$$

where r is the grain radius, ρ_{dust} is the mass density of grain material, ρ_{gas} is the mass gas density, and γ is the dust-to-gas (0.01) mass ratio. Here grains are assumed to be spheres of equal size. As we also assume that the interstellar medium is well-mixed, so that the volume Ω_{MC} is representative for any volume of the real interstellar medium with the same physical conditions.

This setup allows to construct the unified master equation for all three kinds of processes listed above (gas phase reactions, accretion/desorption processes and grain surface reactions). This equation is solved with the stochastic Monte Carlo algorithm described in Gillespie (1976). We implemented this technique in a FORTRAN77 code which allows to simulate all chemical reactions in the network in a self-consistent manner. Such a "brute-force" approach requires substantial CPU power and cannot be utilized in massive calculations. In the present study, it is used as a benchmark method to simulate chemical evolution in astrophysical objects. A typical run on a single Xeon 3.0GHz CPU takes between 10 hours and several days of computational time, and involves several billions of time steps. If one is only interested in a single point then the

model can be used not only for benchmarking, but also for practical purposes. Unfortunately, it becomes impractical if abundances are computed for a number of spatial locations. High density also slows down the computation significantly.
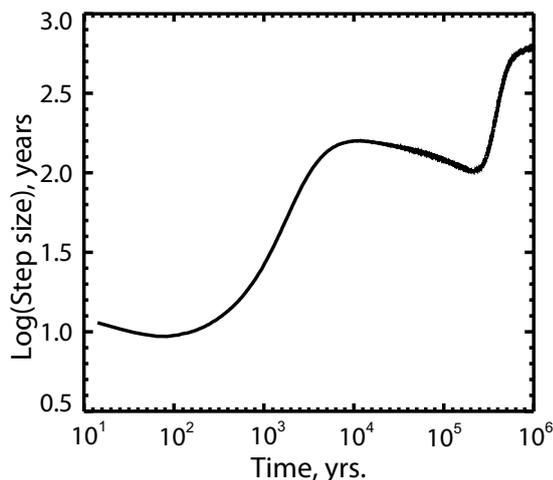
Figure 3.1 The Monte Carlo time step as a function of time in the model of the chemical evolution of a dense cloud.

Due to the fact than the Monte Carlo technique operates with integers, the smallest non-zero abundance of a molecule is 1. Given the dust properties in our model (radius $r = 10^{-5}$ cm, density $\rho_{\mathrm{dust}} = 3 \ \mathrm{g \ cm^{-3}}$), a dust-to-gas ratio of $1/100$ means that volume per one grain is about $10^{12}/n(\mathrm{H}) \ \mathrm{cm^3}$, where $n(\mathrm{H})$ is the number density of hydrogen nuclei. Therefore, an absolute population of 1 corresponds to a relative abundance of 10^{-12} with respect to the total number of hydrogen atoms (see Eq. 3.7). This is the lowest abundance directly resolvable in our model. However, the huge amount of tiny time steps taken during the calculations allows to average stochastic abundances over wider time spans of 10–1 000 years and push the smallest abundance resolvable by the Monte Carlo code below 10^{-12}:

$$\overline{X} = \frac{\sum_{i=1}^{N} X_i \Delta t_i}{\sum_{i=1}^{N} \Delta t_i} \tag{3.8}$$

where X_i is the abundance of species after the ith time step, the Δt_i is the time step in seconds and N is the amount of time steps over which the averaging is performed. In such an averaging procedure, the noise in the random variable X_i decreases with N as $\sqrt{N}$ and enables us to resolve abundances below 10^{-12}. In our simulations we averaged

abundances over 10^6 time steps. Therefore, the resolution of our calculations is about $10^{-15} - 10^{-16}$ cm^{-3}. The average value of the Monte Carlo time step in Gillespie's algorithm is equal to an inverse sum of rates of all chemical reactions in the model. For example, in the dense cloud model many molecules form rapidly at initial times and less actively toward the end of evolution (Fig. 3.1). Time intervals, corresponding to 10^6 time steps in a medium with density 10^4 cm^{-3} vary from 10 to $7 \cdot 10^2$ years for early and late time moments, correspondingly.

3.4 Comparison of the Monte Carlo method with rate equations

While the Monte Carlo (MC) technique seems to be the most adequate method to solve the chemical master equation, it is computationally extremely demanding. Rate equations (RE) do not account for the stochastic nature of surface processes and thus may produce spurious results in some circumstances. On the other hand, they do require much less computer power and are easier to handle. Therefore rate equations will remain an important tool in theoretical astrochemistry.

Given the importance of surface processes, it is thus necessary to isolate regions in the parameter space where rate equations should not be used at all or, at least, should be used with caution. Similar comparisons, having been made so far, are based on a very limited number of species and reactions (e.g. Barzel and Biham, 2007; Caselli et al., 2002; Chang et al., 2007; Charnley, 1998, 2001; Green et al., 2001; Lipshtat and Biham, 2003; Ruffle and Herbst, 2000; Stantcheva and Herbst, 2003, 2004; Stantcheva et al., 2002). As we implemented a unified Monte Carlo approach to the gas-phase and surface chemistry, which is capable to treat a "regular size" chemical network, we are able to perform a comprehensive comparison between predictions of the MC and the (M)RE approaches.

For both the Model T and the Model H, the rate equations (RE), the modified rate approach (MRE) (for surface chemistry) and the Monte Carlo method are used to simulate gas-phase and surface chemistry. The differences in abundances discussed are related to surface chemistry and/or dust-gas interactions. For the gas-phase chemistry, all models produce identical results. Each run represents a combination of the tunneling

treatment (T or H) and the surface chemistry treatment (RE, MRE, or MC). In total, we considered six models denoted as T-RE, T-MRE, etc.

3.4.1 Global Agreement

To perform an overall comparison, in Figures 3.2 and 3.3 we show diagrams of global agreement between MC, RE, and MRE calculations as a function of n and T for evolutionary times 10^4, 10^5, and 10^6 years. For a given species, the two methods, being compared, are assumed to agree at time t if they produce abundances, that differ by no more than an order of magnitude. As we have mentioned above, in the MC method we are able to resolve abundances down to 10^{-15}, which would lead to a formal disagreement between abundances, say, 10^{-15} in the MC method and 10^{-16} (or smaller) in the RE method (all abundances are relative to the total number of H atoms). This kind of disagreement is not meaningful from the observational point of view because such small relative abundances are extremely difficult to observe with a satisfactory accuracy. In addition, even though lower abundances can be calculated by the RE method, their actual accuracy is limited by the numerical interpolation. In the following discussion, species, for which both methods predict relative abundances less than 10^{-12}, are excluded from further consideration. In Figures 3.2 and 3.3, contours labeled with 0.9 mean that the two methods give abundances that differ by less than an order of magnitude for 90% of species with abundances higher than 10^{-12} in both methods.

An order-of-magnitude agreement criterion may seem to be too coarse. However, when stochastic effects do not play an important role, all three method produce results, which are nearly identical. To illustrate this, we show in Figure 3.4 the evolution of the H_2CCCC abundance at $n = 2 \cdot 10^4$ cm^{-3} and $T = 10$ K, simulated with the MC and RE methods. The species is chosen because its abundance strongly varies with time. It can be seen that the difference between the two methods is very small.

3.4.1.1 Model T

In Model T the species are highly mobile—atomic and molecular hydrogen because of tunneling, and all the other species because of the low energy barrier for diffusion. Mobility drives rapid surface reactions with rates which sometimes exceed the accretion/desorption rate. Surface reactions, which are on average faster than accretion, are not permitted in the MC approach when surface populations of their reagents are low

3. A UNIFIED MONTE CARLO TREATMENT OF GAS-GRAIN CHEMISTRY FOR LARGE REACTION NETWORKS: MOLECULAR CLOUDS
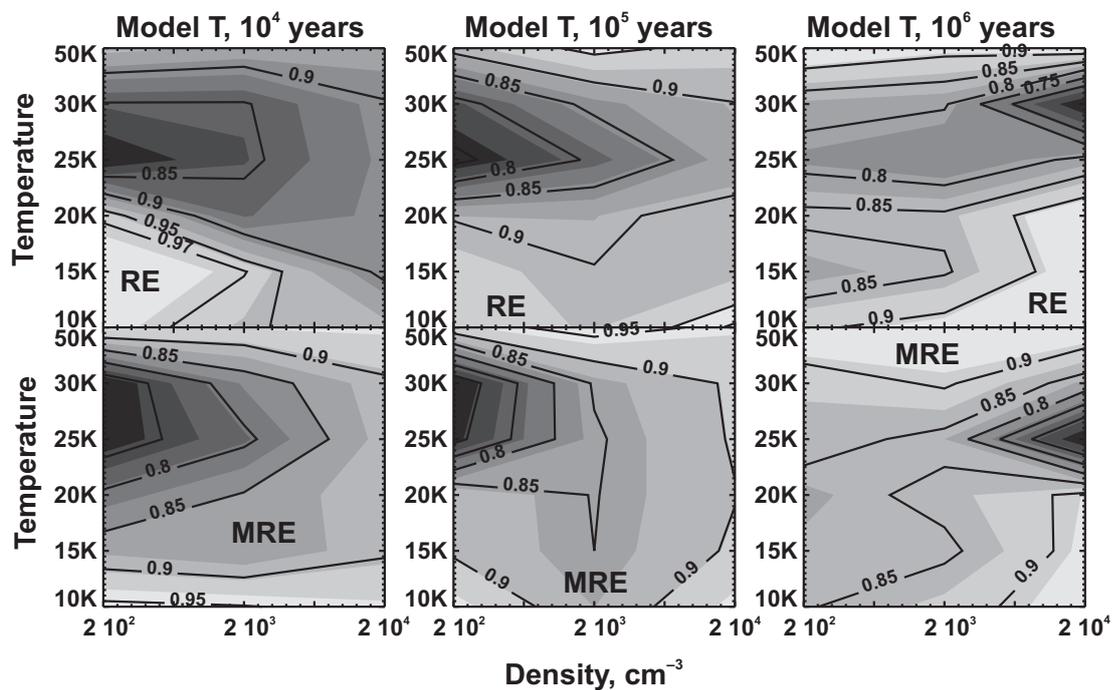
Figure 3.2 Global agreement diagrams for Model T at three time moments. Percentage of species is shown in contour labels, for which abundances computed with the rate equations and with the Monte Carlo method differ by no more than an order of magnitude. Grayscale map with arbitrary contours is added for clarity. Darker color corresponds to worse agreement. Results are presented for conventional rate equations (top row) and for modified rate equations (bottom row).
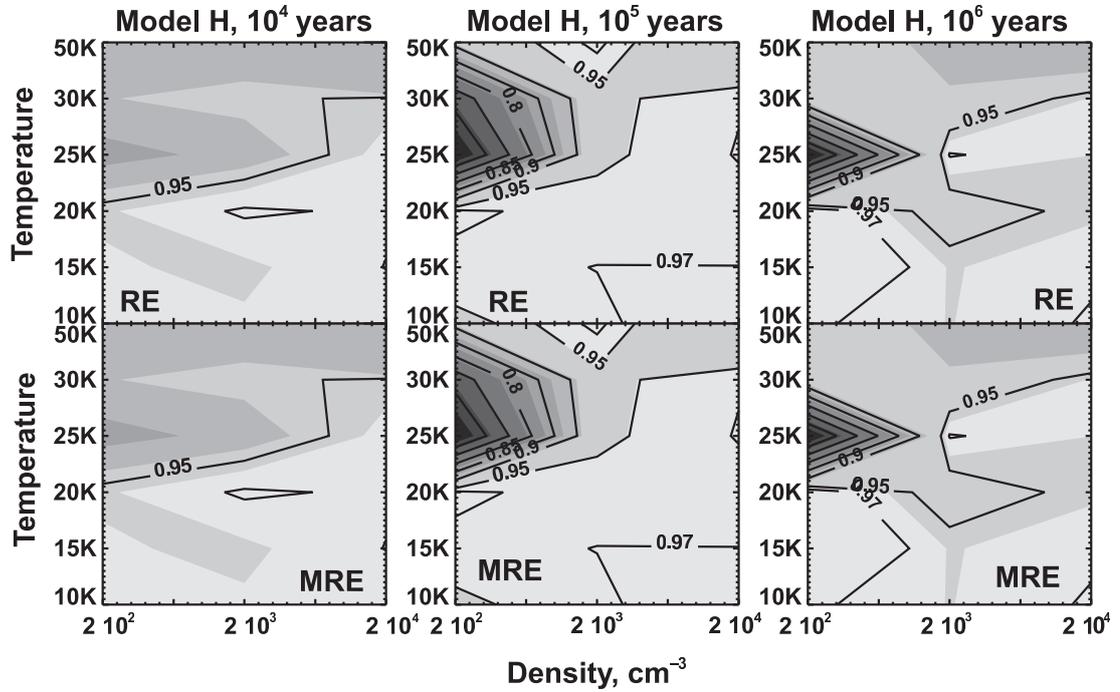
Figure 3.3 Same as in Figure 3.2, but for Model H.
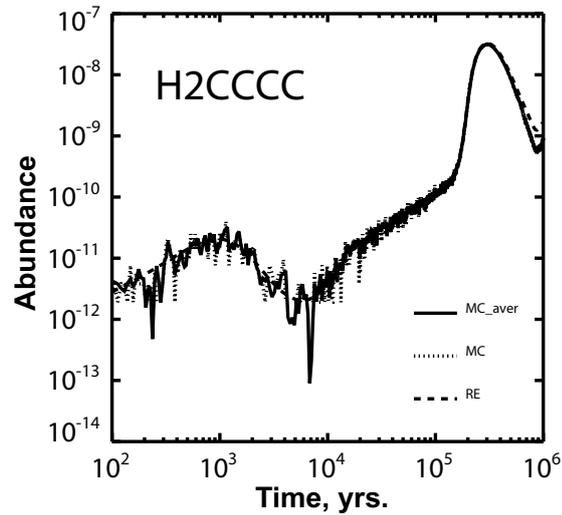
Figure 3.4 Evolution of H$_2$CCCC gas-phase abundance at $n = 2 \cdot 10^4$ cm^{-3} and $T = 10$ K, simulated with the MC and RE methods (Model T). Dotted line indicates raw MC results, solid line shows MC results after averaging. Results of RE integration are shown with dashed line.

3. A UNIFIED MONTE CARLO TREATMENT OF GAS-GRAIN CHEMISTRY FOR LARGE REACTION NETWORKS: MOLECULAR CLOUDS

(~ 1), but they are allowed in the RE approach, where the surface abundance of a species can be much less than one. Because of that, differences between Monte Carlo and rate equation methods are quite noticeable in Model T.

At temperatures below $20\,K$ and above $\sim 40\,K$ the agreement between the stochastic method and the rate equation method (both RE and MRE) is about 85% or better at all times and densities (Figure 3.2). Around $T \sim 10\,K$ the residual discrepancy is mainly caused by complex surface species, which have zero abundances in Model T-MC and are overproduced in Model T-RE and Model T-MRE, so that their abundances are just above the adopted cutoff of 10^{-12}. If we would raise the cutoff to 10^{-11}, the agreement would be almost 100%. At $T \sim 50\,K$ the agreement is also nearly perfect, as the chemistry is almost a purely gas-phase chemistry under these conditions (dust temperature being equal to gas temperature).

All the major discrepancies are concentrated in the temperature range between 25–30 K. In this range the accretion rate (which depends on gas temperature) is high enough to allow accumulation and some processing of surface species, while the correspondingly high desorption rate (which depends on dust temperature and $A_{\rm V}$) precludes surface production of complex molecules. The latter process is adequately described in the MC runs only.

At earlier times ($t \leq 10^5$ years) the largest differences in this temperature range are observed at lower densities. They are caused by an overproduction of 'terminal' surface species, like water, ammonia, hydrogen peroxide, carbon dioxide, etc., in the RE and MRE calculations. At later times ($t \sim 10^6$ years) situation changes drastically. The discrepancies shift toward higher density, and the overall agreement falls off to about 60% for both RE and MRE calculations. Even though the stochastic chemistry is only important on dust surfaces, by this time it also influences many gas-phase abundances due to effective gas-grain interactions.

At $t = 10^6$ years, in the RE calculation at $T = 30\,K$, among 234 species with abundances higher than 10^{-12}, 95 species (including 81 gas-phase species) have an order of magnitude disagreement with the MC run. In the MRE run at $T = 25\,K$, the number of species with abundances above 10^{-12} is 221. Among them 83 species disagree with the MC results by more than an order of magnitude. In both calculations these are mostly carbon-bearing species, like CO, CO_2, CS, to name a few, and, in particular,

carbon chains (like some cyanopolyynes). It is noteworthy that not only the abundances of neutral species disagree, but also the abundances of some ions, including C^+ and S^+.

3.4.1.2 Model H

In Model H the mobility of all species on the surface (including H and H_2) is caused by thermal hopping only, which is slow because of the high E_b/E_D ratio. One of the consequences of these slow surface reaction rates is that results produced by the modified rate equations almost do not differ from results of conventional rate equations. The essence of the modification is to artificially slow down surface reactions to make their rates consistent with accretion/desorption rates. In Model H all surface reactions are slow anyway, so that modifications never occur. Thus, we only compare the results of the MC and RE calculations.

At $t = 10^4$ years the percentage agreement between the two runs never falls below 80% and most often is actually much better than the adopted order-of-magnitude criterion. At later times, the discrepancy appears in the same temperature range as in Model T, i.e., between 25 and 30 K. Unlike Model T, both at $t = 10^5$ years and $t = 10^6$ years the disagreement shows up at low density. The set of discrepant species is nearly identical at both times and consist mostly of ices, overproduced by rate equations. These ices include some key observed species. For example, NH_3, H_2O, CO_2 ices are all abundant in the Model H-RE despite the low density, with a surface H_2O abundance reaching $3 \cdot 10^{-7}$ by 10^6 years. On the other hand, the Model H-MC results in very small or zero abundances for the same species. More chemically rich ices in Model H-RE bring about enhanced gas-phase abundances for the same molecules. The only species which is *under*produced by the rate equation approach is surface C_2O.

3.4.2 Selected Species

The diagrams presented above indicate areas in the parameter space, relevant to molecular clouds, where deterministic methods fail to describe stochastic surface processes. However, a global agreement does not necessarily imply that the abundances of key species are also correctly calculated. In the following we discuss a few important gas-phase species and ices, for which an order of magnitude (or more) disagreement has been found.

3.4.2.1 Model T

Because surface reaction rates are high in this model, there are many species for which stochastic and deterministic methods give quite different results. The most abundant trace molecule, CO, is among these species. In Figure 3.5, we show agreement diagrams for Models T-RE and T-MRE (top row) and the CO abundance evolution for $n - T$ combinations corresponding to the worst agreement. Both the RE and MRE methods fail to reproduce the late CO evolution at high density and temperatures of 25–$30\,\mathrm{K}$ (where the global agreement is also worst in this model), but each in a different way. While in Model T-RE CO is underabundant by an order of magnitude, in Model T-MRE it is overabundant by the similar amount. This difference is related to the treatment of $CO \longrightarrow CO_2$ conversion on dust surfaces, where underabundance of the CO ice in Model T-RE and overabundance in Model T-MRE are observed at almost all times. At later time, these surface abundances just start to propagate to gas-phase abundances.

Overproduction of the CO_2 ice in Model T-RE also consumes carbon atoms which would otherwise be available not only for CO, but also for more complex molecules, in particular, carbon chains, starting from C_2, observed in diffuse clouds, and C_2S, used as a diagnostics in prestellar cores. In the RE and MRE calculations these molecules, like CO, show trends opposite to that of CO_2 ice: when surface CO_2 is overabundant with respect to the MC model, carbon chains are underabundant and vice versa.

When CO molecule sticks to a grain, it either desorbs back to the gas-phase, where it may participate in further processing, or is converted into CO_2. As the desorption energy is quite high for CO_2, it acts as a sink for carbon atoms at these temperatures. In the accretion-limited regime, rate equations overproduce CO_2 with respect to the MC method. Thus, we see less CO and other carbon-bearing species in the gas-phase. The MRE method helps, probably, too much to account for accretion-limited CO processing and essentially quenches surface $CO \longrightarrow CO_2$ conversion. It is worth noting that at high density in this particular temperature range (and for adopted CO desorption energy) CO balances between complete freeze-out (at $T < 20\,\mathrm{K}$) and near absence on dust surface (at $T > 30\,\mathrm{K}$). Thus, even relatively minor changes in treatment may lead to noticeable consequences.

Another carbon-bearing molecule that shows an interesting behavior is methanol in the gas phase. Diagrams, comparing its abundance computed with the MC approach
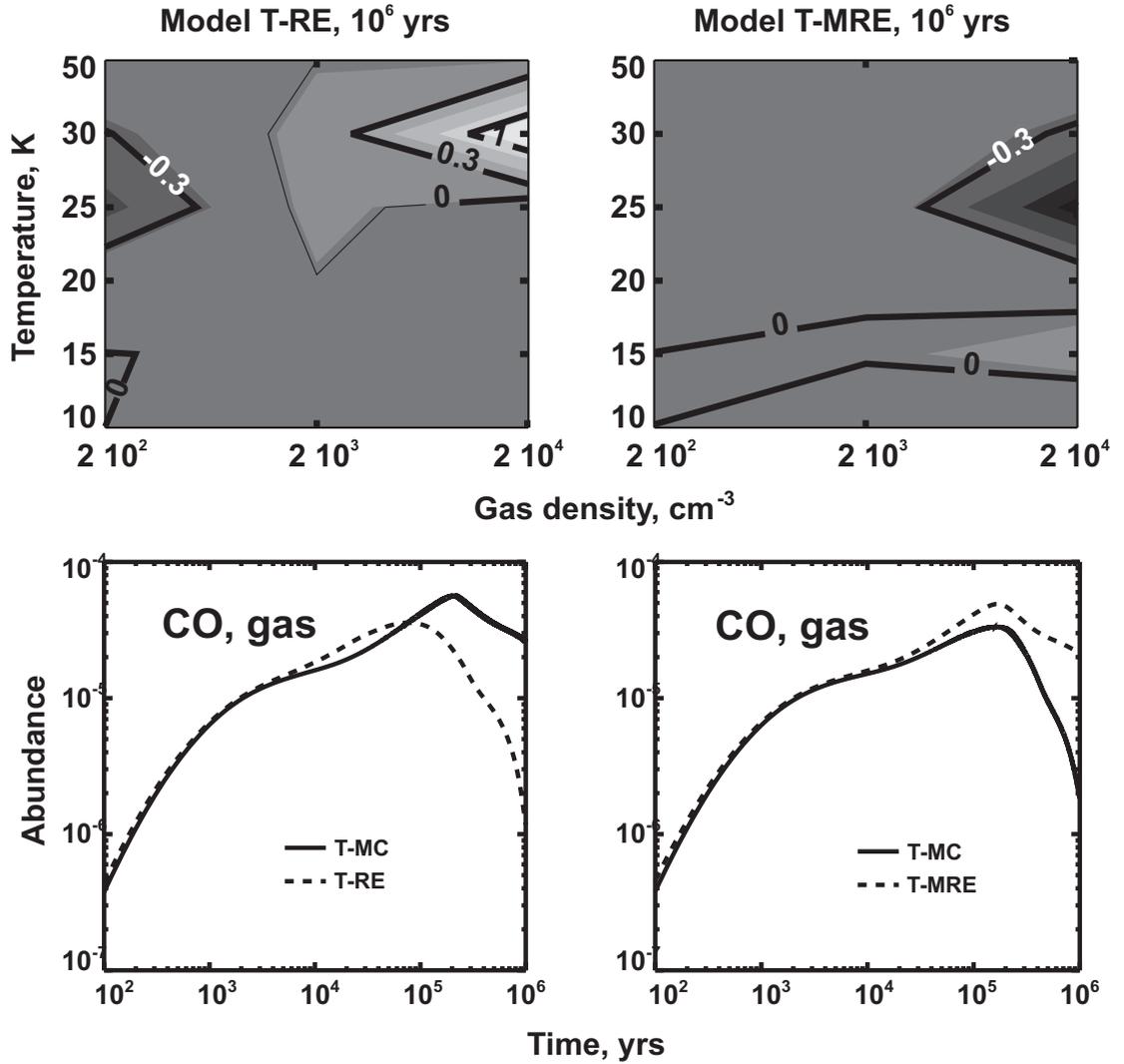
Figure 3.5 (Top row) Agreement diagrams for CO in Model T. Contour labels correspond to the logarithm of the ratio of gas-phase CO abundance in the MC run to that in the RE (top left) and MRE (top right) runs. (Bottom row) Gas-phase CO abundance evolution in the RE run ($n = 2 \cdot 10^4$ cm^{-3} and $T = 30$ K; bottom left) and in the MRE run ($n = 2 \cdot 10^4$ cm^{-3} and $T = 25$ K; bottom right).
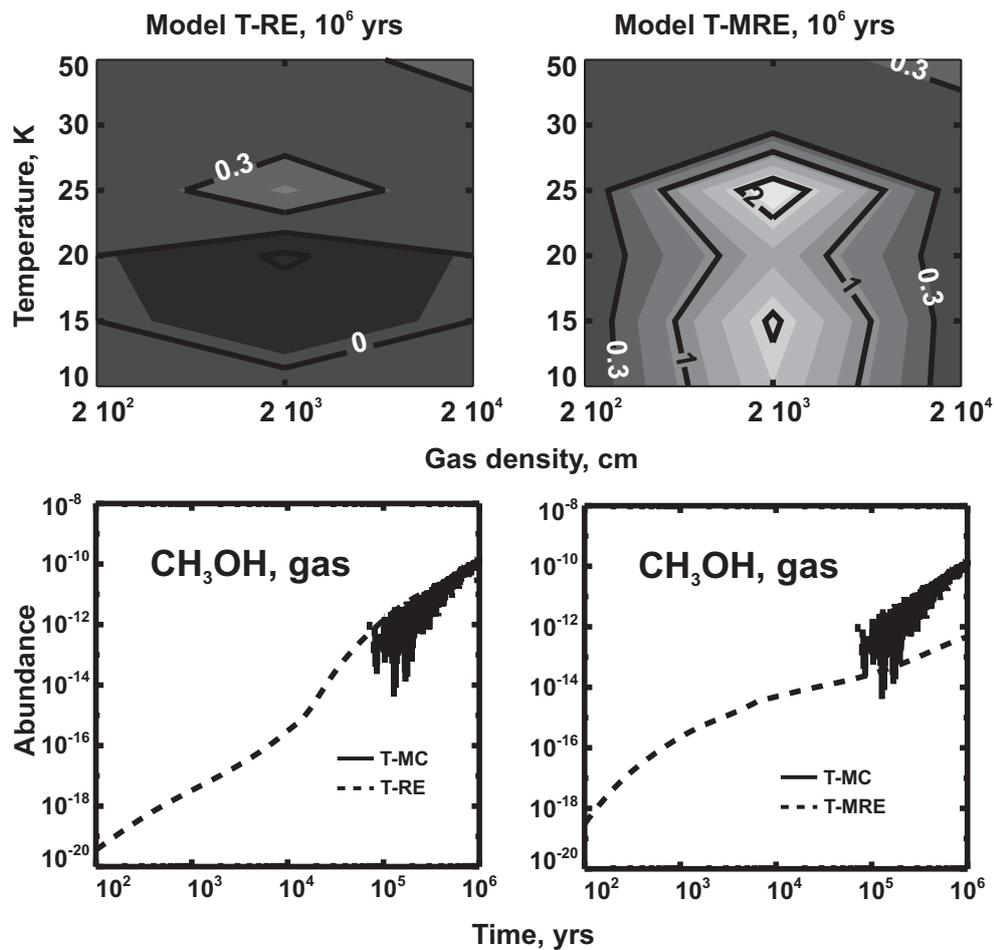
Figure 3.6 (Top row) Agreement diagrams for methanol. Contour labels correspond to the logarithm of the ratio of gas-phase CH_3OH abundance in the MC run to that in the RE (top left) and MRE (top right) runs. (Bottom row) Gas-phase methanol abundance evolution in the RE run ($n = 2 \cdot 10^3$ cm^{-3} and $T = 25$ K; bottom left) and in the MRE run ($n = 2 \cdot 10^3$ cm^{-3} and $T = 25$ K; bottom right).

and with the rate equations, are presented in Figure 3.6. The agreement between results of the MC calculations and the RE calculations is almost perfect, at least, within the scatter produced by the MC simulations. However, the modified rate equations, which tend to improve agreement between stochastic and deterministic methods for many other species, in this particular case underpredict methanol abundance by more than two orders of magnitude in comparison with the MC run. The same is true for surface methanol as well. It is interesting to note that the region in the parameter space, where MC and MRE methanol abundances disagree, extends down to lowest temperatures considered.

An interesting pattern is presented by the abundance of water, ammonia and their ices (Figure 3.7). These species are severely overproduced by the RE methods at $t = 10^5$ years, but after this time the modified rate equations are able to restore the agreement with the MC method, so that by 10^6 years difference between MC and MRE runs is not significant. This is an example of a situation where the MRE help to produce realistic results, at least, at later times. We show plots only for gas-phase abundances because these are what is really observed. However, these abundances are only a reflection of surface processes, and surface water and ammonia abundances behave in exactly the same way. It is hard to name a single reaction which is responsible for the difference between results of RE and MRE methods in this case. Let's consider water as its chemistry is somewhat simpler. The primary formation reaction for water is H + OH, with only a minor contribution from H_2O_2 (see below). However, hydroxyl is not produced in H + O reaction, as one might have expected. Because of the paucity of H atoms on the grain surface, hydroxyl formation is dominated by reaction

$$O + HNO \longrightarrow NO + OH.$$

Abundance of HNO is restored in reaction

$$H + NO \longrightarrow HNO.$$

These two reactions form a semi-closed loop for which the sole result is OH synthesis out of an H atom and an O atom. Evolution of surface O abundance seems to be the key to the difference between the RE and MRE models. In the RE model the number of O atoms on a surface is determined by the balance between their accretion from the gas phase and consumption in O + HNO reaction. The same processes define O abundance
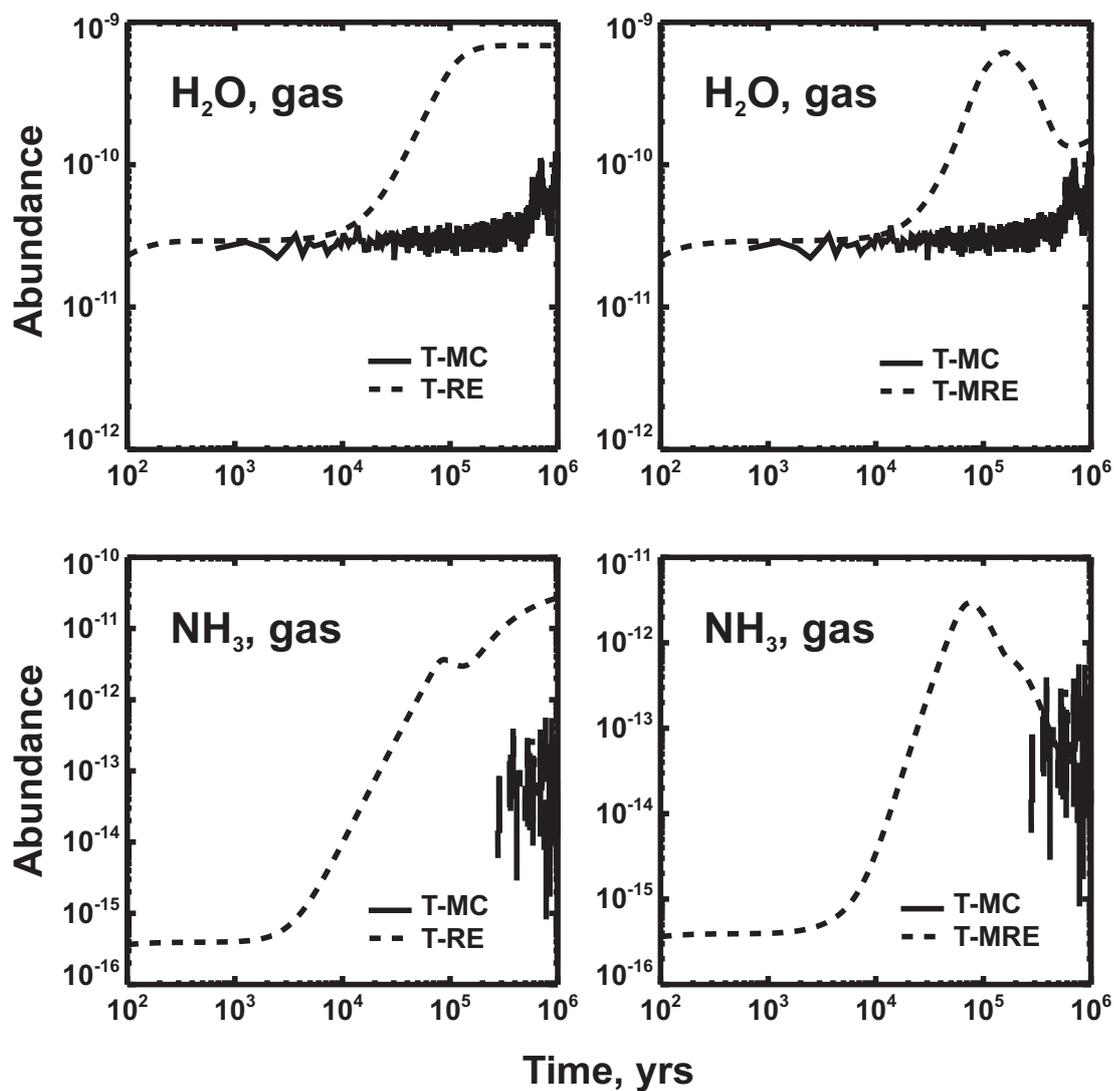
Figure 3.7 Water and ammonia gas-phase abundance evolution in the RE run in Model T ($n = 2 \cdot 10^2$ cm^{-3} and $T = 25$ K; left) and in the MRE run ($n = 2 \cdot 10^2$ cm^{-3} and $T = 25$ K; right).

in the MRE model as well, but only at $t \leq 10^5$ years. After this time O+HNO reaction slows down significantly due to modifying correction, and O abundance is controlled purely by accretion and desorption thereafter (as it is in the MC model at all times). As a result, OH and H_2O abundances decrease, getting closer to the MC model prediction. A similar mechanism is at work in the case of ammonia as well.

3.4.2.2   Model H

The only parameter region where a discrepancy occurs for Model H is located at $n = 2 \cdot 10^2 \text{ cm}^{-3}$ and $T = 25 \text{ K}$. Because of the low density, the degree of molecular complexity at these conditions is also low, and by 10^6 years only 73 species have abundances higher than 10^{-12} at least in one of the calculations. Of these 73 species, 25 show disagreement between the MC calculations and the RE calculations.
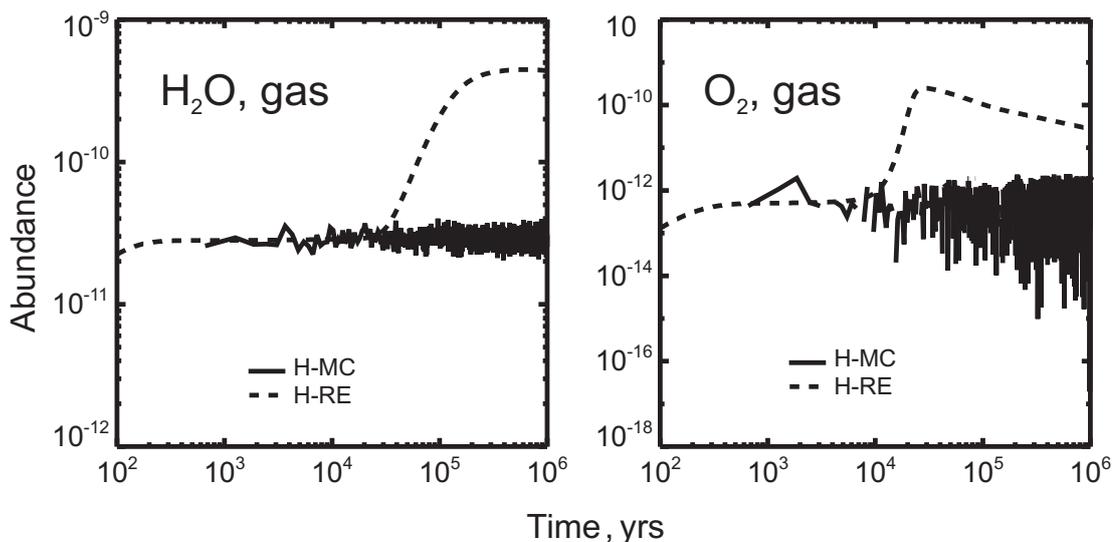
Figure 3.8 Water and molecular oxygen abundances at $n = 2 \cdot 10^2 \text{ cm}^{-3}$ and $T = 25 \text{ K}$ in Model H.

In the top row of Figure 3.8 we show the low density evolution of gas-phase water and molecular oxygen abundances. Both plots show a similar trend. In the MC calculations the abundance of the molecule stays nearly constant. At earlier times this steady-state behavior is reproduced in the RE run as well, but later the abundance grows and exceeds the MC abundance by more than an order of magnitude. It is interesting to note that the *average* O_2 abundance in the MC run seems to decrease somewhat at

later times, and this trend is reproduced by the RE model. The behavior of gas-phase abundances is a reflection of grain-surface abundances. It must be kept in mind that surface water abundance is quite high in the H-RE model, reaching almost 10^{-6}. Even though evaporation rate is not very high, it does increase gas-phase abundance up to a level of a few time 10^{-10}. Also, it is a low density model, so desorption is primarily caused by photons.
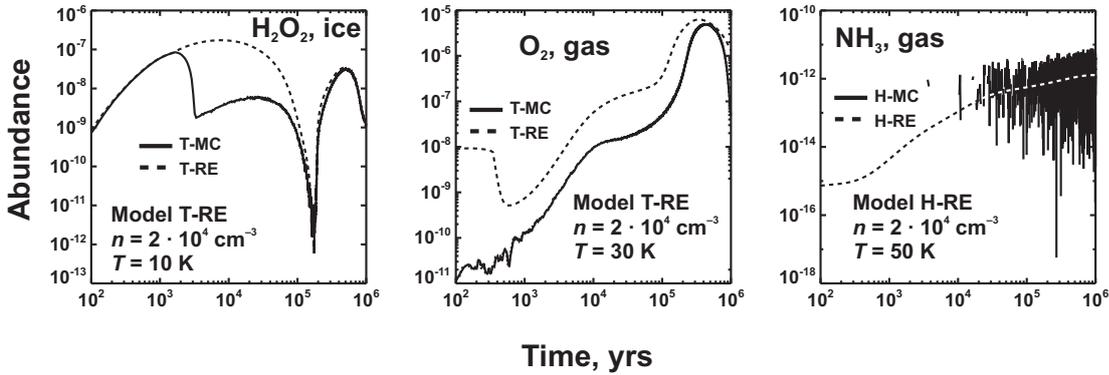
Figure 3.9 Abundance evolution for selected species. Models and physical conditions are indicated on the diagrams.

In Figure 3.9 we show the evolution of H_2O_2 surface abundance and O_2 gas-phase abundance in Model T-RE at $n = 2 \cdot 10^4$ cm^{-3} and the gas-phase ammonia abundance in Model H-RE at $n = 2 \cdot 10^3$ cm^{-3}. These plots demonstrate that disagreement does not always mean simply higher or lower abundances. Different processes determine the H_2O_2 abundance at different times, and while the RE method is able to capture some of these processes, others are obviously missed. Our analysis shows that this behavior is related to the treatment of reaction with H atoms. Specifically, surface abundance of H_2O_2 is controlled by three reactions only. It is produced in a reaction $H + O_2H$ and destroyed by atomic hydrogen in reactions producing either $H_2O + OH$ or $O+2H + H_2$. (Note that in the considered model water ice is almost irreversible sink for O atoms as there are no surface reactions destroying water, and desorption is negligible.) The formation reaction is fast as it does not have an activation barrier. So, initially, as H and O atoms start to stick to a grain, surface abundance of H_2O_2 steadily grows. At the same time, there is not enough H atoms for either of destruction reactions. Then, in the MC model at around 1300 years the first destruction reaction ($H + H_2O_2 \longrightarrow H_2O + OH$), which has a slightly lower activation barrier than the other one ($H + H_2O_2$

$\longrightarrow$ O$_2$H + H$_2$), starts to "steal" some hydrogen atoms from the formation reaction, irreversibly removing one O atom per reaction from the H$_2$O$_2$ (re)formation process. This is the reason for the sharp fall-off of H$_2$O$_2$ abundance. On the other hand, in the RE model both destruction and formation reactions may occur simultaneously, which prevents the first destruction reaction from having such a dramatic effect. Note that the second reaction restores an O$_2$H molecule which may react again with an H atom to restore an H$_2$O$_2$ molecule.

H$_2$O$_2$ is not unique in this kind of behavior. There are some other surface species which show more or less similar trends, that is, almost perfect agreement at some times and quite noticeable disagreement at other times. These are some carbon chains (C$_2$H$_2$, C$_2$N) or simpler molecules (CS, NO). Another equally dramatic example is represented by C$_2$H$_2$. The mechanism is similar, that is, it is related to the sequence of hydrogen additions which is treated differently in the MC model and the RE model.

Evolution of the O$_2$ abundance computed with the RE method follows the evolution computed with the MC model, but most of the time the RE curve is somewhat higher than the MC curve. Finally, the plot for ammonia shows the situation when the RE method correctly describes the average abundance evolution. However, the abundance predicted by the MC method fluctuates so wildly, that at each particular t we can detect disagreement with high probability, using our formal order-of-magnitude criterion.

3.5   Discussion

In the previous sections we investigated the validity of the (modified) rate equation approach to grain surface chemistry under different physical conditions encompassing diffuse clouds, giant molecular clouds, infrared dark clouds etc. Evolution of the medium is studied with an extended gas-grain chemical model over a time period of 10^6 years. We utilize the unified stochastic Monte Carlo approach, applied simultaneously to gas-phase and grain-surface reactions. The results are used to test the validity of conventional deterministic approaches. In general, differences in results obtained with deterministic and stochastic methods strongly depend on the adopted microphysical model of surface chemistry. In Model T, where tunneling for atomic and molecular hydrogen is permitted and diffusion/desorption energies ratio is low ($E_{\rm b}/E_{\rm D} = 0.3$), discrepancy both for RE and MRE methods is very significant. At low temperatures

3. A UNIFIED MONTE CARLO TREATMENT OF GAS-GRAIN CHEMISTRY FOR LARGE REACTION NETWORKS: MOLECULAR CLOUDS

(10 - 20 K) only abundances of surface species are discrepant by more than an order of magnitude. At moderate temperatures (25–40 K), due to active gas-grain interaction, incorrect treatment of grain surface chemistry becomes important for gas-phase abundances, too, and leads to dramatic decrease of overall agreement. At even higher temperatures agreement becomes better again due to limited surface chemistry. In Model H with no tunneling and high E_b/E_D ratio, surface species are much less mobile, and the agreement between deterministic and stochastic methods is better. The only exception is low density ($n(\text{H}) = 10^2$ cm^{-3}) with moderate temperatures (25 – 30 K), where average residence time of species on grain surface is still lower than the average interval between reaction events. In general, the stochastic chemistry severely affects abundances and, thus, must be taken into account in chemical models of a warm and moderately dense medium.

Modifications in rate equations, aimed at taking into account the accretion-limited regime, do not provide a significant improvement over 'canonical' rate equations in Model T. Close inspection of Figure 3.2 shows that at earlier times ($t \leq 10^5$ years) modified rate equations mostly produce results, which are rather *less* consistent with the 'exact' Monte Carlo solution, than results of the RE method. Only at later times ($t \sim 10^6$ years) results of the MRE method become more consistent with the 'exact' solution than the RE results. In the previous section, we have already shown some examples of species, for which the MRE method actually worsens the agreement.

Because at many of considered physical conditions results obtained with Monte Carlo method deviate significantly from those obtained with (modified) rate equations, the natural question to ask is whether the inability of the RE method to treat these combinations of parameters might have caused mis-interpretation of observational data. To answer this question, one would need to consider an object, for which a large volume of observational data is available, so that simultaneous comparison for many molecules is possible. So far, there seems to be just one molecular cloud, which is studied in necessary details. This is a sub-region of the TMC1 cloud where cyanopolyynes reach high concentrations, the so-called TMC1-CP. The physical conditions in this object ($T \sim 10$ K, $n_\text{H} \sim 10^4$ cm^{-3}) do fall into the range adopted in our model (Benson and Myers, 1989). However, the TMC1-CP is probably too cold to show significant dependence of gas-phase abundances from surface processes.

We may expect that the disagreement will be more significant in hotter objects. The range of physical conditions studied in this chapter is quite narrow, as it has only been chosen to provide an initial view on the importance of stochastic treatment for surface chemistry. There are two directions which are worth to follow for further study. One of them is related to diffuse clouds. In this chapter we most of the time assumed initial conditions in which all the hydrogen is molecular even at low density. Another simplification, which is, strictly speaking, not valid in low density medium, is equality of dust and gas temperature. So, it is interesting to check if stochastic effects work in predominantly atomic gas with different gas and dust temperatures. Another direction is chemistry at later stages of star formation, that is, in hot cores, hyper- and ultracompact HII regions, protoplanetary disks. In particular, in dark cold disk midplanes, which are poor in atomic hydrogen, stochastic effects may severely influence surface synthesis of hydrogenated species, like formaldehyde, which are later transferred by turbulent mixing in warmer disk areas and desorbed into gas phase (Aikawa, 2007). In these circumstances one would definitely need to use more accurate methods to model surface chemistry. Stochastic effects may be even more pronounced in the dynamically evolving medium, like during slow warm-up phase in hot cores or "corinos". Complex (organic) molecules will be among the most affected species.

In Figure 3.10 we show the percentage agreement between theoretical predictions and observational data as a function of the cloud age. We take a basic set of abundances from Ohishi et al. (1992), substituting them, when possible, with more recent, higher-resolution measurements, e.g., reported in Pratap et al. (1997). It is assumed that the modeled and observed abundances agree if both quantities differ by no more than an order of magnitude. This criterion include an observational uncertainty of a factor of 3 and a similar modeling uncertainty due to low accuracy of rate constants (Vasyunin et al., 2004; Wakelam et al., 2006a).

Results of comparison for $T = 10\,\mathrm{K}$ and $n = 2 \cdot 10^4$ cm^{-3} do not depend on the adopted treatment of surface chemistry, which is quite expected, as at this temperature and density all the considered models are consistent with each other within not less than 90% (see Figures 3.2 and 3.3).

The best fit chemical age of 10^5 years in the presented models seems to be at odds with earlier estimates by e.g. Semenov et al. (2004) and Garrod et al. (2007), which predicted the best agreement at $\sim 10^6$ years or later. Two comments can be made
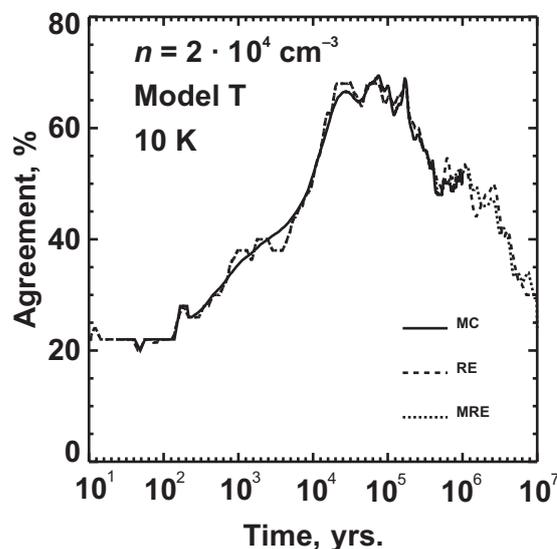
Figure 3.10 Percentage agreement of modeled and observed abundances for 50 molecules in the TMC1-CP within 10 Myr. The observed abundance (or upper limit) is assumed to agree with the model result if both values fall within one order of magnitude. Results are computed with the Monte Carlo model (solid line), the standard rate equation approach (dashed line), and the modified rate equation method (dotted lines), for Model T.

to justify this disagreement. First, in Semenov et al. (2004) lower value for a sticking probability has been adopted, and this parameter is a reciprocal for the chemical age (see e.g. Pavlyuchenkov et al., 2006). In Garrod et al. (2007) elevated ratio of E_b/E_D is adopted, and no tunneling is taken into account, so their model (see their Fig. 9) is best compared with our Model H. For TMC1-CP both models produce two peaks of agreement, one at 10^5 years and another at $> 10^6$ years. The relative height of the peaks is different. In our model the earlier peak seems to be preferable, while in Garrod et al. model the better agreement is achieved at the late peak. This difference is not surprising, given the variety of assumptions and implementations. It may be possible to achieve better agreement for the late time peak in Model H by tuning parameters of the physical or chemical model, like temperature, initial abundances, presence of PAHs etc. However, we did not attempt that, as in this chapter we do not aim at explaining the detailed chemical composition of any particular object.

Table 3.2.   Comparison of observed and modeled gas-phase abundances for
TMC1-CP

Molecule	Abundance[a] (relative to H)	Model T-MC 10 K, 0.1 Myr	H-MC	T-MC 30 K, 0.1 Myr	H-MC	T-MC 30 K, 1 Myr	T-RE
C	1.0(-05)	**2.4(-05)**	**3.2(-05)**	**3.5(-05)**	**3.5(-05)**	7.8(-07)	1.6(-08)
e$^-$	3.0(-07)	**4.3(-08)**	**4.2(-08)**	**5.2(-08)**	**5.2(-08)**	**8.6(-08)**	**6.0(-08)**
CH	2.0(-08)	**8.2(-09)**	**1.0(-08)**	**8.0(-09)**	**8.0(-09)**	**1.5(-08)**	5.0(-10)
C$_2$	5.0(-08)	2.3(-09)	2.4(-09)	1.8(-09)	1.8(-09)	**9.2(-09)**	2.2(-10)
C$_2$H	2.0(-08)	**1.1(-08)**	**1.0(-08)**	**1.1(-08)**	**1.1(-08)**	**2.2(-08)**	2.7(-10)
C$_3$H	3.0(-09)	**1.0(-08)**	**8.6(-09)**	**9.5(-09)**	**9.5(-09)**	**6.7(-09)**	9.6(-12)
C$_3$H$_2$	1.0(-09)	1.2(-08)	**8.4(-09)**	**8.2(-09)**	**8.0(-09)**	**6.3(-09)**	4.0(-11)
C$_4$H	2.0(-08)	**1.1(-08)**	**9.1(-09)**	**9.2(-09)**	**9.1(-09)**	**1.2(-08)**	8.8(-12)
C$_4$H$_2$	3.0(-10)	**2.3(-10)**	**2.2(-10)**	**4.3(-10)**	**4.2(-10)**	**4.2(-10)**	2.7(-12)
C$_5$H	6.0(-10)	**1.2(-09)**	**1.2(-09)**	**1.9(-09)**	**1.9(-09)**	**4.4(-10)**	1.2(-13)
CH$_3$C$_4$H	2.0(-10)	1.3(-11)	1.1(-11)	1.1(-11)	5.9(-12)	0.0	6.7(-16)
C$_6$H	4.0(-10)	**6.0(-10)**	**4.6(-10)**	**6.3(-10)**	**6.1(-10)**	**9.4(-10)**	3.4(-13)
C$_6$H$_2$	3.0(-11)	**1.2(-11)**	5.9(-12)	9.6(-12)	2.8(-12)	**2.4(-11)**	3.5(-15)
CN	3.0(-09)	**2.9(-08)**	**2.8(-08)**	**2.1(-08)**	**2.1(-08)**	**5.2(-08)**	**5.9(-09)**
HCN	2.0(-09)	2.8(-08)	3.3(-08)	4.1(-08)	4.0(-08)	2.1(-08)	**1.0(-08)**
HNC	6.0(-09)	**2.1(-08)**	**2.4(-08)**	**3.6(-08)**	**3.6(-08)**	**2.7(-08)**	**1.3(-08)**
HCNH$^+$	2.0(-09)	1.7(-10)	1.8(-10)	**3.0(-10)**	**2.8(-10)**	**3.1(-10)**	**2.8(-10)**
CH$_2$CN	5.0(-09)	2.1(-10)	2.0(-10)	2.7(-10)	2.7(-10)	1.4(-10)	2.0(-11)
CH$_3$CN	1.0(-09)	**9.6(-10)**	**1.2(-09)**	**2.2(-09)**	**2.3(-09)**	4.9(-11)	7.5(-12)
C$_3$N	1.0(-09)	**6.7(-10)**	**6.2(-10)**	**6.7(-10)**	**6.8(-10)**	**1.6(-09)**	9.8(-13)
CH$_2$CHCN	8.0(-09)	0.0	0.0	3.8(-12)	0.0	0.0	6.9(-16)
CH$_3$C$_3$N	8.0(-11)	**1.0(-10)**	**1.8(-10)**	**1.7(-10)**	**1.5(-10)**	3.8(-12)	1.3(-15)
HC$_3$N	4.0(-09)	**3.9(-09)**	**5.1(-09)**	**1.1(-08)**	**1.1(-08)**	7.8(-10)	2.0(-12)
HC$_5$N	4.0(-09)	**4.5(-10)**	**5.6(-10)**	**1.8(-09)**	**1.6(-09)**	2.1(-11)	5.4(-14)
HC$_7$N	1.0(-09)	4.5(-11)	3.4(-11)	**1.7(-10)**	8.9(-11)	0.0	1.0(-15)
HC$_9$N	5.0(-10)	3.8(-12)	1.5(-11)	2.3(-11)	1.1(-11)	0.0	3.0(-17)
CO	8.0(-05)	**5.6(-05)**	**6.1(-05)**	**8.3(-05)**	**8.2(-05)**	**5.2(-05)**	**2.5(-06)**
HCO$^+$	5.0(-09)	**3.2(-09)**	**3.1(-09)**	**5.6(-09)**	**5.4(-09)**	**8.1(-09)**	**1.6(-09)**
H$_2$CO	2.0(-08)	**1.1(-07)**	**1.2(-07)**	**7.4(-08)**	**7.3(-08)**	**9.4(-09)**	1.1(-09)
CH$_3$OH	2.0(-09)	0.0	0.0	0.0	0.0	0.0	8.0(-15)
HCOOH	< 2.0(−10)	**8.4(-10)**	**9.3(-10)**	**5.7(-10)**	**5.4(-10)**	**0.0**	**2.5(-12)**
H$_2$CCO	6.0(-10)	**4.9(-09)**	6.4(-09)	**4.7(-09)**	**4.7(-09)**	**7.8(-11)**	6.6(-13)
CH$_3$CHO	6.0(-10)	2.3(-11)	1.5(-11)	1.1(-11)	1.1(-11)	0.0	3.1(-14)
C$_2$O	6.0(-10)	**9.6(-11)**	**8.3(-11)**	5.3(-11)	**6.9(-11)**	4.2(-12)	1.8(-14)
C$_3$O	1.0(-10)	**2.5(-10)**	**2.4(-10)**	**4.1(-10)**	**4.3(-10)**	**2.3(-11)**	1.9(-13)
H$_2$S	< 5.0(−10)	**7.6(-12)**	**0.0**	**0.0**	**3.8(-12)**	**2.0(-11)**	**3.5(-11)**

3. A UNIFIED MONTE CARLO TREATMENT OF GAS-GRAIN CHEMISTRY FOR LARGE REACTION NETWORKS: MOLECULAR CLOUDS

Table 3.2 (cont'd)

Molecule	Abundance[a] (relative to H)	Model T-MC 10 K, 0.1 Myr	H-MC	T-MC 30 K, 0.1 Myr	H-MC	T-MC 30 K, 1 Myr	T-RE
SO	2.0(-09)	4.3(-11)	1.5(-11)	1.5(-11)	1.9(-11)	**3.4(-10)**	**1.1(-09)**
SO_2	$< 1.0(-09)$	**0.0**	**0.0**	**0.0**	**0.0**	**3.8(-12)**	**7.9(-11)**
CS	4.0(-09)	**3.4(-09)**	**3.8(-09)**	**6.2(-09)**	**6.5(-09)**	**1.6(-09)**	1.4(-11)
HCS^+	4.0(-10)	1.9(-12)	2.7(-12)	1.5(-12)	2.8(-12)	1.9(-12)	4.0(-14)
H_2CS	3.0(-09)	**8.1(-10)**	**9.8(-10)**	**1.8(-09)**	**1.6(-09)**	2.1(-10)	1.6(-11)
C_2S	8.0(-09)	5.7(-10)	5.0(-10)	**9.6(-10)**	**9.4(-10)**	7.3(-10)	7.3(-13)
C_3S	1.0(-09)	**2.9(-10)**	**2.6(-10)**	**4.6(-10)**	**4.4(-10)**	**2.8(-10)**	7.7(-14)
OCS	2.0(-09)	**2.3(-10)**	**2.6(-10)**	1.3(-10)	**2.0(-10)**	3.0(-11)	7.3(-13)
NH_3	1.0(-08)	**1.3(-08)**	**1.2(-08)**	**2.6(-08)**	**2.6(-08)**	**3.7(-08)**	3.0(-07)
N_2H^+	1.3(-10)	**1.1(-10)**	**1.0(-10)**	**1.3(-10)**	**1.1(-10)**	**7.9(-10)**	2.2(-09)
NO	$< 3.0(-08)$	**2.8(-08)**	**2.0(-08)**	**1.7(-08)**	**1.7(-08)**	3.5(-07)	1.5(-06)
OH	3.0(-07)	**5.2(-08)**	**4.3(-08)**	**3.6(-08)**	**3.7(-08)**	**5.5(-08)**	**1.8(-07)**
H_2O	$< 7.0(-08)$	9.3(-07)	1.0(-06)	1.4(-06)	1.4(-06)	**2.3(-08)**	**6.7(-08)**
O_2	$< 7.7(-08)$	**8.6(-08)**	**6.4(-08)**	**9.7(-08)**	**9.5(-08)**	**1.0(-07)**	2.7(-06)
Agreement		70%	70%	74%	74%	64%	26%

[a]The observed values are taken from Ohishi et al. (1992); Pratap et al. (1997); Schilke et al. (1995); Smith et al. (2004); Turner et al. (2000).

In general, comparing predictions of different methods with observations for TMC1-CP we obtain very similar results, which is not surprising, as the temperature in this object is not high enough to make the stochastic chemistry important (See Table 3.2 that is available in electronic form). However, we may expect that he disagreement will be more significant in hotter objects. The range of physical conditions studied in this chapter is quite narrow, as it has only been chosen to provide an initial view on the importance of stochastic treatment for surface chemistry. There are two directions which are worth to follow for further study. One of them is related to diffuse clouds. In this chapter we most of the time assumed initial conditions in which all the hydrogen is molecular even at low density. Another simplification, which is, strictly speaking, not valid in low density medium, is equality of dust and gas temperature. So, it is interesting to check if stochastic effects work in predominantly atomic gas with different gas and dust temperatures. Another direction is chemistry at later stages of star formation, that is, in hot cores, hyper- and ultracompact HII regions, protoplanetary

disks. In particular, in dark cold disk midplanes, which are poor in atomic hydrogen, stochastic effects may severely influence surface synthesis of hydrogenated species, like formaldehyde, which are later transferred by turbulent mixing in warmer disk areas and desorbed into gas phase (Aikawa, 2007). In these circumstances one would definitely need to use more accurate methods to model surface chemistry. Stochastic effects may be even more pronounced in the dynamically evolving medium, like during slow warmup phase in hot cores or "corinos". Complex (organic) molecules will be among the most affected species.

While the Monte Carlo method is the most direct approach, it is by no means practical. So, other methods are to be developed if we want to understand deeper the chemical evolution in warm and dense astrophysical objects.

3.6 Conclusions

In this study, a gas-grain chemical model is presented, consisting of about 600 species and 6000 reactions with stochastic description of grain surface chemistry. For the first time both gas phase and grain surface reactions are simulated with a unified Monte Carlo approach. This unified model is used to test the validity of rate equations and modified rate equations for a set of physical conditions, relevant to translucent clouds, dark dense cores, and infrared dark clouds.

A comparison of results obtained with deterministic rate equations (RE) and modified rate equations (MRE) with results of Monte Carlo simulations was performed for this set of physical conditions and two different models of surface chemistry. We found that results obtained with both RE and MRE approaches sometimes significantly deviate from those obtained with Monte Carlo calculations in Model T, where surface species are highly mobile and most of the grain chemistry occurs in the accretion limited regime. While at low temperatures ($10\,\mathrm{K}$ – $20\,\mathrm{K}$) mainly RE and MRE abundances of surface species show significant discrepancies, at moderately high temperatures ($25\,\mathrm{K}$ – $30\,\mathrm{K}$) even abundant gas-phase species like CO considerably deviate from the Monte Carlo results. At these temperatures grain surface chemistry is still very active and at the same time processes of accretion and desorption are very efficient. The gas-phase abundances of many species are influenced by surface chemistry that is correctly described in Monte Carlo simulations only. In Model H surface species

are much less mobile than in Model T and the agreement between the (modified) rate equations approach and Monte Carlo simulations is almost perfect. The only parameter region where this discrepancy is significant is at a temperature of $T = 25$ K and at a low density $n(\text{H}) = 2 \cdot 10^2$ cm^{-3}. On the whole, results of modified rate equations seem to be in somewhat closer agreement with Monte Carlo simulations than results of the conventional rate approach. But still, the agreement is far from being perfect, so modified rates should be used with care. We conclude that stochastic effects have a significant impact on chemical evolution of moderately warm medium and must be properly taken into account in corresponding theoretical models. In the studied parameter range, stochastic effects are, in general, not important at low ($T \sim 10$ K) and high ($T \sim 50$ K) temperatures.

Since Monte Carlo simulations are too slow for everyday use, it is of interest to study the validity of other techniques to simulate grain surface chemistry properly. In the next chapter of the thesis we investigate the validity of newly proposed modifications to rate equations (see Garrod, 2008) and apply them to the study of stochastic effects in the chemistry of protoplanetary disks.

4

A new modified-rate approach for gas-grain chemistry: Comparison with a unified large-scale Monte Carlo simulation

4.1   Introduction

From the synthesis of H_2 in molecular clouds (e.g. Gould and Salpeter, 1963), to the formation of complex organic molecules in star-forming regions (e.g. Belloche et al., 2009), a full understanding of interstellar chemistry requires the consideration of both gas-phase and dust grain-surface processes. However, the lack of accurate computational tools for the modeling of coupled gas-grain chemical systems presents a major obstacle to the achievement of this goal, as has long been realized.

Accurate simulation of gas-phase chemistry alone may be achieved using rate equa-

4. A NEW MODIFIED-RATE APPROACH FOR GAS-GRAIN CHEMISTRY:
COMPARISON WITH A UNIFIED LARGE-SCALE MONTE CARLO SIMULATION

tions (RE), and this method is frequently extended to the simulation of the grain-surface chemistry, in the manner of Hasegawa et al. (1992). Such an approach is attractive, due both to the simplicity of solution and the ease with which gas-phase and grain-surface chemistry may be coupled. However, the discreteness of surface processes in some situations (when the number of reacting particles per grain is less than 1) can invalidate the use of rate equations (Biham et al., 2001; Caselli et al., 1998; Tielens and Hagen, 1982; Vasyunin et al., 2009).

Grain-surface chemistry may be accurately simulated using the chemical master equation. A number of attempts have been made to solve this equation in astrochemical contexts; however, these have mostly been limited to small chemical networks, as the numerical methods required for solution place great demands on computer power and processor time. Furthermore, these "exact" methods are so dramatically different from the rate equations used to simulate gas-phase chemistry that, in some implementations, direct coupling between the two phases is intrinsically impossible.

Two straightforward approaches to these problems present themselves. Firstly, one may employ the master equation to treat both gas-phase and grain-surface chemistry; Vasyunin et al. (2009) have demonstrated that this is indeed possible, solving the chemical master equation for a full gas-grain chemical network using the Monte Carlo (MC) method. However, in the considered range of parameters the computation is very time-consuming, taking up to a few days on an average computer for a single set of physical parameters. The computational time required also tends to increase with higher densities and/or higher initial abundance of atomic hydrogen.

Alternatively, one may modify the rate equations to account for the discrete nature of chemical reactions. Crucially, rate equations may be solved quickly and efficiently using a general-purpose ODE integrator. This also makes them attractive for multi-point and/or multi-variant simulations. Modification of the grain-surface reaction-rate coefficients has been attempted previously (Caselli et al., 2002, 1998; Shalabiea et al., 1998; Stantcheva et al., 2001), but without unqualified success. Vasyunin et al. (2009) compared their own master equation results with those obtained using the method of Caselli et al. (1998). While in some cases the modified rate equations were indeed found to ensure closer agreement with the Monte Carlo method, in other cases they produced results less accurate than the unmodified rate equations (as compared with the 'exact' Monte Carlo solution).

Recently, Garrod (2008) proposed another modified rate equation (MRE) scheme, which modifies not simply the rate coefficients but the functional form of the equations. The scheme has shown great success in tests using limited chemical networks to achieve steady-state solutions. However, to properly ascertain its accuracy and applicability, the new method requires testing with a full time-dependent gas-grain chemical model. In this letter we present the first large-scale comparison between the modified-rate method of Garrod (2008) and the exact Monte Carlo method of Vasyunin et al. (2009). We also present the results of standard rate equations.

4.2 Modeling

4.2.1 Physical conditions

We simulate chemical processes under a range of physical conditions, typical of irradiated translucent clouds, cold dark cores and infrared dark clouds. We consider temperatures $T = 10, 15, 20, 25, 30, 50$ K, and gas densities $n_H = 2 \cdot 10^2, 2 \cdot 10^3, 2 \cdot 10^4, 2 \cdot 10^5$ cm^{-3}, with corresponding visual extinctions $A_V = 0.2, 2, 15, 15$ **mag** (e.g., Hassel et al., 2008; Snow and McCall, 2006), giving a grid of 24 points. Dust and gas temperatures are assumed to be equal. Simulations are performed over a timescale of 1 Myr, appropriate for TMC-1 cloud conditions (see e.g. Roberts et al., 2004; Semenov et al., 2004).

4.2.2 Chemical model

The chemical model is that used by Vasyunin et al. (2008), described briefly here. Gas-phase reactions and rates are taken from the RATE 06 database (Woodall et al., 2007); reactions with negative activation energy barriers are excluded. The mean Draine interstellar UV field is assumed, with the rates of photodissociation and photoionization of molecular species by UV photons taken from van Dishoeck et al. (2006b).

Accretion of neutral species onto dust grains occurs with a sticking probability of unity. Evaporation and photodesorption of mantle materials are also included (Semenov et al., 2004). A uniform grain size of $0.1 \, \mu$m is assumed, with a surface density of sites $2 \cdot 10^{14}$ cm^{-2}, giving $\approx 3 \cdot 10^5$ sites per grain (Biham et al., 2001). The gas-to-dust ratio is 100:1.

Surface reactions and desorption energies, E_D, are taken from Garrod and Herbst (2006), with reaction rates calculated following Hasegawa et al. (1992). The low diffusion barriers of Hasegawa et al. (1992) are adopted, i.e. $E_b = 0.3E_D$, and tunneling of atomic and molecular hydrogen is allowed. The case of high $E_b : E_D$ ratios, without tunneling, was considered by Vasyunin et al. (2009); however, standard rate equations were shown to be adequate in this case, with stochastic effects being mostly negligible.

The full network consists of 422 gas-phase and 157 surface species, composed of 13 elements, and 6002 reactions, including 216 surface reactions. The "low metallicity" initial abundances used by Lee et al. (1998) are assumed, with all hydrogen initially in molecular form.

4.3   Algorithm of the new MRE method

The modified-rate approach of Garrod (2008) labelled method C is used. Under this method, the production rate of a surface reaction between species A and B is calculated using expressions appropriate when the averaged populations, $\langle N(A) \rangle$ and $\langle N(B) \rangle$, are much less than unity. For reaction between heterogeneous species, this new production rate is composed of two separate terms, associated with the arrival of either reactant:

$$
\begin{aligned}
R_{mod}(AB) = \quad & R_{arr}(B) \cdot P(A) \cdot \eta_{AB}(A) \\
+ \quad & R_{arr}(A) \cdot P(B) \cdot \eta_{AB}(B)
\end{aligned}
\tag{4.1}
$$

where $R_{arr}(B)$ is the total arrival/formation rate of B, $P(A)$ is the probability of A being present when B arrives, and $\eta_{AB}(A)$ is the efficiency of reaction $A + B$. The components of the second term are defined similarly.

The probability that one or more particles of a reactant be present at any arbitrary moment is approximated using a Poisson probability distribution; hence, $P(i) = 1 - \exp[-\langle N(i) \rangle]$. The efficiency of the reaction takes into account competition between reaction and the evaporation of either species, as well as competition with other reactions that involve species that are present with populations greater than unity (which species we label "deterministic"). Note that the efficiency depends on which species is arriving and which is already present. The arrival/formation of a reactant is typically achieved by accretion from the gas-phase. However, the rates of chemical formation

on the grain surfaces are added to the accretion rate of each species, if such chemical formation takes place "deterministically" (see eq. 2, below).

One further restriction is that $R_{mod}(AB)$ may not exceed the standard deterministic production rate (i.e. the rate-equation rate), which constitutes a theoretical maximum. This allows rate equations to be used when appropriate, even in the case when $\langle N(A) \rangle, \langle N(B) \rangle << 1$. We refer the reader to Garrod (2008) for further details concerning the construction of $R_{mod}(AB)$.

The final production rate for reaction $A + B$ mixes the deterministic rate with $R_{mod}(AB)$:

$$
\begin{aligned}
R_{tot}(AB) = \quad & f_{AB} \cdot R_{mod}(AB) \\
+ \quad & (1 - f_{AB}) \cdot k_{AB} \cdot \langle N(A) \rangle \cdot \langle N(B) \rangle
\end{aligned} \tag{4.2}
$$

where f_{AB} is a switching function that is equal to 1 when both $\langle N(A) \rangle$, $\langle N(B) \rangle \leq 1$, but which falls off quickly when either $\langle N(A) \rangle$ or $\langle N(B) \rangle$ become greater than unity. This allows the expression above to converge quickly with standard rate equations when appropriate. The second term of the above expression represents the "deterministic" part of the production rate. It is this term (including the switching function) that contributes to the arrival/formation rate R_{arr} for the purposes of other reactions, as mentioned above.

4.4   Results

We apply the RE, MRE and MC methods to the same density–temperature parameter space. The level of global agreement between methods is assessed for three different times in the chemical evolution of the models (10^4, 10^5, 10^6 yr) following the procedure of Vasyunin et al. (2009). The global agreement level is given by the number of chemical abundances reproduced by the MRE (or RE) method to within one order of magnitude of the MC value, divided by the number of species considered. Only species with abundances greater than $10^{-12} n_H$ were counted. An order of magnitude agreement threshold used here may seem to be too loose, however, we note that most often results of MC and MRE runs do not differ by more than a factor of 3.

Fig. 4.1 shows the level of global agreement between the MRE and MC methods, which is, in general, very good; most of the parameter space shows agreement greater

4. A NEW MODIFIED-RATE APPROACH FOR GAS-GRAIN CHEMISTRY:
COMPARISON WITH A UNIFIED LARGE-SCALE MONTE CARLO
SIMULATION
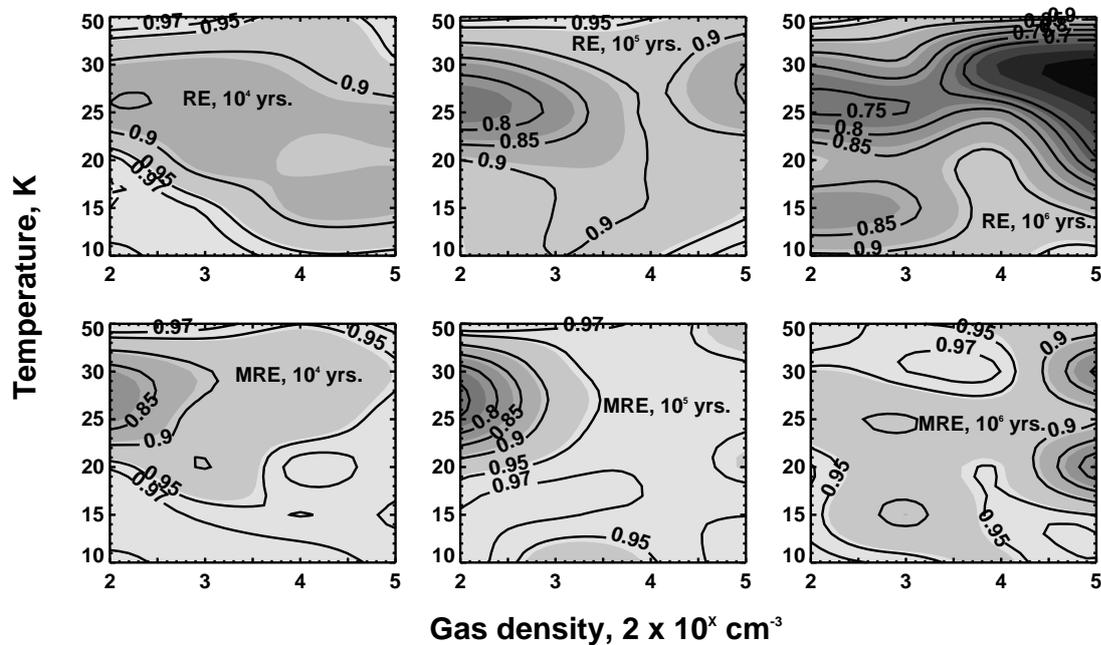
Figure 4.1 Global agreement diagrams at three evolutionary times. Contour labels show the percentage of species whose abundances computed with rate equations (top row) or modified rate equations (bottom row) differ from those of the Monte Carlo method by no more than one order of magnitude. Grayscale map with arbitrary contours is added for clarity. Darker color corresponds to worse agreement.
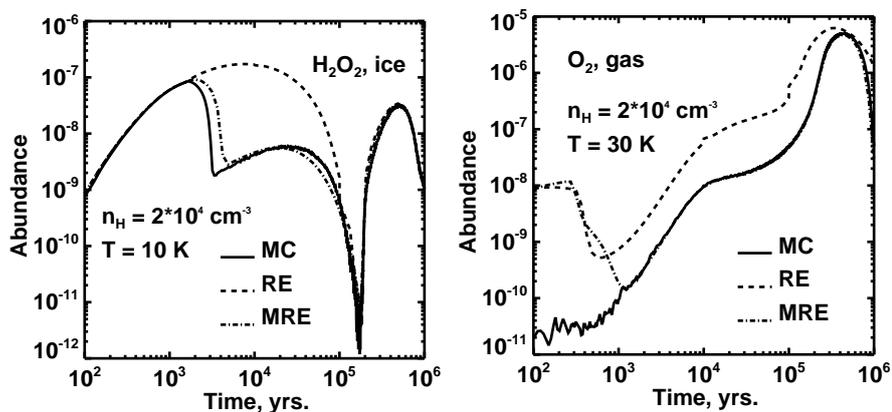
Figure 4.2 Time-dependent abundances of representative species calculated with RE (dashed line), MRE (dotted–dashed line) and Monte Carlo (solid line).
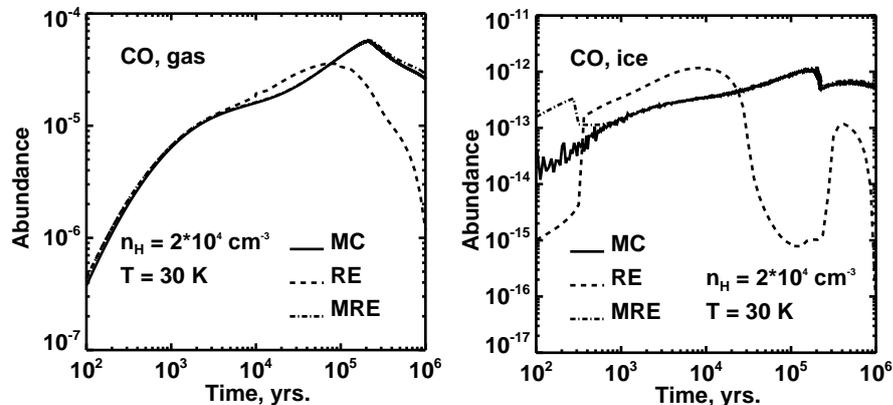
Figure 4.3 Gas-phase and grain-surface abundances of CO in one of the worst cases for rate equation accuracy: $n_H=2\cdot10^4$ cm^{-3},T=30 K.

than 0.9, and large regions show values greater than 0.95, at all three comparison times. Fig. 4.4 shows time-dependent abundances of some typical gas-phase and grain-surface species, calculated using each method. Complex chemical behavior that is missed by the RE method is accurately traced using MRE. Figure 4.4 shows results for gas-phase and grain-surface CO for one of the worst cases of rate-equation inaccuracy.

Agreement of the MRE method with the MC results is superior to that of the RE method over all parameter space, except at two points ($n_H = 2 \cdot 10^2$ cm^{-3}, $T = 25, 30$ K), at which agreement is ~ 0.05 lower at times of 10^4 and 10^5 yr. Agreement with the MC results falls noticeably at two other points in parameter space ($n_H = 2 \cdot 10^5$ cm^{-3}, $T = 20, 30$ K) at time 10^6 yr, although the MRE results are still superior to the RE method.

The lesser agreement at each of these points is, in fact, related to the behavior of grain-surface NO and HNO molecules. The grain-surface chemical network we employ has only a limited number of reactions involving NO and HNO; appropriate for cold (10 K), dark-cloud environments where atomic hydrogen is the dominant mobile reactant. Hydrogenation of NO to HNO proceeds rapidly on the grains; however, at elevated temperatures atomic oxygen also becomes mobile, allowing it to abstract a hydrogen atom from HNO, forming NO + OH. This mechanism can become the dominant formation route for NO, creating a fast loop of NO–HNO inter-conversion. At the same time, this mechanism may become the dominant route for OH formation.

The resultant strong correlation between NO and OH populations, combined with the sparse reaction network for NO, creates a complex behavior that the MRE method does not take into account. For example, with the MRE method, the OH may react with O to form O_2H, which reacts with N to form NH. This NH then reacts with atomic oxygen to form HNO, re-enforcing the NO-HNO loop.

However, with the Monte Carlo method, re-enforcement of the loop does not occur; throughout the NH-formation process, the NO molecule is still present on the grains – a fact which is not taken into account by the MRE method. This NO quickly reacts with NH, preventing the formation of HNO. This apparently small detail creates noticeable differences in abundances between the MRE and MC methods, strongly affecting up to 25% of considered species.

Other, similar NO/HNO-related effects can become important at other points in parameter space. However, the main point highlighted here is the ability of the MC method to trace convoluted correlations between pairs of species (in this case, NO and NH), which the MRE method cannot. Is this failure important to the accuracy of the MRE method? Only if such correlations are realistic. It is the sparsity of the NO/HNO chemistry employed here that allows an NO molecule to be present on the grain for so long, while so much other chemistry goes on around it, unaffected. A more comprehensive reaction network that allowed grain-surface NO to react with, for example, atomic O and N (which the current network does not) would make such correlations very weak, and therefore redundant. To ensure that the MRE method is accurate, therefore, one should provide a sufficiently comprehensive set of destruction mechanisms for species, such as NO and HNO, that may become locked into an inter-conversion loop.

Fig. 4.4 shows the agreement levels within the same parameter space, but with all grain-surface NO and HNO destruction mechanisms switched off. The accuracy of the MRE method is now vastly improved, and far superior to the RE results.

4.5 Summary of methods comparison

Grain surfaces are now well recognized as a site where many important species, including observational tracers and complex organics, are either synthesized or at least preserved in a variety of prestellar, protostellar, and protoplanetary objects. However,
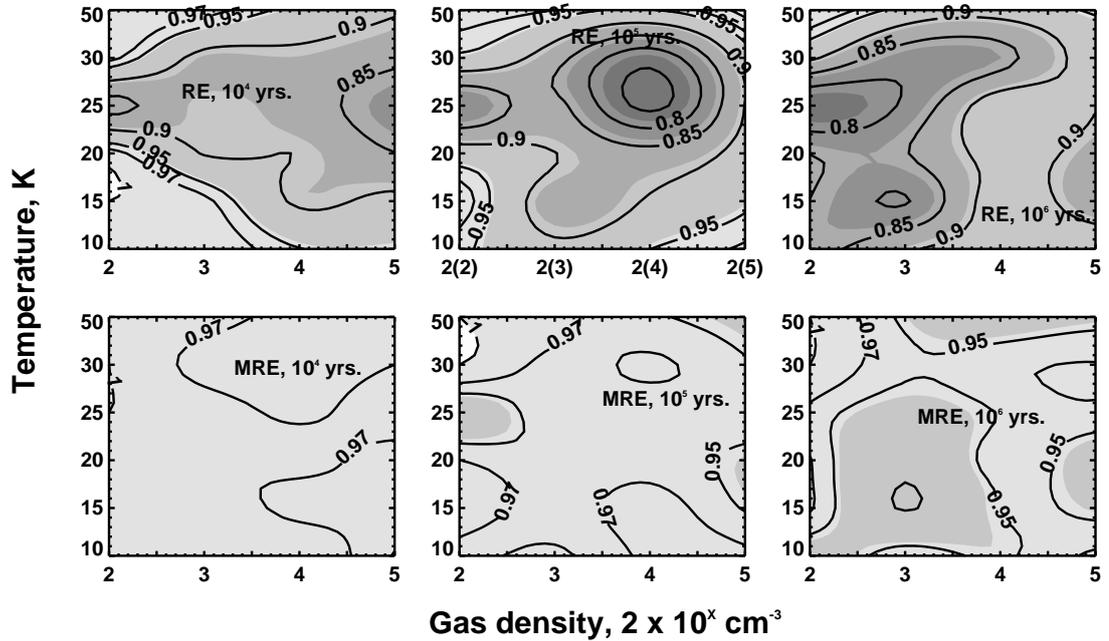
Figure 4.4 Same as fig. 4.1 but calculated for chemical network with NO – HNO loop excluded.

proper understanding of surface chemistry is still hampered, among other reasons, by the lack of an effective and realistic tool for modeling surface reactions.

The new modified-rate method of Garrod (2008) reproduces very well the time-dependent chemical abundances obtained using the exact Monte Carlo method of Vasyunin et al. (2009). Improvement over the standard rate-equation method is especially marked at later times, $> 10^5$ years. The few stronger discrepancies between the MRE and MC results appear to derive from correlations between the populations of certain species, which the MRE method does not take into account. In the considered network these correlations are uniquely associated with the destruction pathways of grain-surface NO molecules, and they are amplified by a chemical loop in which grain-surface NO and HNO undergo fast inter-conversion. These effects may be best remedied by the completion of the NO reaction network, which is not currently sufficient for temperature regimes in which heavier atoms become mobile on the grain-surfaces. The comparison presented here shows the new modified-rate method to be robust over a large range of physical conditions. The method will be useful in allowing fast and accurate simulation of interstellar chemistry using even the most complex chemical networks.

4.6 Importance of stochastic effects for the chemistry of protoplanetary disks

In this section, we apply for the first time the new modified rate equations scheme to chemical modeling of protoplanetary disks. Our main aim is to assess the importance of stochastic effects for the disk chemical evolution and to characterize it's observability with the current or forthcoming observational facilities like ALMA, SOFIA, and Herschel.

We adopted a steady-state 1+1D model of an irradiated protoplanetary disk surrounding a young T Tauri star (D'Alessio et al., 1999a). The central star has a mass of 0.7 $M_\odot$, temperature 4000 K and radius 2.64 $R_\odot$. The disk has a radius of 800 AU, an accretion rate $\dot{M} = 10^{-8} M_\odot \, yr^{-1}$, a viscosity parameter $\alpha = 0.01$, and a mass $M \simeq 0.005 \, M_\odot$. The disk structure is represented by the 2D-grid including 30 radial and 65 vertical points (1950 disk cells in total). The adopted model closely resemble the DM Tau protoplanetary system (e.g., Dartois et al., 2003; Piétu et al., 2007). The thermal and density structure of the disk are shown in the Figure 4.5.

Our chemical model is essentially the same as described in Chapter 2. We considered two different approaches to the surface chemistry modeling (see Chapter 3). The Model T has fast surface recombination rates, as we allow quantum tunneling of light atoms through potential barriers of the neighboring surface sites, and assume low diffusion barriers for thermal hopping of heavy radicals. The Model H has slow rates of surface reactions because tunneling is not allowed and the diffusion energies are high. The dust grains are assumed to be spherical uniform particles with radius of 10^{-5} cm and the same dust-to-gas mass ratio of 1%. Using our disk physical and chemical model, the disk chemical evolution over 1 Myr is simulated.

4.6.1 Global disk chemical structure

The global chemical structure of the disk is dictated by the physical conditions (temperature, the UV and X-ray ionization rates, etc.) and as such does not depend on details of grain surface chemistry. From chemical perspective the disk can be divided on three layers in the vertical direction (see Fig. 4.6). In hot diffuse atmosphere ($Z/R \geq 1.5$) chemistry is dominated by the high-energy irradiation from the star (UV, X-rays) and the interstellar space (UV, CRPs). Surface recombination and hence stochastic effects
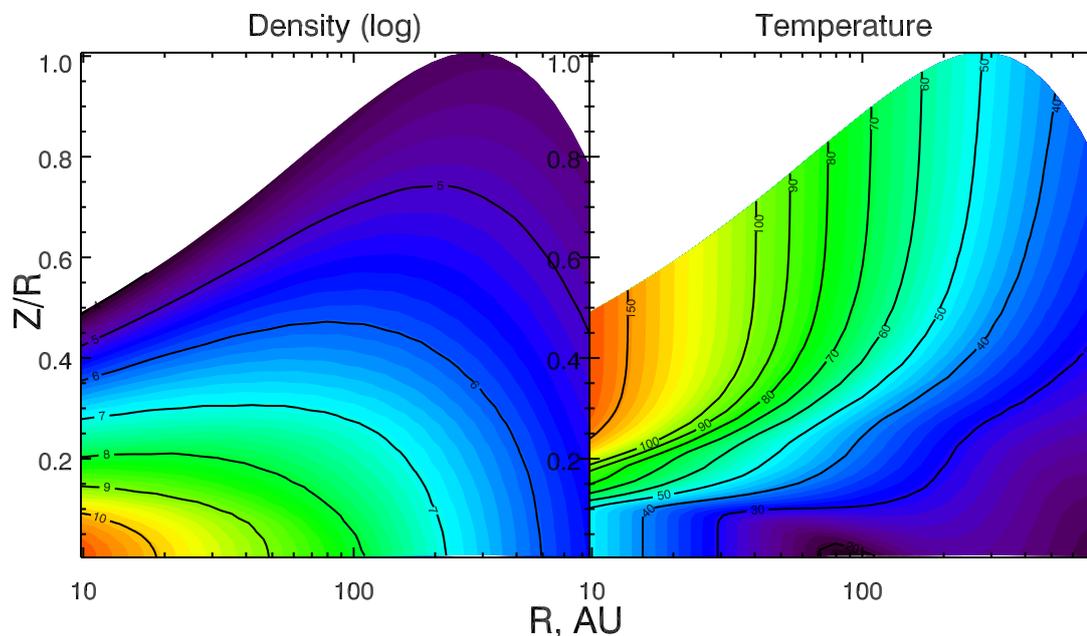
Figure 4.5 Thermal and density structure of the adopted protoplanetary disk

are not important there, and only a handful of atomic ions and simple molecular ions (e.g., CH^+, CH_2^+) are abundant. In contrast, in dark cold disk midplane density is high ($\geq 10^7$ cm^{-3}) while temperature is sufficiently low ($T \leq 20$ K) to allow fast accretion of gas-phase molecules onto grain surfaces. In this region evaporation of mantle materials occurs only via the CRP-heating and is not competitive with accretion. After about $10^4 - 10^5$ years of the disk evolution thick icy mantles are formed, where surface chemistry is active and thus stochastic processes become important. However, it only affects abundances of surface species while concentrations of their gas-phase counterparts remain intact. Between the disk atmosphere and midplane an intermediate layer is located. This warm region ($T \sim 30 - 100$ K) is only partly shielded from the UV radiation, which activates many neutral-neutral and photoreactions and results in its rich molecular complexity (see a molecular peak at $R \sim 100$ AU, $Z/R \sim 0.2$). In this disk region evaporation of ices becomes effective, and evolution of gas-phase and surface species is coupled. Thus the stochastic nature of surface reactions can manifest itself by affecting abundances of both the surface as well as the gas-phase molecules. Indeed, the fraction of species with high relative abundances is the largest in the disk intermediate layer (Fig. 4.6). The "sandwich"-like 3-layered chemical structure of the

disk described by other authors (e.g., Aikawa and Herbst, 1999; Semenov et al., 2004; Vasyunin et al., 2008) appears also in our model.
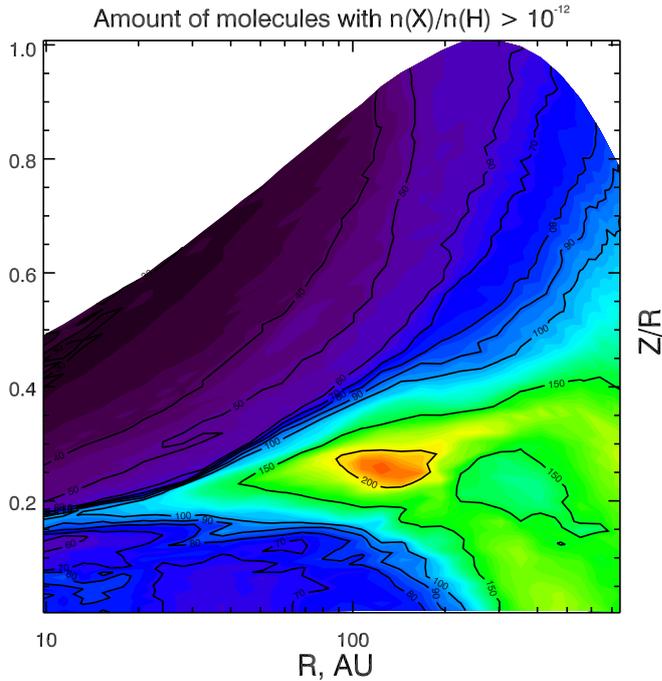
Figure 4.6 Chemical diversity in the disk: amount of species with abundances relative to the total amount of hydrogen nuclei that exceeds 10^{-12}.

4.6.2 Results for Model T

In the Sect. 4.4, we showed that in the model with fast surface recombination rates stochastic effects may be very pronounced in the case of molecular clouds. The importance of stochastic effects for chemical evolution of protoplanetary disks for Model T is presented in Figure 4.7. Shown is the agreement map between the RE and MRE results, that is the percentage of molecules which abundances do not deviate by more than the factor of 10 in both the RE and MRE models.

The agreement level between RE and MRE is below 100% practically everywhere in midplane and intermediate layer of the disk, i.e. in the region where gas and dust temperature is below 40 K. At higher temperatures most of species desorb quickly form grain surfaces and surface chemistry less pronounced, and thus agreement becomes better. The molecular peak of the disk is located within that region and thus is hardly
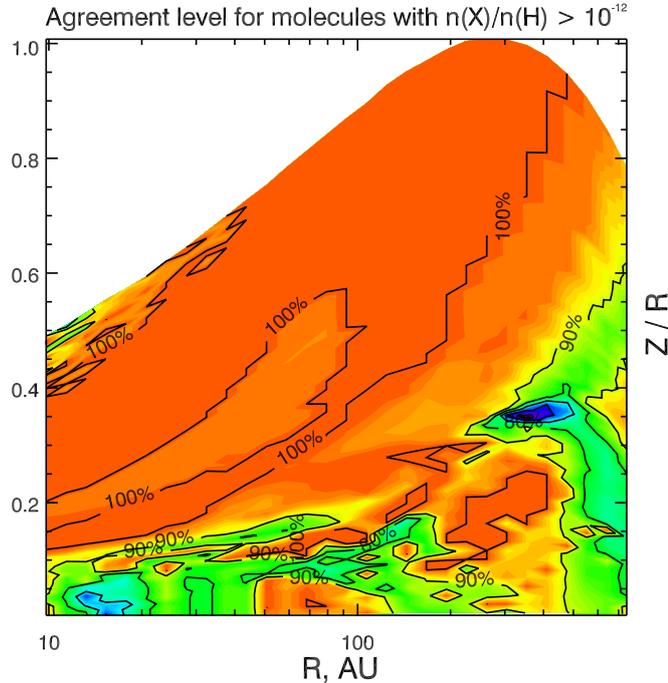
Figure 4.7 Agreement map for RE and MRE approaches in case with tunneling, $a_{gr} = 10^{-5}$ cm.

affected by the stochastic effects. It is even more true for highly-ionized hot disk atmosphere, where disk chemistry is regulated by a short loop of ionization-recombination reactions.

The agreement level over the disk can be as low as $\sim 70\%$, that is $\sim 30\%$ of species are sensitive to stochastic surface processes. This group of sensitive molecules include several abundant and important observable species: CH_3OH, $HCOOH$, NH_3, NH_3 ice, CO_2, CO, H, H_2CO, C_2H_2 ice. However, the vertical column densities of most of these species do not change substantially. This is due to the fact that their abundances are sensitive to stochastic processes only over localized disk zones (e.g., in the inner disk midplane, $R \sim 20$ AU), and often regions of the maximal disagreement do not coincide with regions of maximal molecular concentrations.

We found only two abundant species which column densities are affected by the stochastic effects significantly. These are ammonia NH_3 (see Fig. 4.8) and formic acid $HCOOH$ (see Fig. 4.9). Column densities of both species vary between 10^{10} g·cm^{-2} and 10^{13} g·cm^{-2}. Due to stochastic effects their column densities can be increased by about one order of magnitude compared with the standard RE model. Column density of NH_3
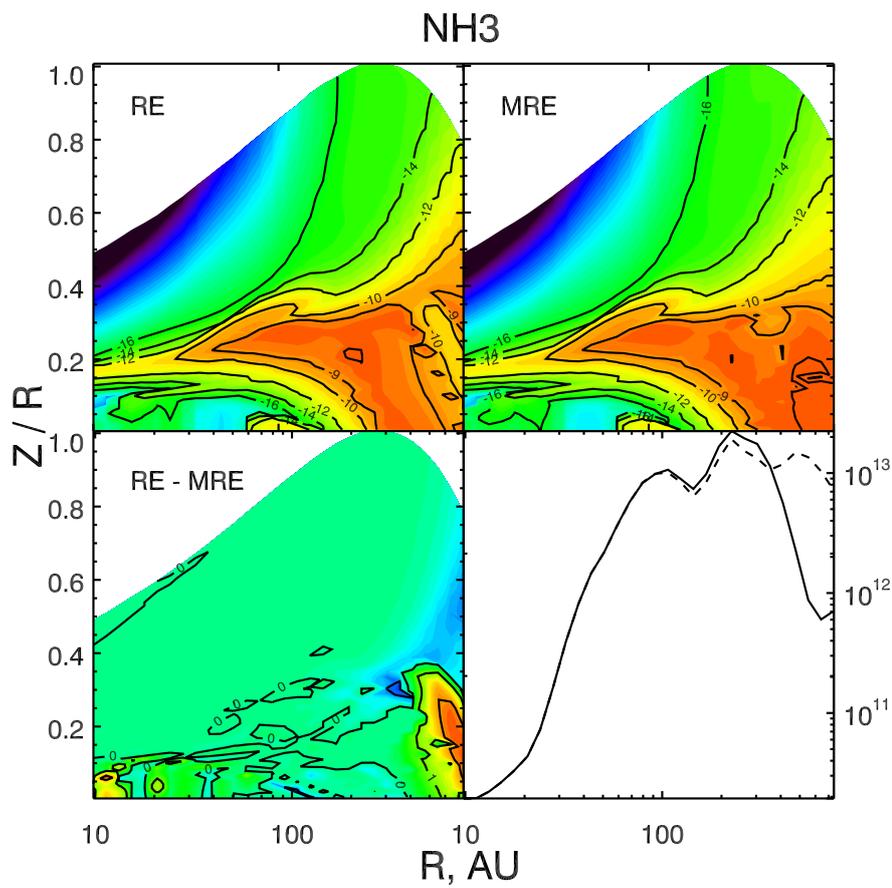
Figure 4.8 Abundances and column density of NH_3 over the disk calculated with the RE and MRE approaches. Solid line corresponds to the RE calculations, dashed line – to the MRE calculations.
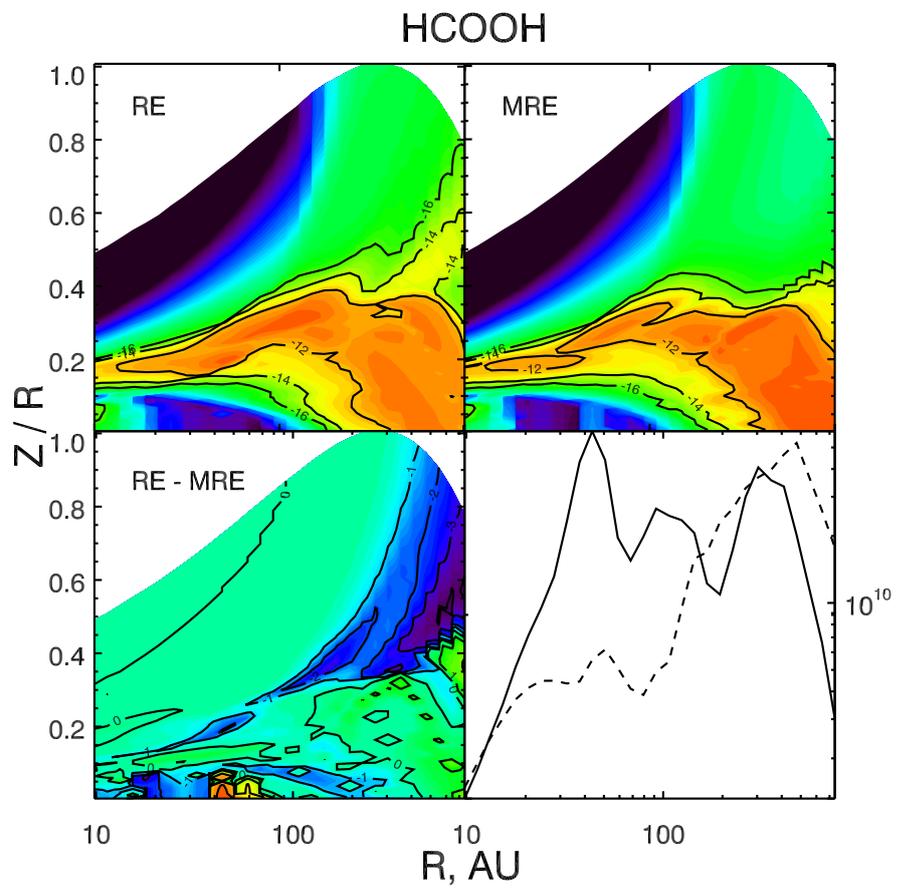
Figure 4.9 The same as in Fig. 4.8 but for HCOOH.

is enhanced in the MRE run in outer disk region: 10^{13} instead of 10^{12} at R $\geq$ 400 AU. This change is caused by higher abundance of NH$_3$ at $R \geq 500$ AU and Z/R between 0 and 0.3, X(NH$_3$)$_{MRE} \sim 10^{-9} - 10^{-8}$ while its RE abundance is only about 10^{-10}.

In the case of HCOOH the entire shape of its column density is different in the both runs. In the inner part of the disk ($R \leq 100$ AU) the HCOOH MRE column density is lower by about an order of magnitude than that of RE, while in the outer disk ($R \geq 300$ AU) it is increased by the same amount. In the inner disk regions this deviation is caused by stochasticity of surface hydrogenation reactions, where abundance of H atoms on grain surfaces is below unity per grain. In this case rate equations overestimate the efficiency of reactions with H. It leads to overproduction of HCO via surface reaction H + CO $\rightarrow$ HCO, and then to overproduction of HCOOH via OH + HCO $\rightarrow$ $HCOOH$. The MRE run leads to higher efficiency of the HCOOH formation in the outer disk region due to higher surface OH abundances, which are treated incorrectly by the RE approach.

None of other molecules detected in protoplanetary disks, like CO, CN, HCN, HNC, H$_2$CO, C$_2$H, CS, HCO$^+$, and N$_2$H$^+$ (see e.g., Dutrey et al., 2007b; Henning and Semenov, 2008)) are sensitive enough to stochastic surface chemistry to be reliable observational tracers of this process.

4.6.3   Results for Model H
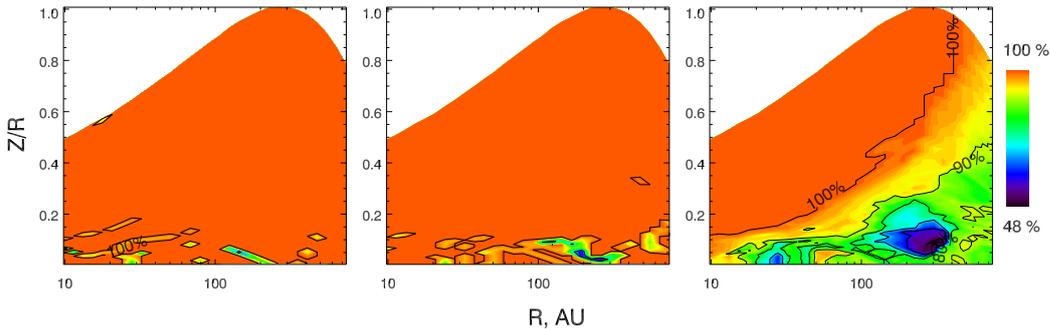
Figure 4.10 The agreement map for the RE and MRE approaches and the disk chemical model with slow surface reactions. From left to right shown are results for various grain radii: $10^{-5}, 10^{-6}, 10^{-7}$ cm.

As it was discussed in Chapter 3, Model H does not show any significant disagreement between abundances calculated with the RE and Monte Carlo approaches for

sub-micron grains (10^{-5} cm). In protoplanetary disks grains can be larger due to collisional growth, fragmentation, and sedimentation (e.g. Brauer et al., 2008a; Przygodda et al., 2003; van Boekel et al., 2005). This should lower gas-grain interaction rate and thus lead to higher probability for stochastic effects to occur in surface chemistry. Therefore, in this Section we investigate the importance of stochastic effects for disk model with slow surface processing but for grains of various sizes.

In Figure 4.10 the agreement maps for the RE and MRE calculations are presented for the grain radii of 10^{-5}, 10^{-6}, and 10^{-7} cm (0.1, 0.01, and 0.001 μm). The radius of 10^{-7} cm represents an extreme case of a PAH-dominated dust mixture and can be appropriate only in the upper disk layers where such tiny grains are kept by turbulence. For 0.1 μm grains agreement between the classical and stochastic approaches is perfect almost everywhere in the disk, except for a few isolated points in the intermediate layer (Fig. 4.10, left panel). In this disk region temperature is in range of $20 - 30$ K. This temperature range is critical for stochastic surface chemistry when reaction rates are fast, which modifies abundances of both the ices and gaseous species (Vasyunin et al., 2008). But in Model H surface reaction rates are slow, and accretion-limited stochastic regime almost never occurs.

When grain radius gets smaller ($r = 10^{-6}$ cm, Fig. 4.10, middle panel), rates of surface reactions increase as r^2, while accretion rates of gas-phase species decrease linearly with radius r (e.g., Hasegawa et al., 1992). This leads to a wider disk region where accretion-limited regime operates, and thence to moderate expansion of the disagreement zones. The largest disagreement zone is located in the lower part of the intermediate layer, between 100 and 300 AU. In this region, temperature varies between 25 and 30 K and density is $\approx 10^7 - 10^8$ cm^{-3}.

One may expect that for even smaller grains stochastic effects should become more pronounced. In the extreme case of the PAH-like tiny grains the entire picture changes dramatically (Fig. 4.10, right panel). Disagreement between the RE and MRE results appears in all disk regions where temperature is below 40 K. In the inner zone and the far-distant part of the disk the agreement level is about 90%, i.e. just some of species are reproduces incorrectly with the rate equations approach. Among them are mostly complex (organic) species that forms solely on grain surfaces, e.g. C_{10}, HC_9N, CH_3OH, HC_9N, CH_3CCH, HC_7N. The region of maximal stochasticity is located between 100

and 400 AU in intermediate layer and partly in midplane. There the agreement drops down to ~ 70.

The reason for that is similar to those described in Chapter 3 ($n_{\rm H} = 10^4$ cm^{-3}, $T = 30$ K). In this moderately warm and dense region accretion and desorption of CO is very active. At the same time, surface reactions involving CO are also active. The rate of surface conversion of CO to CO$_2$, CO + O $\rightarrow$ CO$_2$, is highly overestimated in the RE run. This inaccuracy propagates to many carbon- and oxygen-bearing species in the model, as CO is an essential molecule in the C- and O-reaction networks.

4.7   Conclusions

Main results of this study can be summarized as following:

1. For disk chemical model with fast surface reactions stochastic effects are important in almost all disk regions (apart from hot atmosphere.) But at the same time the resulting column densities of observable species do not show large deviations. The only candidates to trace a magnitude of the stochastic effects in disk chemical evolution are NH$_3$ and HCOOH. Their column densities are increased in the stochastic model by a factor of ~ 10. Similar changes in resultant column densities can be also caused by e.g. uncertainties in reaction rates, unknown physical conditions in the disk, transport processes, etc. The forthcoming observational instruments like ALMA, SOFIA, and Herschel may be able to finally resolve this puzzle.

2. Stochastic effects in the disk chemical model with slow surface reaction rates are unimportant even for sub-micron-sized dust grains. In the extreme case of the PAH-like particles some of molecular abundances become affected. However, in protoplanetary disks these tiny grains reside in the hot atmosphere and thus have no active surface chemistry. Therefore, the classical rate equations approach is appropriate for chemical modeling of protoplanetary disks if surface reaction rates are slow

In the last Chapter of the thesis we will use these findings and study chemical evolution of protoplanetary disks with grain growth and sedimentation, using the RE approach to surface chemistry.

5

Chemistry in disks with grain evolution

Content of the chapter is to appear in *Chemistry in evolving disks with grain evolution*, A.I. Vasyunin et al., The Astrophysical Journal (2010), in preparation.

5.1 Introduction

Our own existence and the presence of numerous exoplanets as well as protoplanetary disks orbiting various stars strongly suggest that the planet formation process is ubiquitous in the Milky Way (e.g., Mayor and Frei, 2003; Mayor and Queloz, 1995b; Udry and Santos, 2007). It remains one of the most challenging problems of the modern astronomy to understand how planets form. This topic covers a tremendous range of micro- and macrophysics, and involves a variety of physical, dynamical, and chemical processes.

It is now commonly believed that planets are assembled in protoplanetary disks surrounding young stars, starting from coagulation of sub-micron dust grains into larger grains and bodies (e.g., Natta et al., 2007a). The presence of micron-sized grains in disks have been found by mid-infrared spectroscopy (Apai et al., 2004; Bouwman et al., 2008, 2001; Kessler-Silacci et al., 2006; van Boekel et al., 2004) A number of nearby protoplanetary disks have been imaged at the VLA and Australia Telescope Compact Array (ATCA) at millimeter and centimeter wavelengths and show evidence of significant grain growth up to at least pebble-like (cm) sizes (Cortes et al., 2009;

5. CHEMISTRY IN DISKS WITH GRAIN EVOLUTION

Lommen et al., 2009; Rodmann et al., 2006; Wilner et al., 2005)).

Large-scale IR spectroscopic surveys of young stars in stellar clusters of various ages have placed tight constraints on typical dispersal timescales of prominent circumstellar disks of $t \sim 5$ Myr, and mass accretion rates of $\dot{M}_{Sun} \sim 10^{-8}$ M_{Sun} yr^{-1} (Haisch et al., 2001; Hernández et al., 2008; Oliveira et al., 2009; Sicilia-Aguilar et al., 2009, 2006). It has been found that the inner, planet-forming zones of some older disks are cleared of sub-micron-sized dust grains within just ~ 1 Myr (e.g., Dutrey et al., 2008; Graham et al., 2007; Salyk et al., 2009). Furthermore, the analysis of the mineralogical and chemical composition of unaltered chondritic meteorites has shown that different types of meteorites have condensed and formed via grain agglomeration within $\sim 2 - 5$ Myr in the Solar Nebula (e.g., Podosek and Cassen, 1994; Thrane et al., 2006; Wasson and Kallemeyn, 1988).

In essence, grain evolution is controlled by collisions leading to coagulation and fragmentation of dust particles, and radial drift and sedimentation to disk midplane when they become bigger ($\gtrsim 1$ cm). Grains evolve faster in dense disk interior ($\lesssim 10 - 20$ AU), while in the outer region ($R \gtrsim 100$ AU) grain ensemble may remain ISM-like for the entire lifespan of the system (Birnstiel et al., 2009; Brauer et al., 2008b; Ciesla, 2007; Ormel et al., 2007; Weidenschilling, 1997). In principle, it is reasonable to expect that the grain evolution is somehow reflected in the physical and chemical structure of the disk. Due to grain growth and sedimentation, dust opacities become lower, and stellar X-ray and UV photons penetrate more easily into the disk interior, heating it and thus preventing rapid freeze-out of molecules and increasing photodegradation of gas-phase chemical species (e.g., Aikawa and Nomura, 2006; Jonkheid et al., 2006a,b)). Also, local variations in the dust-to-gas ratio, dust density and average grain size may affect efficiency of gas-grain interaction and thus freeze-out and surface chemistry.

Jonkheid et al. (2004) have studied importance of dust settling on the disk chemical evolution, assuming that dust distribution remain the same along the disk radius. It has been found that dust and gas temperature deviate substantially in the optically-thin disk region, and that dust sedimentation has a great impact on the gas temperature in the disk. On the other hand, it does not strongly influence the gas-phase chemistry in the considered model due to the assumption that PAHs are still well-mixed with the gas and therefore efficiently absorb stellar and interstellar UV photons. At the same time,

elevated temperatures of the upper disk layer in the model with grain sedimentation lead to excitation of higher-lying transitions.

Aikawa and Nomura (2006) have studied an effect of dust growth on the chemical abundances in a well-mixed disk around a low-mass star. They have modeled dust and gas temperature of the disk self-consistently and adopted a power-law grain size distribution. The grain growth has been simulated by varying of the maximum size of the grains up to 10μm. An extended chemical network with gas-grain interactions and surface processes have been applied. Aikawa and Nomura (2006) have found that molecular column densities for many species are not affected by grain growth, despite the fact that molecular layers shift closer to the disk midplane. They have identified a few sensitive tracers of grain growth in disks, such as HCO^+, H_3^+, H_2D^+.

Later, Jonkheid et al. (2006a) have modeled chemistry and gas temperature of evolving Herbig Ae disks with decreasing mass or dust settling. They have utilized a 2D UV radiative transfer to model gas/dust temperature and photodissociation rates. It has been found that the disk chemical structure shows a strong correlation with disk mass. While some photofragile molecules like HCN are abundant only in massive disks, their fragments, like CN and CCH, become abundant in low-mass disks. Dust settling affects the gas temperature in the disk atmosphere, and thus high-temperature tracers like O and C^+. They have identified that the line ratios of $CO/^{13}CO$, CO/HCO^+ and [OI] 63μm/146μm can be used to distinguish between disks with undergoing grain evolution and photoevaporative disks.

In the present work we focus on the effects of dust evolution on the chemistry in the protoplanetary disk around a T Tauri star. We employ a large gas-grain chemical network with surface reactions, and realistic 2D dust distribution from the modeling results of Birnstiel et al. (2009). In the grain evolutionary model dust coagulation, fragmentation, and sedimentation are taken into account, assuming the equilibrium between turbulent stirring and gravitational settling as proposed in Dullemond and Dominik (2004).

To better assess the importance of different factors for the disk chemical structure (UV strength, average grain size), we consider 4 different dust models: (1) Model S5 is the "standard" model with dust particles having single radius of 10^{-5} cm and dust-to-gas mass ratio of 0.01, (2) Model D is the model with detailed treatment of dust evolution, (3) Model DAv is the same as Model D but without updated modeling of

the UV penetration into the disk, and (4) Model S4 is the "a poor man's grain growth" model where grain evolution is crudely approximated by a uniform increase of the grain size by one order of magnitude (and without taking sedimentation into account).

As we have already mentioned, evolution of grain size distribution and sedimentation affect chemistry in two ways. First, these processes lead to evolution of opacities and, thus, result in different rates of photoprocesses. Second, changes in the properties of the dust ensemble may affect rates of surface reactions and gas-dust exchange rates. The reason to introduce Model DAv is to separate the influence of these two factors.

5.2 Model outline

Since chemical evolution of the disk depends on its physical structure, in this study we employ four-step approach to derive disk temperature and density. First, we calculate disk thermal and density structure using a D'Alessio-like 1+1D steady-state model. Second, evolution of dust grain ensemble in the disk due to grain coagulation, fragmentation and sedimentation is modeled according to Birnstiel et al. (2009). Fast timescale of grain evolution ($\sim 10^3$-10^5 yrs) allow us to utilize the final steady-state dust distribution for chemical simulations. Third, vertical structure of the dust in the disk is reconstructed using the outcome of the first two models of Dullemond and Dominik (2004). At this step, we obtain mean grain size from calculated grain size distribution in each disk cell, as well as dust-to-gas ratios and visual extinctions. As a final step, we computed the chemical structure of the disk at $t = 2$ Myr.

Our disk evolutionary model is still not fully consistent, yet it is a major step forward in chemical modeling of evolving protoplanetary disks. For example, we do not separate between dust and gas temperature, which is not valid for very upper disk layer. We also do not iteratively update the vertical gas structure when dust distribution changes. All these effects are important for accurate estimation of the temperature in disk atmosphere but not so much for molecular layers.

5.2.1 Disk model

5.2.1.1 Overall disk structure

A popular formalism, which is used in many studies of disks surrounding young stars, is based upon the so-called α-model of Shakura and Sunyaev (1973). In this model it

is assumed that transport of angular momentum in the disk is caused by the turbulent viscosity, with the viscosity coefficient ν expressed as $\alpha H c_{\rm s}$, where H is the disk semi-thickness at a given radius, $c_{\rm s}$ is the isothermal sound speed, and α is the viscosity parameter, which is usually assumed to be of the order of 10^{-2}.

The disk structure is calculated with a simplified version of the disk model by D'Alessio et al. (1998) and D'Alessio et al. (1999b). Unlike D'Alessio et al., in the calculation of gas temperature we take into account only two heating sources, namely, viscous dissipation and disk irradiation by the central star. Thorough comparison of our disk models with the D'Alessio et al. results shows that this simplification does not hamper derived disk physical structure, and thus chemistry modeling is accurate.

The following equations are used to describe the disk vertical structure:

$$\frac{dP}{dz} = -g\rho, \tag{5.1}$$

$$\frac{dT}{dz} = -\frac{3\kappa\rho F}{4acT^3}, \tag{5.2}$$

$$\frac{dF}{dz} = \frac{9}{4}\alpha P \Omega(R) + \Gamma_{\rm irr}. \tag{5.3}$$

Here P is the gas pressure, g is the gravity acceleration, ρ is the gas density, T is the gas temperature, F is the flux of the disk thermal emission, $\Omega(R)$ is the disk angular (Keplerian) velocity at a distance R from the central object, and $\Gamma_{\rm irr}$ is the heating rate due to disk irradiation by the central object.

Two-dimensional structure of the disk is modeled in the so-called 1+1D approximation. It is assumed that at each radius the disk is in the hydrostatic equilibrium (Eq. 5.1). Thus, the disk vertical structure can be found from the solution to the expressions (5.1–5.3) independently at each R. To calculate the disk temperature at each vertical slice we integrate the transfer equation (5.2) in the Eddington approximation. First term in the right hand side of equation (5.3) gives the viscous heating of the disk. The disk is described by the following parameters:

- accretion rate $\dot{M}$;

- viscous parameter α;

- temperature, radius, and mass of the central object T_*, R_*, M_* (radiation is assumed to be that of a black body);

- inner and outer disk radii R_{in} and R_{out}.

Output of the model are gas surface density distribution $\Sigma_{gas}(R)$, and the 2D structure of gas density and temperature. Strengths of the UV and X-ray fields over the disk can be calculated separately using the data about dust properties in the disk.

5.2.1.2 Model of dust evolution in the disk

Grain growth model Several authors have constructed theoretical models for grain growth in protoplanetary disks (e.g. Nakagawa et al., 1981; Weidenschilling, 1997; Dullemond and Dominik, 2005; Ormel et al., 2007; Zsom and Dullemond, 2008; Brauer et al., 2008a). The main challenges of modeling grain growth are the following:

First, growth from e.g. sub-micrometer grains to centimeter-sized grains involves already 15 orders of magnitude, which is more than the numerical precision of *double-precision* computer variables. Still, the codes must be able to conserve mass, since large particles could grow by accreting large numbers of very small grains.

Second, particle size is not the only parameter determining the properties of grains: porosity, composition and the various possible outcomes of collisions further extend the parameter space (see Guettler et al., in prep.).

Here, we use a slightly modified version of the code presented in Brauer et al. (2008a), a statistical, mass conserving code which implicitly solves the Smoluchowski equation, taking coagulation, fragmentation and cratering into account. It is important to note that we ignore radial drift of dust particles in the present study.

Mathematical formalism of the model is the following.

The number density distribution $n(m, r, z)$ is a function of mass m, radius r, height above the midplane z, and time. We define the vertically integrated number density per mass m as

$$N(m,r) \equiv \int_{-\infty}^{\infty} n(m,r,z)\,\mathrm{d}z. \tag{5.4}$$

By assuming the coagulation and fragmentation Kernels K and L (defined below) to be independent of z and the dust to be distributed according to

$$n(m,z) = \frac{N(m)}{\sqrt{2\pi}\,h(m)} \exp\left(-\frac{z^2}{2\,h^2(m)}\right), \tag{5.5}$$

Table 5.1 Notation

parameter	symbol
speed of sound	c_{s}
Kepler frequency	Ω_{K}
gas scale height	$H_{\mathrm{p}} = \frac{c_{\mathrm{s}}}{\Omega_{\mathrm{K}}}$
the turbulence parameter	α
solid density of dust grains	ρ_{s}
gas surface density	Σ_{g}
grain size	a
Stokes number	$\mathrm{St} = \frac{a\rho_{\mathrm{s}}}{\Sigma_{\mathrm{g}}} \cdot \frac{\pi}{2}$
number density	n
Vert. integrated number density	N
fragmentation velocity	u_{f}
relative particle velocity	Δu
geometric cross section	$\sigma = \pi(a_1 + a_2)^2$
coagulation Kernel	K
fragmentation Kernel	L
distribution of fragments	S
coagulation probability	p_{c}
fragmentation probability	p_{f}

with the dust scale height given by

$$h_{\mathrm{d}} = H_{\mathrm{p}} \cdot \min\left(1, \sqrt{\frac{\alpha}{\min(\mathrm{St}, \frac{1}{2})(1 + \mathrm{St}^2)}}\right),\qquad(5.6)$$

we can now describe the time-evolution of this distribution by a vertically integrated version of the Smoluchowski equation

$$
\begin{aligned}
\frac{\partial N(m)}{\partial t} \;=\; & +\int_0^{m/2} N(m')\,N(m-m')\,K(m',m-m')\,\mathrm{d}m' \\
& -\int_0^\infty N(m')\,N(m)\,K(m,m')\,\mathrm{d}m' \\
& +\tfrac{1}{2}\iint_0^\infty N(m')\,N(m'')\,L(m',m'')\,S(m,m',m'')\,\mathrm{d}m'\,\mathrm{d}m'' \\
& -\int_0^\infty N(m')\,N(m)\,L(m,m')\,\mathrm{d}m',
\end{aligned}
\qquad(5.7)
$$

where the radial dependence was omitted since we treat each radius independently, neglecting radial motion of dust. The right-hand side terms of Eq. 5.7 (from top

to bottom) correspond to gain and loss by coagulation and gain and loss through fragmentation.

The coagulation kernel $K(m, m')$ and the fragmentation kernel $L(m, m')$ are then given by

$$
\begin{aligned}
K(m, m') &= \frac{1}{\sqrt{2\pi(h^2 + h'^2)}} \cdot p_c \cdot \sigma(m, m') \cdot \Delta u(m, m') \\
L(m, m') &= \frac{1}{\sqrt{2\pi(h^2 + h'^2)}} \cdot p_f \cdot \sigma(m, m') \cdot \Delta u(m, m'),
\end{aligned}
\tag{5.8}
$$

with p_c and p_f being the coagulation and fragmentation probabilities, respectively, which sum up to unity. In this work, we consider Brownian motion, relative radial motion, vertical settling (see Brauer et al., 2008a), and turbulent motion (see Ormel et al., 2007) as physical effects that produce the relative particle velocities.

Particles colliding with a relative velocity higher than the critical velocity u_f, are assumed to fragment into a power-law size distribution of fragments (i.e., $S(m, m', m'') \propto m^{-1.83}$, see Brauer et al., 2008a) if the particle masses differ by less than one order of magitude. Otherwise the smaller body is assumed to excavate mass from the larger one by cratering where the amount of excavated mass equals the mass of the smaller body. The fragmentation velocity u_f is a free parameter in our model, and unless otherwise noted is taken to be 10 m/s.

This model connected with model of gas disk structure through just two input parameters: radial midplane temperature distribution $T_{mid}(R)$ and radial gas surface density distribution $\Sigma_{gas}(R)$. A more comprehensive description of the physics of coagulation/fragmentation and of the numerical implementation can be found in Brauer et al. (2008a).

Vertical dust distribution   The numerical model described above provides us with the gas surface densities of grains of different masses integrated over vertical direction. To calculate the vertical dust distribution $\rho_i(R, z)$ we assume that vertical distribution of grains is dictated by the equilibrium between gravitational settling and turbulent stirring as proposed in Dullemond and Dominik (2004). Grain size distribution for the chemistry calculations was obtained from the equilibrium grain surface density distribution.

Average grain properties   In astrochemical calculations presented in previous chapters of this thesis, dust is characterized by the two parameters: dust-to-gas mass ratio of 0.01 and a single constant grain radius of 0.1μm, representing an average grain size from the ISM grain size distribution. Model of dust evolution described above gives us the evolution of grain size distribution function across the disk with time. In our spatially local chemical model grains are represented as spheres of equal size with certain mass and total dust-to-gas mass ratio. Hence, in the formalism of our chemical model, dust evolution in any isolated volume can be described as evolution of mean grain size and dust-to-gas mass ratio with time. Dust-to-gas mass ratio was obtained as described in previous paragraph. Calculation of mean grain size from grain size distribution was done following the assumption that total surface area and mass of a "mean" grain should be equal to those of grains from distribution obtained from dust evolution model.

Let's introduce a grain size distribution $f(a)$ such that $f(a)da$ is the number of grains with radii from a to $a + da$. The total number of grains per unit volume is then

$$n_{tot} = \int_{a_{min}}^{a_{max}} f(a)da. \tag{5.9}$$

This average particle should allow to retain two main characteristics of the dust distribution, namely, the total dust mass and total grain surface area in the unit volume:

$$\frac{4}{3}\pi\overline{a}^3\overline{n} = \frac{4}{3}\pi \int_{a_{min}}^{a_{max}} f(a)a^3da, \tag{5.10}$$

$$4\pi\overline{a}^2\overline{n} = 4\pi \int_{a_{min}}^{a_{max}} f(a)a^2da, \tag{5.11}$$

where $\overline{n}$ is the total number density of "representative" particles. By dividing eq. 5.10 by eq. 5.11 one can obtain

$$\overline{a} = \frac{\int_{a_{min}}^{a_{max}} f(a)a^3da}{\int_{a_{min}}^{a_{max}} f(a)a^2da}. \tag{5.12}$$

Mean grain radius $\overline{a}$ defined in such a way conserves total grain mass and surface area in a unit volume. We use it in our astrochemical model below every time when dealing with gas-grain interactions and surface chemical processes.

5.2.2 Chemical model

Modeling time-dependent evolution of disk chemistry with grain evolution requires a non-local chemical model. That is due to the fact that grains not only grow but also move within the disk due to e.g. sedimentation and radial drift (Brauer et al., 2008a, e.g.). Since gaseous molecules can accrete onto dust grains in cold disk regions and form icy mantles, one has to take transport terms into account in chemical rate equations describing evolution of molecular concentrations. Coupled chemo-dynamical disk models are computationally expensive and are hard to analyze from chemical point of view, so in the present study we neglect these effects. Thus we consider a chemical structure of the disk in which dust properties and physical conditions are taken from the final step of the time-dependent disk model with dust evolution due to grain growth and sedimentation ($t = 2$ Myr). For each disk cell local dust grain distributions are assumed to be uniformly-sized, with the averaged radius of the dust population and appropriate variable gas-to-dust ratio. Using this disk modeling setup, we calculated the structure of a low-mass protoplanetary disk around a low-mass T Tauri star. We utilize the chemical model described in Vasyunin et al. (2008) to simulate chemical evolution of the disk over 2 Myr.

5.3 Results and Discussion

A DM Tau-like system is modeled. The disk has a radius of 700 AU, an accretion rate $\dot{M} = 2 \cdot 10^{-9}\,M_\odot\,\mathrm{yr}^{-1}$, and a viscosity parameter $\alpha = 0.01$. The disk is illuminated by the UV radiation from the central star with an intensity $G = 410\,G_0$ at $R = 100$ AU ($G(R)$ represents the mean IS UV field of Draine 1978) and by the interstellar UV radiation in a plane-parallel geometry. The disk mass is $M = 0.055\,M_\odot$. The density and thermal structure of the disk are shown in Fig. 5.2. The disk surface density profile and its power-law approximation are depicted in Fig. 5.1. The best-fit line has a slope of 0.84, which is somewhere in between of the Minimum Mass Solar Nebula index of 1.5 (Hayashi, 1981; Weidenschilling, 1977) and the value derived for PPDs from Spectral Energy Distribution (SED) at millimeter wavelengths, ≥ 0.5 (Andrews and Williams, 2007).

Figure 5.1 Total surface density in the disk (solid line) and its best power-law fit (dashed line)
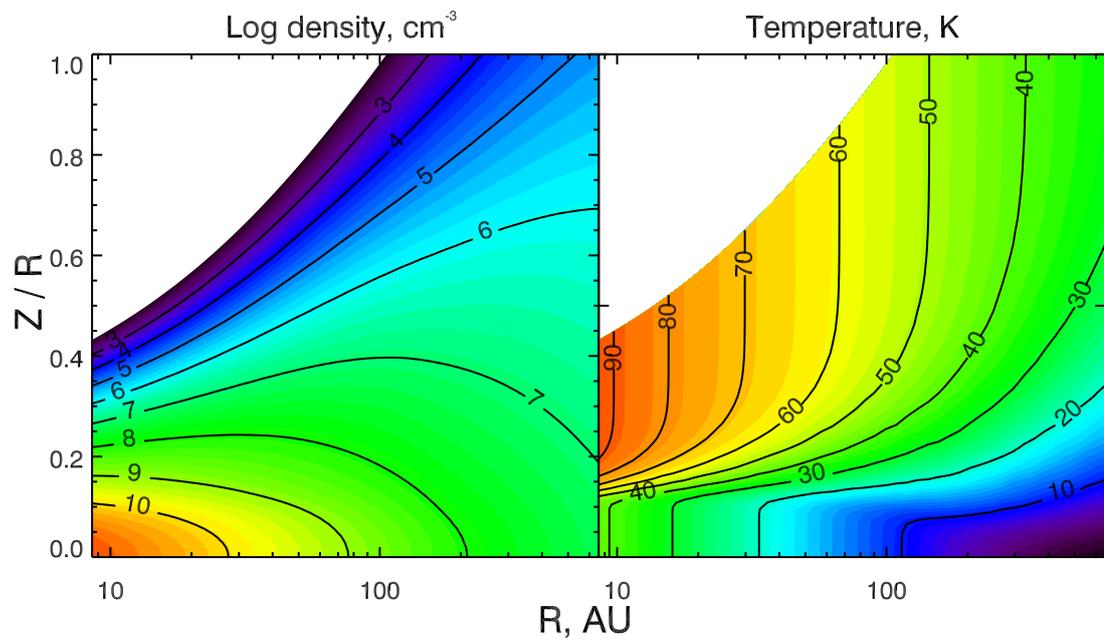
Figure 5.2 Density and temperature distribution in the disk.
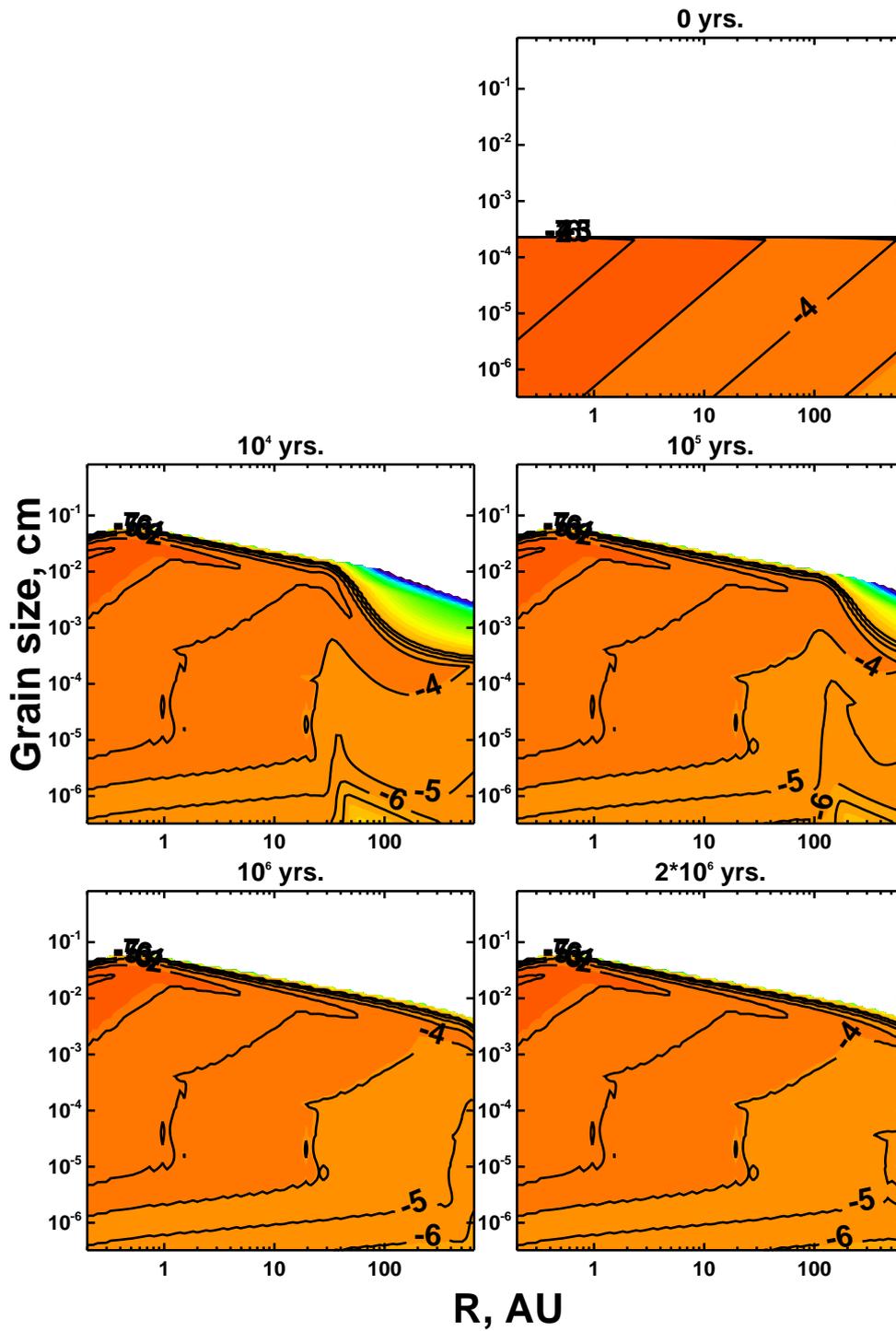
Figure 5.3 Evolution of surface density $(\mathrm{g\,cm^{-2}})$ of growing dust in the disk
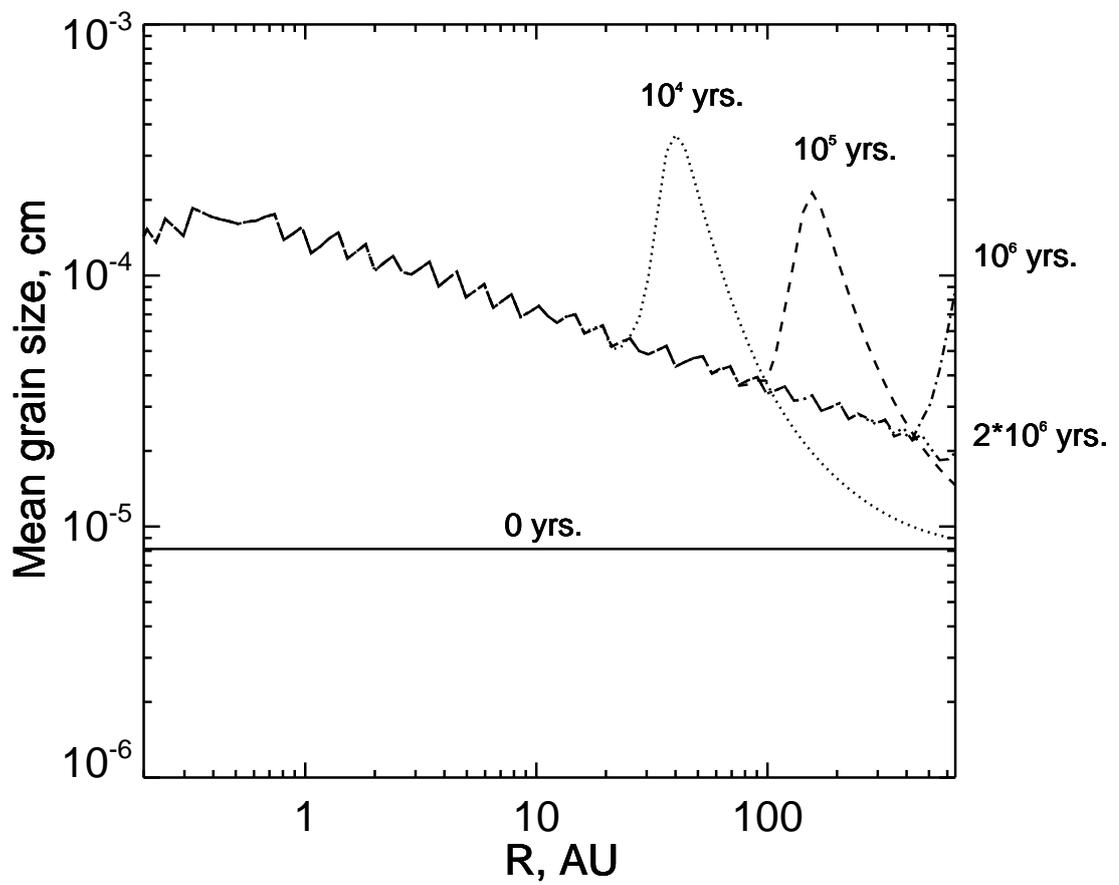
Figure 5.4 Radial distribution of the vertically-integrated average grain radius at different time moments. Averaging is performed such that the total grain mass and surface area are preserved.

5. CHEMISTRY IN DISKS WITH GRAIN EVOLUTION

5.3.1 Dust evolution in the disk

Using the model of grain growth in the disk described in Section 5.2.1.2, we calculated the evolution of surface densities of grains of different masses for 2 Myr, assuming the standard MRN grain size distribution at $t = 0$. (Mathis et al., 1977). Snapshots of surface densities of grains of distinct sizes at various time moments are shown in Fig. 5.3. The corresponding vertically-integrated average grain radius calculated according to eq. 5.12 is shown in Fig. 5.4.

Since disk density is higher closer to the star, the grain growth proceeds faster there. One can see that at $R \leq 30$ AU a steady-state in the grain surface density distribution is reached in less than 10^4 yrs. In outer disk ($R \geq 100$ AU) grain surface density evolves much slower. A steady-state distribution is barely reached there within 10^6 yrs. In our model we do not consider fast radial drift of mm-sized grains, and thus in the inner disk region a steady-state is quickly attained. It is important to point out that the maximum surface density in Fig. 5.3 corresponds to grains which are bigger than the average particle size shown in Fig. 5.4. It is in these large grains most of the dust mass is contained, while small grains dominate the dust surface area.

Therefore, the presence of small grains in the disk significantly reduces the net effect of grain growth for the point of view of gas-grain interactions. The largest increase in the averaged grain size is only by the factor of 10 and is achieved in the inner disk midplane ($R \geq 10$ AU). In the outer disk region average grain radius increases by a modest factor of 3 only ($R \geq 100$ AU). This result implies that the grain growth in low-mass disks could be hard to discover from interferometric observations of molecular lines.

In contrast, differential dust settling seems to be much more important both for the disk structure and its chemical evolution. In Fig. 5.5 2D distributions of the total dust-to-gas mass ratio and mean grain sizes are shown.

Dust settling in the disk leads to the reduction of the dust-to-gas mass ratio in disk regions above the midplane. Everywhere above $Z/R \geq 0.05$ dust-to-gas mass ratio is significantly below the canonical value of 0.01. In chemically rich intermediate layer it varies between 0.001 and 0.01, while in the disk atmosphere it drops down to $10^{-4} - 10^{-5}$. At the same time, in the midplane dust-to-gas mass ratio value can reach 0.02. Similarly, the mean grain radius is getting smaller above the midplane, though
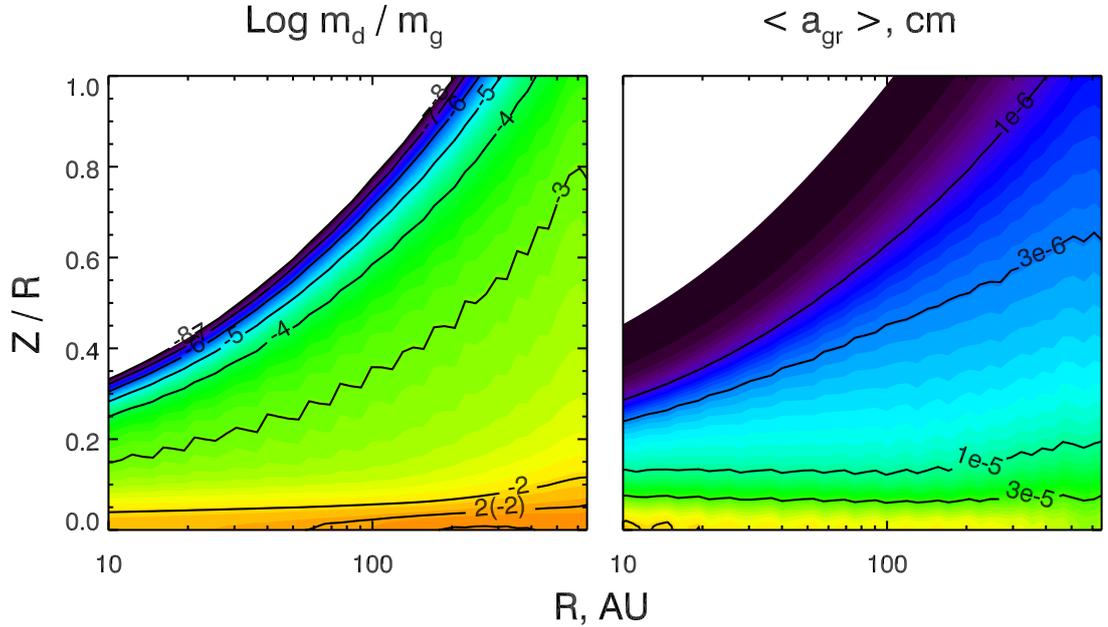
Figure 5.5 2D distributions of dust-to-gas ratio and average grain size over the disk.

its change is not that dramatic. The biggest grain radius is $3 \cdot 10^{-5}$ cm in the midplane and 10^{-6} cm in the atmosphere.

The overall effect of the grain growth and sedimentation in our disk model is the global decrease of the total surface area of dust grains (see Fig. 5.6). It is not that significant in the outer part of the disk ($R \geq 100$ AU), a factor of 2-3 only. In the inner disk region ($R \leq 100$ AU) the decrease of the dust surface area is more prominent, up to one order of magnitude. Note that the ratio of new to old grain surface area has steeper radial dependence than variations in the vertical direction.

5.3.1.1   UV field in the disk

In our model, disk is illuminated by both the stellar and interstellar UV radiation. For the disk chemistrythe strength and the shape of the UV field is of primary importance as it controls the rates of photoionization and photodissociation and efficiency of photodesorption of grain mantles (e.g., Bourdon et al., 1982; Öberg et al., 2007; van Zadelhoff et al., 2003a; Westley et al., 1995). Due to the presence of dust, the UV field is attenuated upon penetration deeply into the disk. In terms of simple 1D-slab model visual extinction A_V for the UV radiation at any disk location can be described
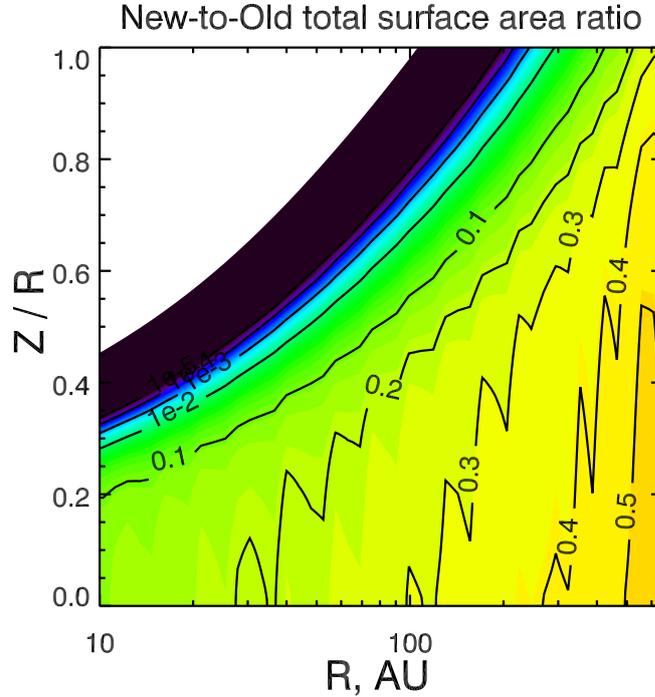
Figure 5.6 Ratio of the total grain surface area in Model D to that in Model S5.

as follows:

$$A_{\mathrm{V}} = \frac{N_{\mathrm{H}}}{f_d} \frac{mag}{cm^{-2}} \tag{5.13}$$

where N_{H} is the column density of hydrogen nuclei between star and disk location and the factor f_d is the hydrogen column density producing the visual extinction of 1 (Aikawa et al., 2002). In the case of the standard uniform 0.1μm spherical grains and dust-to-gas mass ratio of 0.01 $f_d = 1.59 \cdot 10^{21}$ cm^{-2} (Draine and Lee, 1984b). We re-calculate the value of f_d in every disk cell with respect to the local dust properties.

In Fig. 5.7 the distribution of the UV strength over the disk is shown (in units of the interstellar UV radiation field). In both models with crude and accurate treatment of grain growth the disk becomes more transparent to the impinging UV radiation. While in Model S5 (top left panel) one can clearly see the dark zone at the disk midplane (up to $Z/R = 0.15$), in Models D and S4 this region is significantly shrunk. In both evolutionary models, the midplane can be divided into two parts. Inner part at $R \leq$ 100 AU remains as opaque to UV as in the standard model, while the outer midplane hardly can be called "dark" anymore. In Model S4 the UV strength in this region is
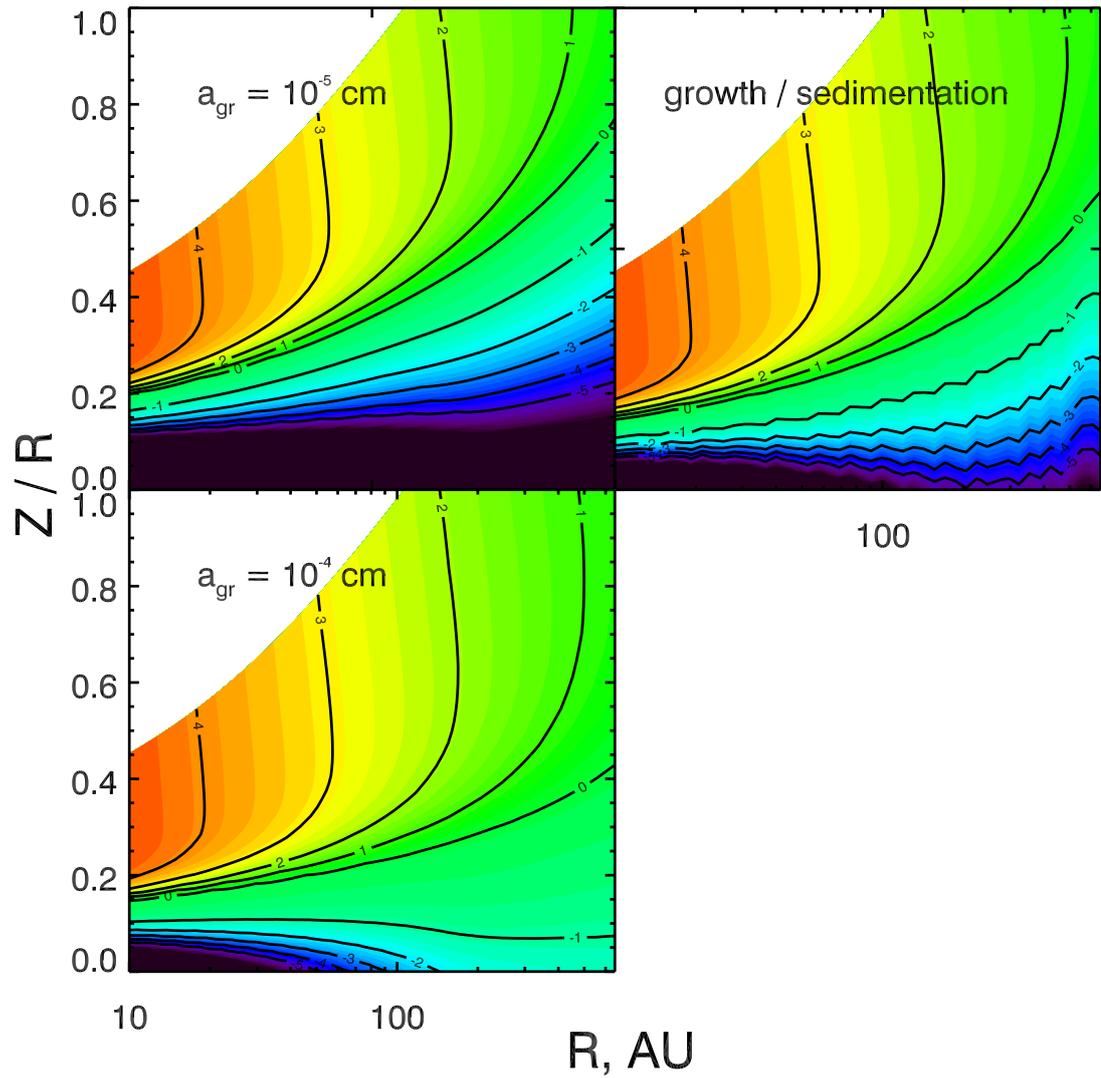
Figure 5.7 Distribution of the UV intensity in units of the Draine IS UV intensity over the disk. (Top to bottom) Shown are Model S5, Model D, and Model S4

$\approx 10^5$ times higher than in Model S5. Thus the outer disk consists of only two layers: the atmosphere and the moderately UV-illuminated intermediate layer. In Model D it is not so transparent. The inner dark region of midplane is narrower in comparison to that in Model S5. The UV strength in the outer disk region is higher than in Model S5 by a factor of $10 - 10^3$, and is only a small fraction of the UV strength in the intermediate layer. Therefore, three-layered disk chemical structure is preserved in Model D but midplane is rather "dim" than "dark".

5.3.2 Chemistry in the disk: importance of dust evolution

As we have shown in previous sections, changes in the dust opacities and the UV irradiation rates in Model D with grain evolution are significant compared to the canonical Model S5. To investigate importance of grain evolution for disk molecular structure, we focus on tracers of density, temperature, ionization degree, etc. that have been detected (CO, CS, N_2H^+, (Dutrey et al., 2007a)) or expected to be detected soon (H_2O, H_3^+, C^+). The influence of the grain growth on the electron concentrations in the disk is also interesting.

In Fig. 5.8–5.15 computed distributions of molecular abundances and vertical column densities for several observationally important species are shown. The left top panel corresponds to Model S5 where dust grains are single-sized olivine spheres of the 10^{-5} cm radius and the dust-to-gas mass ratio is 0.01 everywhere over the disk. The left middle panel depicts the most advanced Model D with the grain growth and sedimentation. In the top middle panel we show Model DAv, that is, the same disk model as in the left middle panel but with the UV field from Model S5, and the right top panel shows the "poor man's" grain growth Model S4 with the big uniform grains of 10^{-4} cm. In the right middle panel the corresponding molecular column densities are presented. The relative molecular abundances for all models at $R = 10$, 100, and 550 AU are drawn in the bottom row.

As can be clearly seen, essentially all considered species exhibit an increase in the column densities in Model D compared to Model S5. This is due to easier UV penetration into the disk interior caused by the sedimentation of growing particles toward the midplane. Increased rate of photodesorption enhance interactions between gas-phase species and surface molecules. On the other hand, gas densities are so high in protoplanetary disks, while grain growth in our model is still moderate, that efficiency of

surface processes is not much affected. Thus, from chemical perspective grain evolution shifts molecular layers closer to the dense midplane, and makes these layers broader (see bottom rows in Fig. 5.8–5.15). Lower UV opacities in the disk lead to greater photoionization rates and, consequently, higher ion abundances. This effect is also discussed in Aikawa and Nomura (2006) and Jonkheid et al. (2006a). Note that grain evolution proceeds rapidly in the planet-forming disk region at $R \leq 20 - 50$ AU. It is the disk region where increase of the molecular column densities is most pronounced.

Below some interesting cases are investigated in detail. The CO molecular layer is broadened by the grain growth, in particular in Model S4 without sedimentation (Fig. 5.8). Enhanced photodesorption rates toward the midplane slow down substantially the surface recombination of CO and O into CO_2. Thus, more CO molecules can be retained in the gas-phase. This effects is most prominent in Model S4. Overall increase of the CO column densities is not large: by the factor of ≈ 3 in Model D, and by one order of magnitude in Model S4.

Similar behaviour is demonstrated by the abundances and column densities of N_2H^+, NH_3, CS, and H_2O. While in Model S5 their column densities decrease toward the inner disk, in models with grain growth these column densities are almost constant. This is again the manifestation of the faster grain evolution in disk interior with respect to the outer region ($R \geq 50 - 100$ AU). Model S4 tends to overestimate this increase of the column densities. The same is true for many other, less abundant molecules, including those that are mainly produced on dust grains. Thus, within the framework of our modeling approach, the most important factor for chemical evolution in protoplanetary disks with grain growth is the change in the UV intensity.

Naturally, disk ionization degree is also increased in the models with grain growth (see Fig. 5.13). In all models the fractional ionization is the same in the disk atmosphere where chemistry is essentially dust-free. The dominant charged ion there is C^+ (see Fig. 5.12). In the intermediate layer complex molecular ions (e.g., HCO^+, N_2H^+, H_3^+) dominate the electron concentration. As their abundances do partly depend on the gas-grain interactions, the electron abundances become sensitive to the adopted dust properties. Differences between electron concentrations calculated with Model D and Model S4 can be as high as two orders of magnitude. The advanced grain evolutionary models are especially important for correct estimations of the boundary of the "dead" zone in disks.

Protonated dihydrogen H_3^+ behaves differently (see Fig. 5.14). In Aikawa and Nomura (2006) this ion is indicated as one among a few species sensitive to the grain growth process. In our study, Model S4 is similar to the model of Aikawa and Nomura (2006), and the results are comparable. However, in Model D the column density of H_3^+ does not change substantially in comparison with Model S5 . The formation of H_3^+ proceeds in two steps, (1) ionization of H_2, and (2) reaction of H_2^+ with H_2.

The destruction of H_3^+ is mainly by dissociative recombination with electrons, and ion-molecule reactions with CO, CN, and other radicals. Model S4 is the most transparent for the UV photons and hence most ionized. Higher electron concentration leads to faster recombination of H_3^+. Also, in this model molecular layers are wider and thus protonation reactions involving H_3^+ are active in a broader disk zone. In Model D a significant fraction of small grains remains, making it not that extremely UV-transparent as in the crude-growth case. Thence, the abundance of H_3^+ is not sensitive to grain evolution in Model D.

How reliable are these results? Strong points of our model is the detailed treatment of grain evolution based on the recent results of Birnstiel et al. (2009); Brauer et al. (2008a), and the large-scale gas-grain chemical model (Semenov et al., 2005; Vasyunin et al., 2008). For the fist time we calculated 2D distributions of *evolved* dust in the disk by coupling the results of the robust grain growth simulations with the vertical dust structure for an non-isothermal disk. Shortcomings of our model are the absence of truly time-dependent updates to the disk structure due to grain evolution, and the equality of dust and gas thermal structures. Another important issue is the absence of PAHs in our model, which could be an important source for scattering the UV photons off the disk (e.g., Jonkheid et al., 2004, 2006b). These macro-molecules should efficiently freeze-out onto dust grains everywhere in the disk apart from the hot atmosphere. It remains to be investigated whether grain growth, sedimentation, and turbulent stirring can leave a substantial fraction of these particles in the intermediate molecular layer.

5.4 Conclusions

We investigated the chemical evolution of the protoplanetary disk around the T Tauri star. The disk thermal and density structures are calculated with a 1+1D α-model. The processes of grain coagulation, fragmentation, and sedimentation are modeled as

described in Brauer et al. (2008a). The initial dust ensemble is the standard MRN grain size distribution (Mathis et al., 1977). Using the final grain size distribution (at $t = 2$ Myrs) and the 1+1D disk structure, we calculated vertical dust distribution in the disk assuming mixing-settling equilibrium according to Dullemond and Dominik (2004). For this distribution we calculated the UV strength over the disk and simulated its chemical evolution over 2 Myr. Modeling results of four dust models were compared: (1) the classical dust model with uniform spherical particles of 0.1μm and the gas-to-dust mass ratio of 100 (Model S5), (2) the "poor man's" grain growth model with bigger grains of 1μm (Model S4), (3) the detailed grain growth model (Model D), and (4) the model in which grains evolve but the UV irradiation rate remains as in the model (1) (Model DAv). The main results of the work can be summarized as follows:

- Grain growth in low-mass T Tauri disks at distances $\geq 20 - 50$ AU is limited and leads to the increase of the average grain size by not more than one order of magnitude. After 2 Myrs of evolution the average grain size in the disk varies between 10^{-4} cm at $R = 10$ AU to $2 \cdot 10^{-5}$ cm at $R = 550$ AU, and dust-to-gass mass ratios are between $\sim 10^{-6}$ and 0.02.

- The net effect of the dust settling and growth is the reduction of the total grain surface, and higher UV irradiation rates. Chemical structure of an evolved disk still has three layers, but the intermediate molecular layer gets wider and moves closer to the midplane. Abundances and column densities of many species are enhanced even by such a moderate grain growth, by a factor of $3 - 100$. As the column densities of observational tracers become larger in the disk with large grains, from observational point of view such a disk is indistinguishable from a more massive younger disk with pristine grains.

- Simple "poor man" model of grain growth in which dust-to-gas mass ratio kept to be constant and grain size simply increased by a certain factor, e.g. by 1 order of magnitude is not sufficient to reproduce chemical evolution of a disk with evolving dust. For example, column density of H_3^+ which is proposed as a sensitive species to grain growth in Aikawa and Nomura (2006) indeed exhibits high sensitivity to grain growth in simple model but not in model with detailed treatment of grain growth and sedimentation.
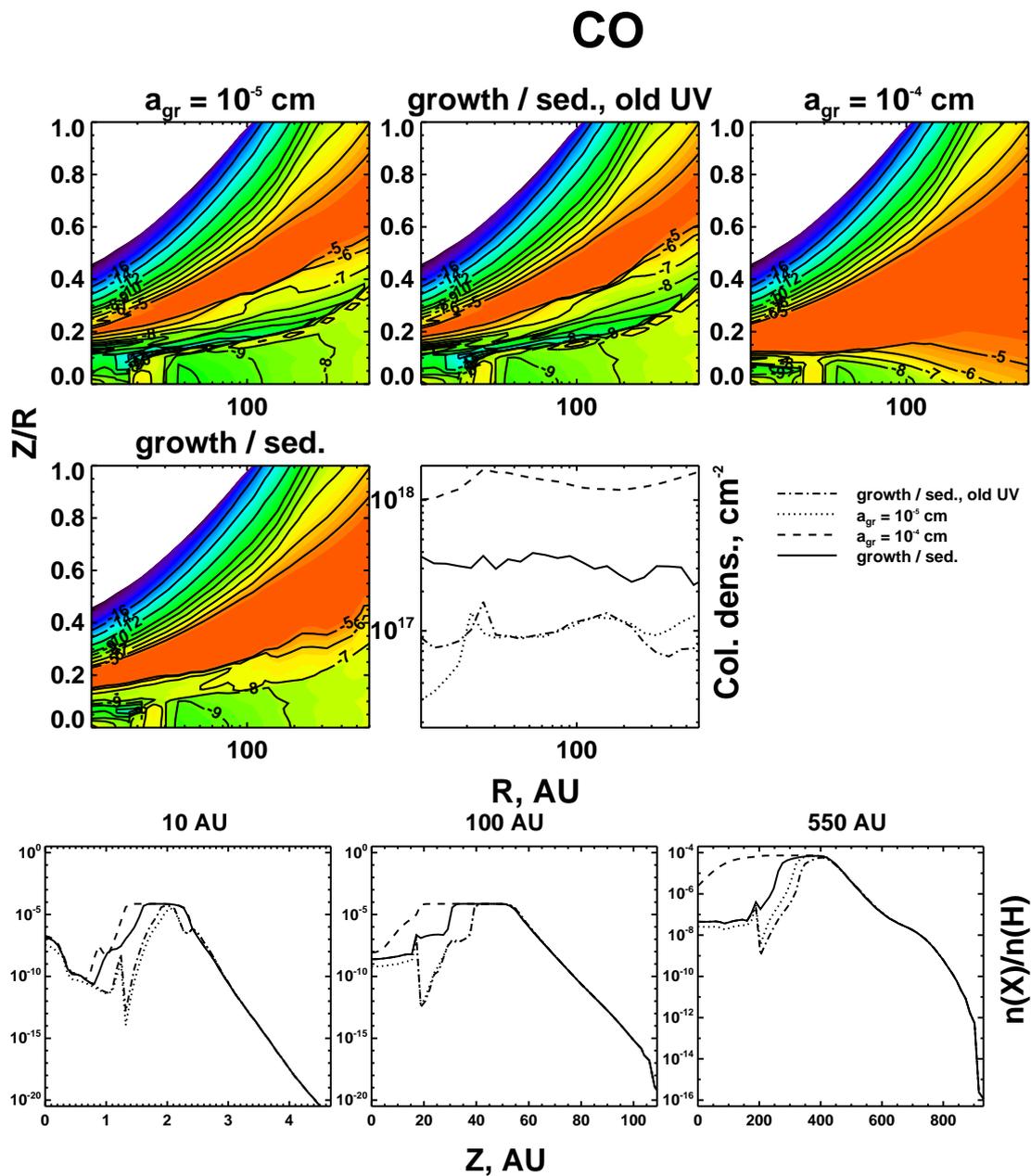
Figure 5.8 2D CO abundance across the disk and vertical profiles of CO abundance at different radii. Solid line corresponds to Model D, dashed — to Model S4, dotted — Model S5, dot-dashed — to Model DAv.

HN2+
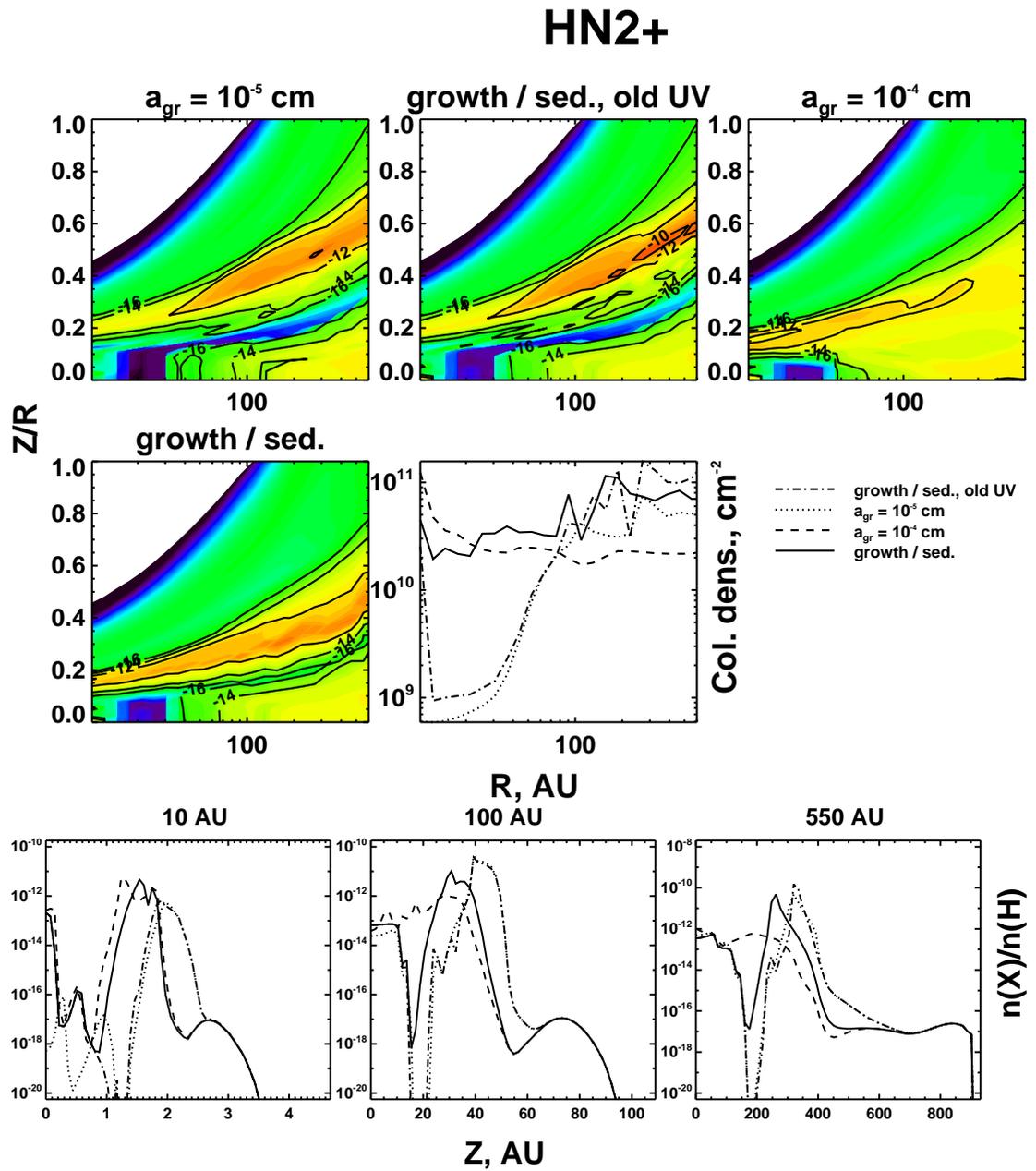
Figure 5.9 Same as on Fig. 5.8 but for N_2H^+.

NH3
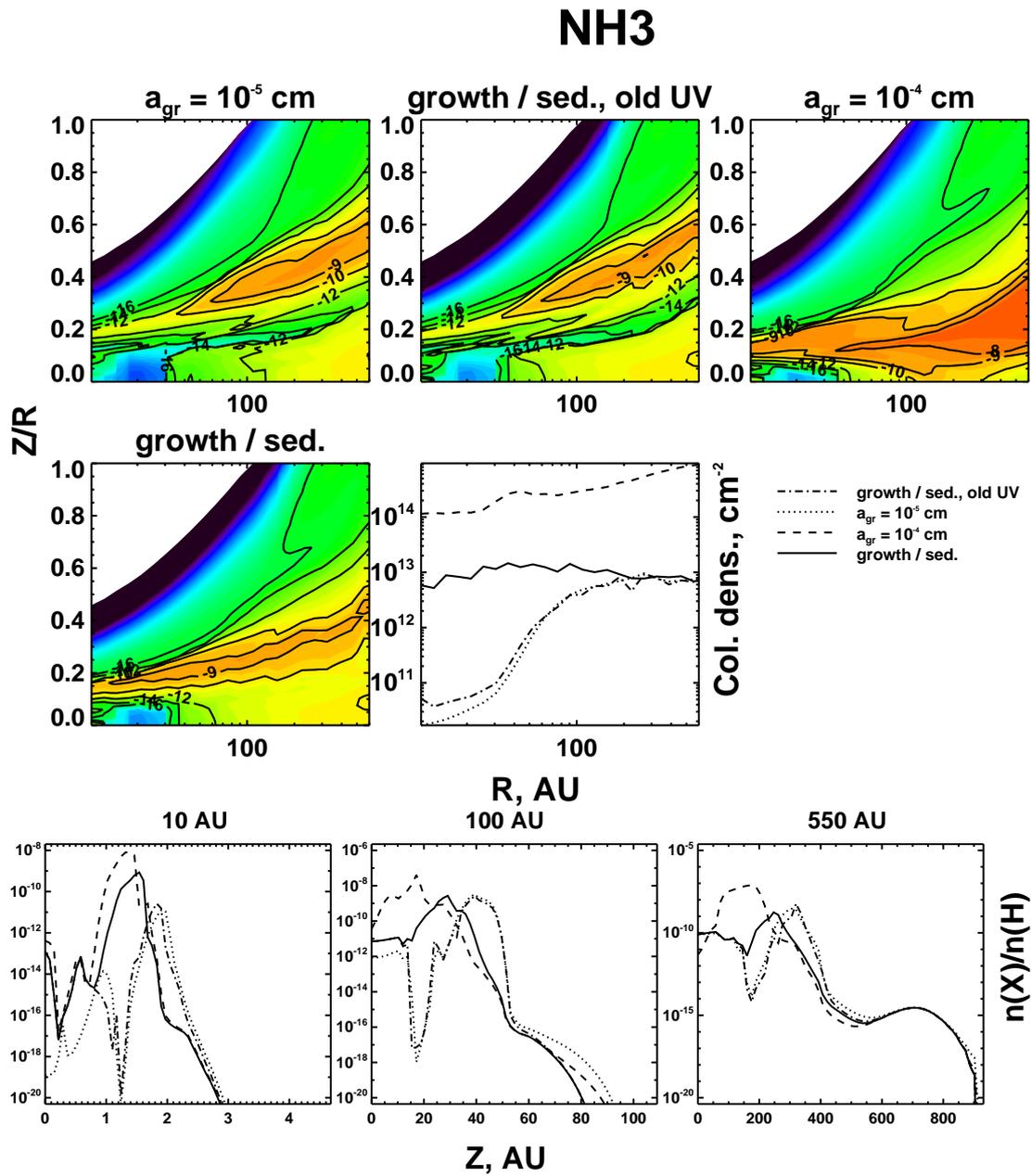
Figure 5.10 Same as on Fig. 5.8 but for NH₃.
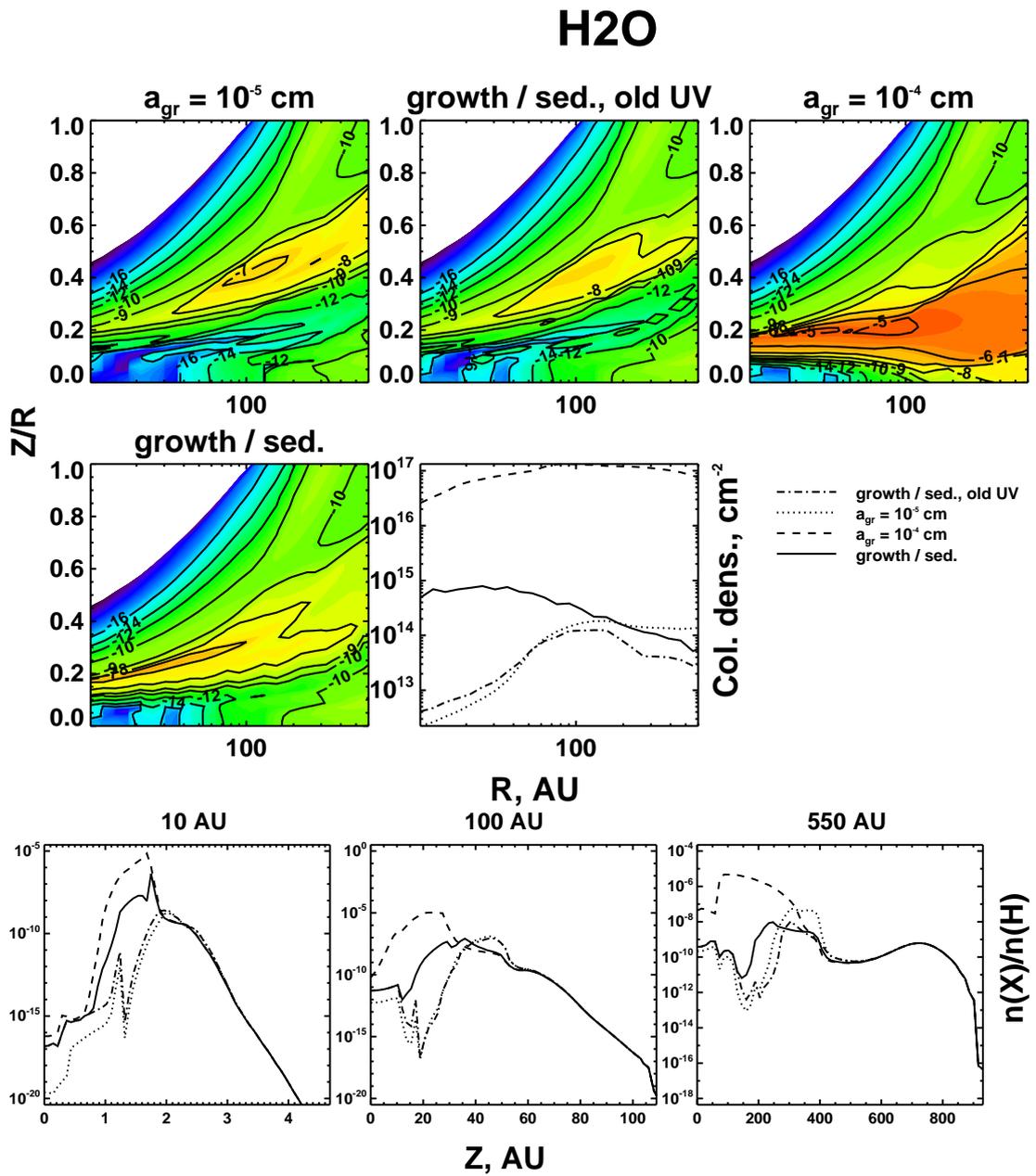
Figure 5.11 Same as on Fig. 5.8 but for H$_2$O.
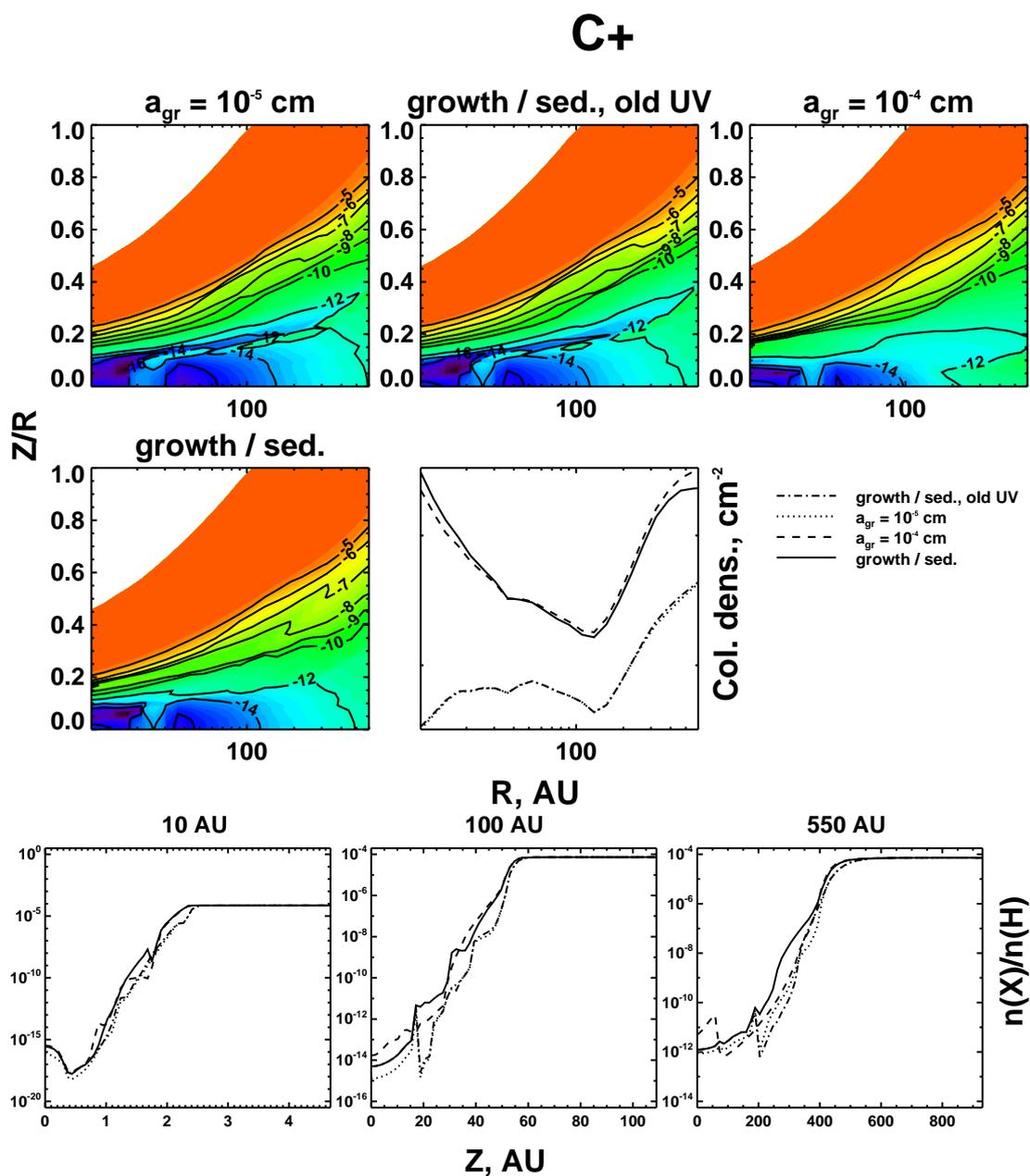
Figure 5.12 Same as on Fig. 5.8 but for C$^+$.
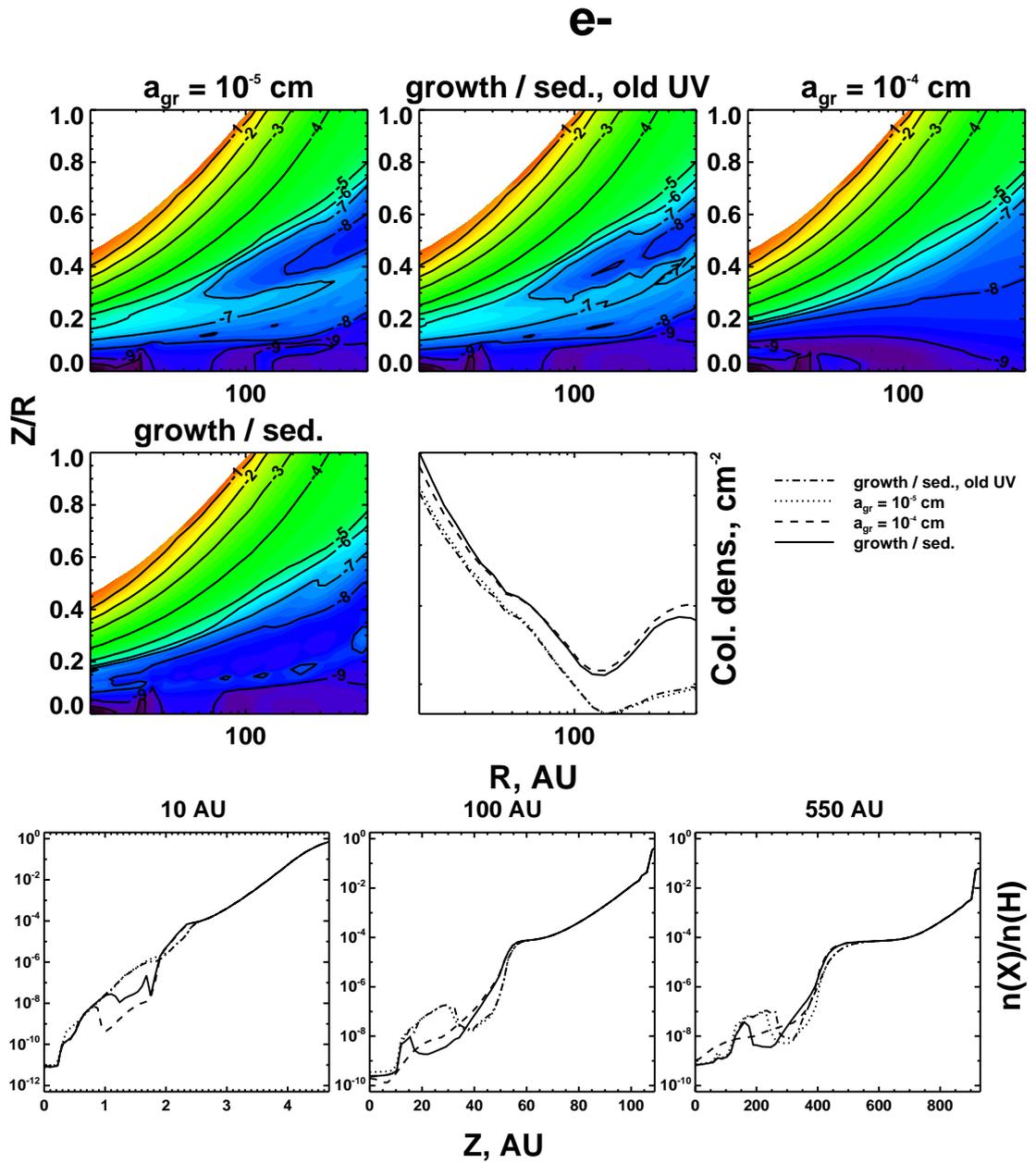
Figure 5.13 Same as on Fig. 5.8 but for e⁻.

H3+

Figure 5.14 Same as on Fig. 5.8 but for H_3^+.

CS
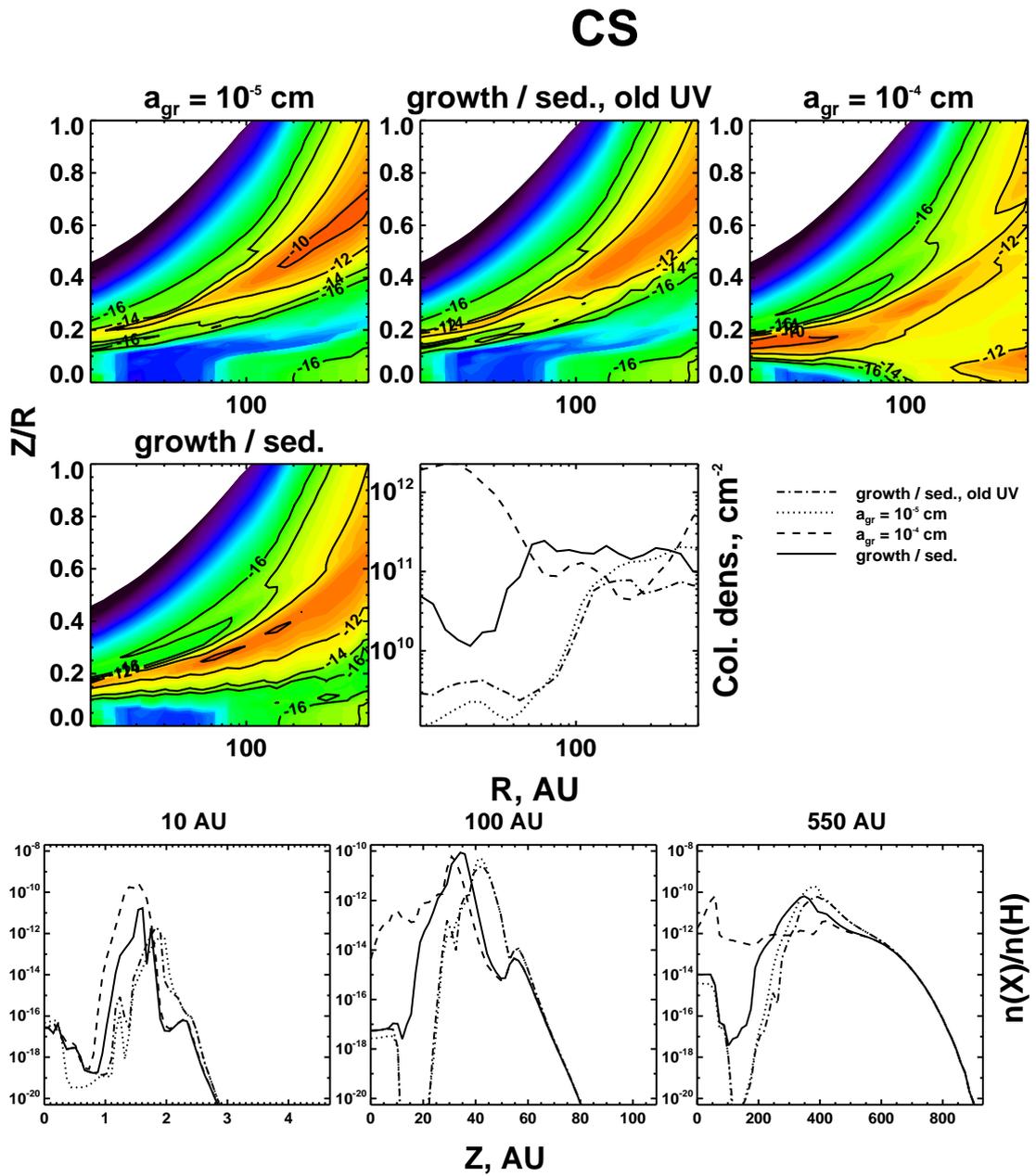
Figure 5.15 Same as on Fig. 5.8 but for CS.

6

Conclusions and future prospects

In this thesis, I considered several important questions of theoretical astrochemistry. Namely, the influence of uncertainties in rates of chemical reactions on the results of astrochemical modeling of protoplanetary disks has been studied, the importance of stochastic effects in grain surface chemistry has been investigated and a model of chemical evolution of the protoplanetary disk with account for grain growth and sedimentation has been constructed. The main results of this thesis are the following.

- The influence of uncertainties in the rates of chemical reactions on the results of astrochemical modeling of protoplanetary disks is investigated for the first time. Modern astrochemical databases include up to a few thousand gas-phase chemical reactions. However, rates of only $10 - 20\%$ of them are measured accurately, with uncertainties of about 25%. The rates of the remaining chemical reactions are estimated even more roughly, and have uncertainties of about an order of magnitude. In my work, I quantitatively investigated the influence of inaccuracies in the rates of the gas-phase chemical reactions on the results of astrochemical modeling. I found that the resulting uncertainty in the modeled abundance of a species depends on its complexity (i.e., the number of atoms it consists of), and for most of the observable species does not exceed a factor of $3 - 4$, which is comparable with the observational uncertainties. Using a sensitivity analysis, I found that for observed molecules the accuracy of astrochemical modeling could be greatly improved if only a few tens of key reaction rates were re-measured in the lab or theoretically predicted (Table 2.3).

6. CONCLUSIONS AND FUTURE PROSPECTS

- For the first time a full-scale model of the chemical evolution of the interstellar medium in which gas-phase and grain surface chemistry are treated simultaneously with a Monte Carlo approach is constructed. Usually, the chemical rate equations are used for astrochemical modeling. The fundamental principles behind them are the continuous change of abundances of species, and the negligibility of fluctuations. These principles are satisfied in the case of gas-phase species, but may not be valid for surface molecules with low populations per grain (≤ 1). In this situation, both the discrete nature of chemical processes and fluctuations in the abundances of species become very important, and the use of the rate equations may lead to spurious results.

My model treats both gas-phase and grain surface reactions simultaneously with a unified Monte Carlo approach, and includes a large amount of reactions. With this model, I investigated the importance of stochastic effects for the chemical evolution of molecular clouds and protoplanetary disks. A stochastic approach is a must if quantum tunneling is allowed for light species and diffusion energies of other species are low. At $10 - 15$ K, in the absence of effective desorption mechanisms, stochastic processes are most important for ices, but at $20 - 30$ K gas-phase abundances become affected. The MC model is rigorous, but computationally very intensive. Using my MC results, I tested the validity of the new approximate modified rate equations method of Garrod (2008). It is confirmed that the new MRE approach is quite accurate and relatively fast and easy to implement. It is recommended for modeling surface chemistry in cases when stochastic effects can arise.

With the new MRE, I investigated the importance of stochastic effects in the chemistry of protoplanetary disks, assuming various grain sizes. It was found that without surface tunneling, stochastic effects are unimportant even for tiny (10^{-6} cm) grains. However, if smaller catalytic particles are considered (e.g., PAHs), stochastic effects may become of great importance, even for surface radicals with high diffusion energies.

- Finally, the chemical structure of a protoplanetary disk around a T Tauri star was investigated, where both grain growth and sedimentation is taken into account. There is observational evidence for substantial grain growth in protoplanetary

systems (up to mm-sized particles). The grain evolution in protoplanetary disks involves different processes, e.g. coagulation and fragmentation of particles, radial drift, vertical sedimentation, and is intimately connected with the physical structure of the disk. Grains are an important factor for enriching the chemical complexity of protoplanetary disks through catalytic grain surface reactions, freeze-out of gaseous molecules, and ion recharging on grains. Many previous works on disk chemistry assumed a standard grain particle of radius of 10^{-5} cm and a dust-to-gas ratio of 0.01. In the last chapter of my thesis, I performed a detailed modeling of dust evolution in the disk. It is found that the main effect of grain growth on disk chemistry is an increase in the UV radiation rates. When the disk becomes more transparent to stellar and interstellar UV photons, the rate of photodesorption of icy mantles increases, while surface recombination rates only slightly decrease. This increases column densities of many gas-phase species such as H_2O, CS, NH_3 and others by a factor of a few. The overall effect is well-pronounced in the inner dense disk region ($R \leq 100$ AU), since grains grow and sediment there more efficiently. Additionally, grain growth results in a higher total ionization degree in the disk. It is shown that crude-growth disk models, e.g., where the mean grain size is varied by a certain factor, should be used with care. The model, presented in the thesis, does not confirm previous claims, based on less detailed computations, that the H_3^+ ion is a sensitive tracer of grain growth in planet-forming systems.

6.1 Prospects for the future work

The work presented in this thesis is just a small contribution to astronomy of the 21st century. Forthcoming observational facilities such as ALMA and Herschel, as well as lab experiments and theoretical advances, will push astrochemistry forward during the coming decade. Below I outline a few further directions for research, based on what is done in this thesis:

6.1.1 Uncertainties in rates of chemical reactions

The estimation of uncertainties in astrochemical networks and their further improvement (e.g., more reactions, better rate coefficients) are necessary tasks if we are aiming

at better models. I plan to continue my work on finding the most problematic reactions for various interesting species. Absolute values of gas-phase reaction rates, their temperature dependence, and branching ratios are among the quantities to be derived. This work will be carried out in close cooperation with lab scientists and quantum chemists. Synergy with expertise in the chemistry community is natural for such a project.

6.1.2 Modeling of grain surface chemistry

Grain surface processes in space pose another interesting and poorly-understood problem. Here, there are a few possible directions of research. First is the further improvement of computational techniques. The Monte Carlo method used in this thesis is rigorous, but very slow. More advanced and faster Monte Carlo techniques have been developed in molecular biology to model the chemical evolution of a living cell. It is very exciting to investigate which of these methods could be utilized for astrochemical simulations. Making use of such fast, yet accurate, stochastic methods will allow us to include these approaches into chemo-dynamical disk models.

While the recent modified rate equations by Garrod (2008) are a fast and quite accurate approach, they are still based on empirical assumptions and cannot properly account for all the possible processes in surface chemical networks, e.g., for the correlations in the abundances of some species (see Chapter 4). Therefore, it should be most interesting to try to use some other approximate stochastic approaches. For example, the moment equations method developed by Lipshtat and Biham (2003) looks very promising, as it is rigorous for surface chemical systems, where surface populations of a reactant is low ($\sim 1 - 3$).

Next, more detailed models of grain surface chemistry are needed. Icy grain mantles can consist of many distinct monolayers, and, therefore, can be divided into a surface layer and a bulk component of ice. When the mantle is thick, desorption of frozen molecules is described by the zero-order kinetics (Bisschop et al., 2006). When it is thin, not only molecules form the surface, but also from the entire mantle can desorb back into the gas phase. These details are currently not in our model. The inclusion of mantle structure into gas-grain chemical models will be important for modeling the disk chemistry under non-stationary physical conditions, e.g., in shocks and outflows where grain mantles evaporate.

Finally, the influence of detailed mantle properties (roughness, porosity etc.) on surface chemistry should be considered. This has been partially attempted by Chang et al. (2005, 2007); Cuppen and Herbst (2007), but with the main focus on surface structures. Detailed surface chemistry, coupled to an advanced gas-phase network in astrochemical models, could be attempted either with more advanced Monte Carlo techniques, or approximate stochastic methods. Such a detailed model may be important when both chemistry and grain growth are modeled together in greater detail.

6.1.3 Chemistry in disks with grain evolution

The evolving disk model presented in Chapter 5 is straightforward. We do not follow the real time-dependent grain evolution but, instead, use the final steady-state grain distribution. Next, no elaborate heating and cooling processes are considered to model gas and dust thermal disk structures separately. As a next step, a series of gaseous disk structures for various time moments can be utilized and coupled with the chemical network. Furthermore, a better description of dust microphysics is required. In the current dust model, the evolving dust distribution is represented by an ensemble of averaged spherical particles of equal size. Instead, a grain size distribution law could be introduced into the astrochemical model. Evolving grains are hardly ideal spheres; they may have a fluffy structure or a complex fractal shape. Such structures imply completely different mass-to-surface ratios for individual grains, and a high degree of porosity, which will make surface chemistry more stochastic. On the other hand, the presence of an icy mantle should definitely affect grain coagulation, compactification, cratering, fragmentation, etc. A more detailed grain growth model using new lab data will allow us to obtain high-quality predictions, which future observations will have to justify or falsify.

The tasks outlined above are just a few possible directions of my further work. The fascinating field of astrochemistry is a treasury of interesting yet unsolved questions which are of the uttermost importance for determining the conditions and compositions of young planetary systems. The coming decade will be a period of significant advantages in exploring of this treasury and I hope to be able to contribute in it with my research.

6. CONCLUSIONS AND FUTURE PROSPECTS

Bibliography

Adams, N. G. and Smith, D. A study of the reactions of NH_3^+ and ND_3^+ with H_2 and D_2 at several temperatures. *Int. J. Mass Spectrom. Ion Proc.*, 61:133–139 (1984). 41

Adams, N. G., Smith, D., and Clary, D. C. Rate coefficients of the reactions of ions with polar molecules at interstellar temperatures. *Astrophys. J., Lett*, 296:L31–L34 (1985). doi:10.1086/184543. 40

Aikawa, Y. Cold CO Gas in Protoplanetary Disks. *Astrophys. J., Lett*, 656:L93–L96 (2007). doi:10.1086/512674. 71, 75

Aikawa, Y. and Herbst, E. Molecular evolution in protoplanetary disks. Two-dimensional distributions and column densities of gaseous molecules. *Astron. Astrophys*, 351:233–246 (1999). 22, 88

Aikawa, Y., Momose, M., Thi, W.-F., et al. Interferometric Observations of Formaldehyde in the Protoplanetary Disk around LkCa 15. *Publ. Aston. Soc. Jpn*, 55:11–15 (2003). 9, 20

Aikawa, Y. and Nomura, H. Physical and Chemical Structure of Protoplanetary Disks with Grain Growth. *Astrophys. J*, 642:1152–1162 (2006). doi:10.1086/501114. 10, 96, 97, 113, 114, 115

Aikawa, Y., Ohashi, N., Inutsuka, S.-I., et al. Molecular Evolution in Collapsing Prestellar Cores. *Astrophys. J*, 552:639–653 (2001). doi:10.1086/320551. 4

Aikawa, Y., van Zadelhoff, G. J., van Dishoeck, E. F., et al. Warm molecular layers in protoplanetary disks. *Astron. Astrophys*, 386:622–632 (2002). doi:10.1051/0004-6361: 20020037. 4, 22, 110

BIBLIOGRAPHY

Andre, P., Ward-Thompson, D., and Barsony, M. From Prestellar Cores to Protostars: the Initial Conditions of Star Formation. *Protostars and Planets IV*, pages 59–+ (2000). 3

Andrews, S. M. and Williams, J. P. High-Resolution Submillimeter Constraints on Circumstellar Disk Structure. *Astrophys. J*, 659:705–728 (2007). doi:10.1086/511741. 104

Apai, D., Pascucci, I., Sterzik, M. F., et al. Grain growth and dust settling in a brown dwarf disk. Gemini/T-ReCS observations of CFHT-BD-Tau 4. *Astron. Astrophys*, 426:L53–L57 (2004). doi:10.1051/0004-6361:200400080. 95

Barzel, B. and Biham, O. Efficient Simulations of Interstellar Gas-Grain Chemistry Using Moment Equations. *Astrophys. J., Lett*, 658:L37–L40 (2007). doi:10.1086/513421. 47, 56

Bates, D. R. Rate of formation of molecules by radiative association. *Mon. Not. R. Astron. Soc*, 111:303–+ (1951). 10

Bates, D. R. and Herbst, E. Radiative Association. In T. J. Millar and D. A. Williams, editors, *Rate Coefficients in Astrochemistry*, Proc. Conf. held in UMIST, Manchester, United Kingdom, September 21-24, 1987, pages 17–37. Kluwer Academic Publishers, Dordrecht (1988). 36

Belloche, A., Garrod, R. T., Mueller, H. S. P., et al. Increased complexity in interstellar chemistry: Detection and chemical modeling of ethyl formate and n-propyl cyanide in Sgr B2(N). *ArXiv e-prints* (2009). 77

Benson, P. J. and Myers, P. C. A survey for dense cores in dark clouds. *Astrophys. J., Suppl. Ser*, 71:89–108 (1989). doi:10.1086/191365. 70

Bergin, E., Calvet, N., D'Alessio, P., et al. The Effects of UV Continuum and Lyα Radiation on the Chemical Equilibrium of T Tauri Disks. *Astrophys. J., Lett*, 591:L159–L162 (2003). doi:10.1086/377148. 12, 39

Bergin, E. A. and Langer, W. D. Chemical Evolution in Preprotostellar and Protostellar Cores. *Astrophys. J*, 486:316–+ (1997). doi:10.1086/304510. 4

Biham, O., Furman, I., Pirronello, V., et al. Master Equation for Hydrogen Recombination on Grain Surfaces. *Astrophys. J*, 553:595–603 (2001). doi:10.1086/320975. 46, 51, 78, 79

Birnstiel, T., Dullemond, C. P., and Brauer, F. Dust retention in protoplanetary disks. *Astron. Astrophys*, 503:L5–L8 (2009). doi:10.1051/0004-6361/200912452. 96, 97, 98, 114

Bisschop, S. E., Fraser, H. J., Öberg, K. I., et al. Desorption rates and sticking coefficients for CO and N2 interstellar ices. *Astron. Astrophys*, 449:1297–1309 (2006). doi:10.1051/0004-6361:20054051. 20, 128

Boger, G. I. and Sternberg, A. Bistability in Interstellar Gas-Phase Chemistry. *Astrophys. J*, 645:314–323 (2006). doi:10.1086/502624. 11, 46

Bourdon, E. B., Prince, R. H., and Duley, W. W. An experimental determination of the cross section for photodesorption. *Astrophys. J*, 260:909–913 (1982). doi: 10.1086/160309. 109

Bouwman, J., Henning, T., Hillenbrand, L. A., et al. The Formation and Evolution of Planetary Systems: Grain Growth and Chemical Processing of Dust in T Tauri Systems. *Astrophys. J*, 683:479–498 (2008). doi:10.1086/587793. 95

Bouwman, J., Meeus, G., de Koter, A., et al. Processing of silicate dust grains in Herbig Ae/Be systems. *Astron. Astrophys*, 375:950–962 (2001). 95

Brauer, F., Dullemond, C. P., and Henning, T. Coagulation, fragmentation and radial motion of solid particles in protoplanetary disks. *Astron. Astrophys*, 480:859–877 (2008a). doi:10.1051/0004-6361:20077759. 4, 93, 100, 102, 104, 114, 115

Brauer, F., Dullemond, C. P., and Henning, T. Coagulation, fragmentation and radial motion of solid particles in protoplanetary disks. *Astron. Astrophys*, 480:859–877 (2008b). doi:10.1051/0004-6361:20077759. 96

Brauer, F., Dullemond, C. P., Johansen, A., et al. Survival of the mm-cm size grain population observed in protoplanetary disks. *Astron. Astrophys*, 469:1169–1182 (2007). doi:10.1051/0004-6361:20066865. 4

BIBLIOGRAPHY

Brownsword, R. A., Sims, I. R., Smith, I. W. M., et al. The Radiative Association of CH with H 2: A Mechanism for Formation of CH 3 in Interstellar Clouds. *Astrophys. J*, 485:195 (1997). doi:10.1086/304402. 37

Canosa, A., Sims, I. R., Travers, D., et al. Reactions of the methylidine radical with CH4, C2H2, C2H4, C2H6, and but-1-ene studied between 23 and 295K with a CRESU apparatus. *Astron. Astrophys*, 323:644–651 (1997). 40

Carmona, A., van den Ancker, M. E., Henning, T., et al. A search for mid-infrared molecular hydrogen emission from protoplanetary disks. *Astron. Astrophys*, 477:839–852 (2008). doi:10.1051/0004-6361:20077846. 4

Carr, J. S., Tokunaga, A. T., Najita, J., et al. The inner-disk and stellar properties of the young stellar object WL 16. *Astrophys. J., Lett*, 411:L37–L40 (1993). doi:10.1086/186906. 4

Caselli, P., Stantcheva, T., Shalabiea, O., et al. Deuterium fractionation on interstellar grains studied with modified rate equations and a Monte Carlo approach. *Planet. Space Sci*, 50:1257–1266 (2002). 46, 47, 51, 56, 78

Caselli, P., Walmsley, C. M., Terzieva, R., et al. The Ionization Fraction in Dense Cloud Cores. *Astrophys. J*, 499:234 (1998). doi:10.1086/305624. 5, 6, 38, 45, 46, 47, 51, 78

Cazaux, S. and Tielens, A. G. G. M. H_2 Formation on Grain Surfaces. *Astrophys. J*, 604:222–237 (2004). doi:10.1086/381775. 49

Chang, Q., Cuppen, H. M., and Herbst, E. Continuous-time random-walk simulation of H_2 formation on interstellar grains. *Astron. Astrophys*, 434:599–611 (2005). doi:10.1051/0004-6361:20041842. 47, 129

Chang, Q., Cuppen, H. M., and Herbst, E. Gas-grain chemistry in cold interstellar cloud cores with a microscopic Monte Carlo approach to surface chemistry. *Astron. Astrophys*, 469:973–983 (2007). doi:10.1051/0004-6361:20077423. 48, 56, 129

Charnley, S. B. Stochastic Astrochemical Kinetics. *Astrophys. J., Lett*, 509:L121–L124 (1998). doi:10.1086/311764. 47, 56

Charnley, S. B. Stochastic Theory of Molecule Formation on Dust. *Astrophys. J., Lett*, 562:L99–L102 (2001). doi:10.1086/324753. 47, 56

Chastaing, D., Le Picard, S. D., Sims, I. R., et al. Rate coefficients for the reactions of C(3PJ) atoms with C2H2, C2H4, CH3C = CH and H2C = C = CH2 at temperatures down to 15 K. *Astron. Astrophys*, 365:241–247 (2001). doi:10.1051/0004-6361:20000026. 40

Ciesla, F. J. Dust Coagulation and Settling in Layered Protoplanetary Disks. *Astrophys. J., Lett*, 654:L159–L162 (2007). doi:10.1086/511029. 96

Clary, D. C. Theory of Reactive Collisions at Low Temperatures. In T. J. Millar and D. A. Williams, editors, *ASSL Vol. 146: Rate Coefficients in Astrochemistry*, pages 1–24. Kluwer Academic Publishers, Dordrecht (1988). 40

Clary, D. C., Haider, N., Husain, D., et al. Interstellar carbon chemistry: Reaction rates of neutral atomic carbon with organic molecules. *Astrophys. J*, 422:416–422 (1994). 40

Clary, D. C., Smith, D., and Adams, N. G. Temperature dependence of rate coefficients for reactions of ions with dipolar molecules. *Chemical Physics Letters*, 119:320–326 (1985). 40, 42

Cortes, S. R., Meyer, M. R., Carpenter, J. M., et al. Grain Growth and Global Structure of the Protoplanetary Disk Associated with the Mature Classical T Tauri Star, PDS 66. *Astrophys. J*, 697:1305–1315 (2009). doi:10.1088/0004-637X/697/2/1305. 95

Cuppen, H. M. and Herbst, E. Simulation of the Formation and Morphology of Ice Mantles on Interstellar Grains. *Astrophys. J*, 668:294–309 (2007). doi:10.1086/521014. 47, 129

D'Alessio, P., Calvet, N., Hartmann, L., et al. Accretion Disks around Young Objects. II. Tests of Well-mixed Models with ISM Dust. *Astrophys. J*, 527:893–909 (1999a). doi:10.1086/308103. 12, 86

D'Alessio, P., Calvet, N., Hartmann, L., et al. Accretion Disks around Young Objects. II. Tests of Well-mixed Models with ISM Dust. *Astrophys. J*, 527:893–909 (1999b). doi:10.1086/308103. 99

D'Alessio, P., Canto, J., Calvet, N., et al. Accretion Disks around Young Objects. I. The Detailed Vertical Structure. *Astrophys. J*, 500:411–+ (1998). doi:10.1086/305702. 99

Dalgarno, A. and McCray, R. A. Heating and Ionization of HI Regions. *Ann. Rev. Astron. Astrophys*, 10:375–424 (1972). 38

Dalgarno, A. and Stephens, T. L. Discrete Absorption and Photodissociation of Molecular Hydrogen. *Astrophys. J., Lett*, 160:L107–L109 (1970). 39

Dartois, E., Dutrey, A., and Guilloteau, S. Structure of the DM Tau Outer Disk: Probing the vertical kinetic temperature gradient. *Astron. Astrophys*, 399:773–787 (2003). doi:10.1051/0004-6361:20021638. 20, 86

Dobrijevic, M., Ollivier, J. L., Billebaud, F., et al. Effect of chemical kinetic uncertainties on photochemical modeling results: Application to Saturn's atmosphere. *Astron. Astrophys*, 398:335–344 (2003). doi:10.1051/0004-6361:20021659. 16

Dobrijevic, M. and Parisot, J. P. Effect of chemical kinetics uncertainties on hydrocarbon production in the stratosphere of Neptune. *Planet. Space Sci*, 46:491–505 (1998). 16

Dolginov, A. Z. and Stepinski, T. F. Are cosmic rays effective for ionization of protoplanetary disks? *Astrophys. J*, 427:377–383 (1994). 38

Draine, B. T. Photoelectric heating of interstellar gas. *Astrophys. J., Suppl. Ser*, 36:595–619 (1978). doi:10.1086/190513. 12, 39

Draine, B. T. and Lee, H. M. Optical properties of interstellar graphite and silicate grains. *Astrophys. J*, 285:89–108 (1984a). doi:10.1086/162480. 48

Draine, B. T. and Lee, H. M. Optical properties of interstellar graphite and silicate grains. *Astrophys. J*, 285:89–108 (1984b). doi:10.1086/162480. 110

Dullemond, C. P. and Dominik, C. The effect of dust settling on the appearance of protoplanetary disks. *Astron. Astrophys*, 421:1075–1086 (2004). doi:10.1051/0004-6361:20040284. 4, 97, 98, 102, 115

Dullemond, C. P. and Dominik, C. Dust coagulation in protoplanetary disks: A rapid depletion of small grains. *Astron. Astrophys*, 434:971–986 (2005). doi:10.1051/0004-6361:20042080. 100

Dutrey, A., Guilloteau, S., and Guelin, M. Chemistry of protosolar-like nebulae: The molecular content of the DM Tau and GG Tau disks. *Astron. Astrophys*, 317:L55–L58 (1997). 9, 12, 20

Dutrey, A., Guilloteau, S., and Ho, P. Interferometric Spectroimaging of Molecular Gas in Protoplanetary Disks. In B. Reipurth, D. Jewitt, & K. Keil, editor, *Protostars and Planets V*, pages 495–506 (2007a). 112

Dutrey, A., Guilloteau, S., Piétu, V., et al. Cavities in inner disks: the GM Aurigae case. *Astron. Astrophys*, 490:L15–L18 (2008). doi:10.1051/0004-6361:200810732. 96

Dutrey, A., Henning, T., Guilloteau, S., et al. Chemistry in disks. I. Deep search for N_2H^+ in the protoplanetary disks around LkCa 15, MWC 480, and DM Tauri. *Astron. Astrophys*, 464:615–623 (2007b). doi:10.1051/0004-6361:20065385. 9, 12, 20, 22, 92

Fehsenfeld, F. C., Lindinger, W., Schmeltekopf, A. L., et al. Energy dependence of the reaction $NH_3^+ + H_2 = NH_4^+ + H$. *J. Chem. Phys*, 62:2001–2003 (1975). 41

Finocchi, F. and Gail, H.-P. Chemical reactions in protoplanetary accretion disks. III. The role of ionisation processes. *Astron. Astrophys*, 327:825–844 (1997). 13

Florescu-Mitchell, A. I. and Mitchell, J. B. A. Dissociative recombination. *Phys. Rep*, 430:277–374 (2006). doi:10.1016/j.physrep.2006.04.002. 10, 43

Gammie, C. F. Layered Accretion in T Tauri Disks. *Astrophys. J*, 457:355 (1996). doi:10.1086/176735. 38

Garrod, R. T. A new modified-rate approach for gas-grain chemical simulations. *Astron. Astrophys*, 491:239–251 (2008). doi:10.1051/0004-6361:200810518. 6, 76, 79, 85, 126, 128

Garrod, R. T. and Herbst, E. Formation of methyl formate and other organic species in the warm-up phase of hot molecular cores. *Astron. Astrophys*, 457:927–936 (2006). doi:10.1051/0004-6361:20065560. 5, 14, 22, 23, 51, 80

Garrod, R. T., Wakelam, V., and Herbst, E. Non-thermal desorption from interstellar dust grains via exothermic surface reactions. *Astron. Astrophys*, 467:1103–1115 (2007). doi:10.1051/0004-6361:20066704. 71, 72

Garrod, R. T., Weaver, S. L. W., and Herbst, E. Complex Chemistry in Star-forming Regions: An Expanded Gas-Grain Warm-up Chemical Model. *Astrophys. J*, 682:283–302 (2008). doi:10.1086/588035. 5

Geppert, W. D., Thomas, R. D., Ehlerding, A., et al. Dissociative recombination branching ratios and their influence on interstellar clouds. *Journal of Physics Conference Series*, 4:26–31 (2005a). doi:10.1088/1742-6596/4/1/004. 10, 43

Gerlich, D. Ion-neutral collisions in a 22-pole trap at very low energies. *Physica Scripta*, 1995(T59):256–263 (1995). URL `http://stacks.iop.org/1402-4896/T59/256`. 36

Gillespie, D. T. A General Method for Numerically Simulating the Stochastic Time Evolution of Coupled Chemical Reactions. *Journal of Computational Physics*, 22:403 (1976). 45, 47, 52, 54

Glassgold, A. E., Feigelson, E. D., Montmerle, T., et al. X-Ray Flares of Sun-like Young Stellar Objects and Their Effects on Protoplanetary Disks. In A. N. Krot, E. R. D. Scott, and B. Reipurth, editors, *Chondrites and the Protoplanetary Disk*, volume 341 of *Astronomical Society of the Pacific Conference Series*, page 165 (2005). 13

Glassgold, A. E. and Langer, W. D. Heating of Molecular-Hydrogen Clouds by Cosmic Rays and X-Rays. *Astrophys. J*, 186:859–888 (1973). 38

Glassgold, A. E., Najita, J., and Igea, J. X-Ray Ionization of Protoplanetary Disks. *Astrophys. J*, 480:344 (1997a). doi:10.1086/303952. 13, 26

Glassgold, A. E., Najita, J., and Igea, J. X-Ray Ionization of Protoplanetary Disks: Erratum. *Astrophys. J*, 485:920–+ (1997b). doi:10.1086/304476. 13

Gould, R. J. and Salpeter, E. E. The Interstellar Abundance of the Hydrogen Molecule. I. Basic Processes. *Astrophys. J*, 138:393 (1963). 5, 77

Graham, J. R., Kalas, P. G., and Matthews, B. C. The Signature of Primordial Grain Growth in the Polarized Light of the AU Microscopii Debris Disk. *Astrophys. J*, 654:595–605 (2007). doi:10.1086/509318. 96

Green, N. J. B., Toniazzo, T., Pilling, M. J., et al. A stochastic approach to grain surface chemical kinetics. *Astron. Astrophys*, 375:1111–1119 (2001). doi:10.1051/0004-6361:20010961. 46, 56

Haisch, K. E., Lada, E. A., and Lada, C. J. Disk Frequencies and Lifetimes in Young Clusters. *Astrophys. J., Lett*, 553:L153–L156 (2001). 96

Hasegawa, T. I. and Herbst, E. Three-Phase Chemical Models of Dense Interstellar Clouds - Gas Dust Particle Mantles and Dust Particle Surfaces. *Mon. Not. R. Astron. Soc*, 263:589 (1993). 22

Hasegawa, T. I., Herbst, E., and Leung, C. M. Models of gas-grain chemistry in dense interstellar clouds with complex organic molecules. *Astrophys. J., Suppl. Ser*, 82:167–195 (1992). doi:10.1086/191713. 5, 49, 51, 52, 78, 80, 93

Hassel, G. E., Herbst, E., and Garrod, R. T. Modeling the Lukewarm Corino Phase: Is L1527 unique? *Astrophys. J*, 681:1385–1395 (2008). doi:10.1086/588185. 50, 79

Hayashi, C. Formation of the planets. In D. Sugimoto, D. Q. Lamb, & D. N. Schramm, editor, *Fundamental Problems in the Theory of Stellar Evolution*, volume 93 of *IAU Symposium*, pages 113–126 (1981). 104

Henning, T. and Semenov, D. The birth and death of organic molecules in protoplanetary disks. In S. Kwok and S. Sandford, editors, *IAU Symposium*, volume 251 of *IAU Symposium*, pages 89–98 (2008). doi:10.1017/S1743921308021261. 92

Herbst, E. An additional uncertainty in calculated radiative association rates of molecular formation at low temperatures. *Astrophys. J*, 241:197–199 (1980). 10, 36

Herbst, E. An update of and suggested increase in calculated radiative association rate coefficients. *Astrophys. J*, 291:226–229 (1985). doi:10.1086/163060. 16, 36

Herbst, E. Chemistry in the ISM: the ALMA (r)evolution. The cloudy crystal ball of one astrochemist. *Astrophys. Space. Sci*, 313:129–134 (2008). doi:10.1007/s10509-007-9639-9. 5

Herbst, E. and Klemperer, W. The Formation and Depletion of Molecules in Dense Interstellar Clouds. *Astrophys. J*, 185:505–534 (1973). 4, 38

Herbst, E. and Shematovich, V. I. New approaches to the modelling of surface chemistry on interstellar grains. *Astrophys. Space. Sci*, 285:725–735 (2003). 5, 45

Hernández, J., Hartmann, L., Calvet, N., et al. A Spitzer View of Protoplanetary Disks in the γ Velorum Cluster. *Astrophys. J*, 686:1195–1208 (2008). doi:10.1086/591224. 96

Hogerheijde, M. R. and van der Tak, F. F. S. An accelerated Monte Carlo method to solve two-dimensional radiative transfer and molecular excitation. With applications to axisymmetric models of star formation. *Astron. Astrophys*, 362:697–710 (2000). 4

Hollenbach, D. and McKee, C. F. Molecule formation and infrared emission in fast interstellar shocks. I Physical processes. *Astrophys. J., Suppl. Ser*, 41:555–592 (1979). doi:10.1086/190631. 13

Hollis, J. M., Lovas, F. J., Remijan, A. J., et al. Detection of Acetamide (CH_3CONH_2): The Largest Interstellar Molecule with a Peptide Bond. *Astrophys. J., Lett*, 643:L25–L28 (2006). doi:10.1086/505110. 9

Ilgner, M., Henning, T., Markwick, A. J., et al. Transport processes and chemical evolution in steady accretion disk flows. *Astron. Astrophys*, 415:643–659 (2004). doi:10.1051/0004-6361:20034061. 10

Ilgner, M. and Nelson, R. P. On the ionisation fraction in protoplanetary disks. I. Comparing different reaction networks. *Astron. Astrophys*, 445:205–222 (2006). doi:10.1051/0004-6361:20053678. 38

Ishii, K., Tajima, A., Taketsugu, T., et al. Theoretical Elucidation of the Unusually High [HNC]/[HCN] Abundance Ratio in Interstellar Space: Two-dimensional and Two-State Quantum Wave Packet Dynamics Study on the Branching Ratio of the

Dissociative Recombination Reaction $HCNH^+ + e^- \rightarrow HNC/HCN + H$. *Astrophys. J*, 636:927–931 (2006). doi:10.1086/498343. 10

Izzard, R. G., Lugaro, M., Karakas, A. I., et al. Reaction rate uncertainties and the operation of the NeNa and MgAl chains during HBB in intermediate-mass AGB stars. *Astron. Astrophys*, 466:641–648 (2007). doi:10.1051/0004-6361:20066903. 11

Johns-Krull, C. M., McCullough, P. R., Burke, C. J., et al. XO-3b: A Massive Planet in an Eccentric Orbit Transiting an F5 V Star. *Astrophys. J*, 677:657–670 (2008). doi:10.1086/528950. 3

Jonkheid, B., Faas, F. G. A., van Zadelhoff, G.-J., et al. The gas temperature in flaring disks around pre-main sequence stars. *Astron. Astrophys*, 428:511–521 (2004). doi:10.1051/0004-6361:20048013. 96, 114

Jonkheid, B., Kamp, I., Augereau, J.-C., et al. Modeling the gas-phase chemistry of the transitional disk around HD 141569A. *Astron. Astrophys*, 453:163–171 (2006a). doi:10.1051/0004-6361:20054769. 39, 96, 97, 113

Jonkheid, B., Kamp, I., Augereau, J.-C., et al. Modeling the gas-phase chemistry of the transitional disk around HD 141569A. *Astron. Astrophys*, 453:163–171 (2006b). doi:10.1051/0004-6361:20054769. 96, 114

Kastner, J. H., Zuckerman, B., Weintraub, D. A., et al. X-ray and molecular emission from the nearest region of recent star formation. *Science*, 277:67–71 (1997). 9, 20

Katz, N., Furman, I., Biham, O., et al. Molecular Hydrogen Formation on Astrophysically Relevant Surfaces. *Astrophys. J*, 522:305–312 (1999). doi:10.1086/307642. 49, 51, 52

Kessler-Silacci, J., Augereau, J.-C., Dullemond, C. P., et al. c2d Spitzer IRS Spectra of Disks around T Tauri Stars. I. Silicate Emission and Grain Growth. *Astrophys. J*, 639:275–291 (2006). doi:10.1086/499330. 95

Kim, J. K., Theard, L. P., and Huntress, Jr., W. T. Proton transfer reactions from H_3^+ ions to N_2, O_2, and CO molecules. *Chemical Physics Letters*, 32:610–614 (1975). 42

Lahuis, F., van Dishoeck, E. F., Boogert, A. C. A., et al. Hot Organic Molecules toward a Young Low-Mass Star: A Look at Inner Disk Chemistry. *Astrophys. J., Lett*, 636:L145–L148 (2006). doi:10.1086/500084. 4

Le Bourlot, J., Pineau des Forets, G., Roueff, E., et al. Bistability in Dark Cloud Chemistry. *Astrophys. J., Lett*, 416:L87 (1993). doi:10.1086/187077. 46

Le Teuff, Y. H., Millar, T. J., and Markwick, A. J. The UMIST database for astrochemistry 1999. *Astron. Astrophys. Suppl. Ser*, 146:157–168 (2000). 10, 37, 42

Lee, H.-H., Herbst, E., Pineau des Forets, G., et al. Photodissociation of H2 and CO and time dependent chemistry in inhomogeneous interstellar clouds. *Astron. Astrophys*, 311:690–707 (1996). 13, 39, 50

Lee, H.-H., Roueff, E., Pineau des Forets, G., et al. Bistability in large chemical networks: a global view. *Astron. Astrophys*, 334:1047–1055 (1998). 14, 46, 51, 80

Leger, A., Jura, M., and Omont, A. Desorption from interstellar grains. *Astron. Astrophys*, 144:147–160 (1985). 38

Leger, A., Rouan, D., Schneider, J., et al. Transiting exoplanets from the CoRoT space mission VIII. CoRoT-7b: the first Super-Earth with measured radius. *ArXiv e-prints* (2009). 3

Lepp, S. and Dalgarno, A. X-ray-induced chemistry of interstellar clouds. *Astron. Astrophys*, 306:L21–L24 (1996). 38

Lipshtat, A. and Biham, O. Moment equations for chemical reactions on interstellar dust grains. *Astron. Astrophys*, 400:585–593 (2003). doi:10.1051/0004-6361:20021902. 45, 47, 56, 128

Lipshtat, A., Biham, O., and Herbst, E. Enhanced production of HD and D2 molecules on small dust grains in diffuse clouds. *Mon. Not. R. Astron. Soc*, 348:1055–1064 (2004). doi:10.1111/j.1365-2966.2004.07437.x. 46

Lommen, D., Maddison, S. T., Wright, C. M., et al. Large grains in discs around young stars: ATCA observations of WW Chamaeleontis, RU Lupi, and CS Chamaeleontis. *Astron. Astrophys*, 495:869–879 (2009). doi:10.1051/0004-6361:200810999. 96

Mac Low, M.-M. and Klessen, R. S. Control of star formation by supersonic turbulence. *Reviews of Modern Physics*, 76:125–194 (2004). doi:10.1103/RevModPhys.76.125. 3

Maloney, P. R., Hollenbach, D. J., and Tielens, A. G. G. M. X-Ray–irradiated Molecular Gas. I. Physical Processes and General Results. *Astrophys. J*, 466:561–584 (1996). 38

Markwick, A. J., Ilgner, M., Millar, T. J., et al. Molecular distributions in the inner regions of protostellar disks. *Astron. Astrophys*, 385:632–646 (2002). doi:10.1051/0004-6361:20020050. 10

Mathis, J. S., Rumpl, W., and Nordsieck, K. H. The size distribution of interstellar grains. *Astrophys. J*, 217:425–433 (1977). doi:10.1086/155591. 108, 115

Mayor, M., Bonfils, X., Forveille, T., et al. The HARPS search for southern extra-solar planets XVIII. An Earth-mass planet in the GJ 581 planetary system. *ArXiv e-prints* (2009). 3

Mayor, M. and Frei, P.-Y. *New Worlds in the Cosmos*. New Worlds in the Cosmos, by Michel Mayor and Pierre-Yves Frei and Translated by Boud Roukema, pp. 260. ISBN 0521812070. Cambridge, UK: Cambridge University Press, October 2003. (2003). 95

Mayor, M. and Queloz, D. A Jupiter-mass companion to a solar-type star. *Nature*, 378:355–359 (1995a). doi:10.1038/378355a0. 3

Mayor, M. and Queloz, D. A Jupiter-Mass Companion to a Solar-Type Star. *Nature*, 378:355–+ (1995b). doi:10.1038/378355a0. 95

McKee, C. F. and Ostriker, E. C. Theory of Star Formation. *Ann. Rev. Astron. Astrophys*, 45:565–687 (2007). doi:10.1146/annurev.astro.45.051806.110602. 3

Millar, T. J., Defrees, D. J., McLean, A. D., et al. The sensitivity of gas-phase models of dense interstellar clouds to changes in dissociative recombination branching ratios. *Astron. Astrophys*, 194:250–256 (1988). 10, 43

Millar, T. J., Farquhar, P. R. A., and Willacy, K. The UMIST Database for Astrochemistry 1995. *Astron. Astrophys. Suppl. Ser*, 121:139–185 (1997). 10, 37

Milligan, D. B. and McEwan, M. J. H_3^+ + O: an experimental study. *Chemical Physics Letters*, 319:482–485 (2000). 42

Mitchell, J. B. A. The dissociative recombination of molecular ions. *Phys. Rep*, 186:215–248 (1990). 43

Mohanty, S., Jayawardhana, R., Huélamo, N., et al. The Planetary Mass Companion 2MASS 1207-3932B: Temperature, Mass, and Evidence for an Edge-on Disk. *Astrophys. J*, 657:1064–1091 (2007). doi:10.1086/510877. 3

Nahar, S. N. and Pradhan, A. K. Electron-Ion Recombination Rate Coefficients, Photoionization Cross Sections, and Ionization Fractions for Astrophysically Abundant Elements. I. Carbon and Nitrogen. *Astrophys. J., Suppl. Ser*, 111:339 (1997). doi:10.1086/313013. 37

Nakagawa, Y., Nakazawa, K., and Hayashi, C. Growth and sedimentation of dust grains in the primordial solar nebula. *Icarus*, 45:517–528 (1981). doi:10.1016/0019-1035(81)90018-X. 4, 100

Natta, A., Testi, L., Calvet, N., et al. Dust in Protoplanetary Disks: Properties and Evolution. In B. Reipurth, D. Jewitt, and K. Keil, editors, *Protostars and Planets V*, pages 767–781 (2007a). 4, 95

Natta, A., Testi, L., Calvet, N., et al. Dust in Protoplanetary Disks: Properties and Evolution. In B. Reipurth, D. Jewitt, & K. Keil, editor, *Protostars and Planets V*, pages 767–781 (2007b). 4

Neufeld, D. A., Maloney, P. R., and Conger, S. Water maser emission from X-ray-heated circumnuclear gas in active galaxies. *Astrophys. J., Lett*, 436:L127–L130 (1994). 38

Öberg, K. I., Fuchs, G. W., Awad, Z., et al. Photodesorption of CO Ice. *Astrophys. J., Lett*, 662:L23–L26 (2007). doi:10.1086/519281. 109

Ohishi, M., Irvine, W. M., and Kaifu, N. Molecular Abundance Variations among and Within Cold, Dark Molecular Clouds(rp). In P. D. Singh, editor, *Astrochemistry of Cosmic Phenomena*, volume 150 of *IAU Symposium*, page 171 (1992). 71, 74

Öjekull, J., Andersson, P. U., Nagard, M. B., et al. Dissociative recombination of ammonia clusters studied by storage ring experiments. *J. Chem. Phys*, 125:4306–+ (2006). doi:10.1063/1.2387174. 10

Oliveira, I., Merín, B., Pontoppidan, K. M., et al. Optical Characterization of A New Young Stellar Population in the Serpens Molecular Cloud. *Astrophys. J*, 691:672–686 (2009). doi:10.1088/0004-637X/691/1/672. 96

Ormel, C. W., Spaans, M., and Tielens, A. G. G. M. Dust coagulation in protoplanetary disks: porosity matters. *Astron. Astrophys*, 461:215–232 (2007). doi: 10.1051/0004-6361:20065949. 96, 100, 102

Pavlyuchenkov, Y., Wiebe, D., Launhardt, R., et al. CB 17: Inferring the Dynamical History of a Prestellar Core with Chemodynamical Models. *Astrophys. J*, 645:1212–1226 (2006). doi:10.1086/504372. 4, 72

Perets, H. B., Biham, O., Manicó, G., et al. Molecular Hydrogen Formation on Ice Under Interstellar Conditions. *Astrophys. J*, 627:850–860 (2005). doi:10.1086/430435. 49

Petrignani, A., van der Zande, W. J., Cosby, P. C., et al. Vibrationally resolved rate coefficients and branching fractions in the dissociative recombination of O_2^+. *J. Chem. Phys*, 122:4302 (2005). doi:10.1063/1.1825991. 43

Pety, J., Gueth, F., Guilloteau, S., et al. Plateau de Bure interferometer observations of the disk and outflow of HH 30. *Astron. Astrophys*, 458:841–854 (2006). doi: 10.1051/0004-6361:20065814. 9

Piétu, V., Dutrey, A., and Guilloteau, S. Probing the structure of protoplanetary disks: a comparative study of DM Tau, LkCa 15, and MWC 480. *Astron. Astrophys*, 467:163–178 (2007). doi:10.1051/0004-6361:20066537. 12, 86

Pineau des Forets, G., Roueff, E., and Flower, D. R. The two chemical phases of dark interstellar clouds. *Mon. Not. R. Astron. Soc*, 258:45P–47P (1992). 11

Pirronello, V., Biham, O., Liu, C., et al. Efficiency of Molecular Hydrogen Formation on Silicates. *Astrophys. J., Lett*, 483:L131 (1997a). doi:10.1086/310746. 49

Pirronello, V., Liu, C., Roser, J. E., et al. Measurements of molecular hydrogen formation on carbonaceous grains. *Astron. Astrophys*, 344:681–686 (1999). 49

Pirronello, V., Liu, C., Shen, L., et al. Laboratory Synthesis of Molecular Hydrogen on Surfaces of Astrophysical Interest. *Astrophys. J., Lett*, 475:L69 (1997b). doi: 10.1086/310464. 49

Podosek, F. A. and Cassen, P. Theoretical, observational, and isotopic estimates of the lifetime of the solar nebula. *Meteoritics*, 29:6–25 (1994). 96

Prasad, S. S. and Huntress, Jr., W. T. A model for gas phase chemistry in interstellar clouds. I - The basic model, library of chemical reactions, and chemistry among C, N, and O compounds. *Astrophys. J., Suppl. Ser*, 43:1–35 (1980). doi:10.1086/190665. 36

Prasad, S. S. and Tarafdar, S. P. UV radiation field inside dense clouds - Its possible existence and chemical implications. *Astrophys. J*, 267:603–609 (1983). 39

Pratap, P., Dickens, J. E., Snell, R. L., et al. A Study of the Physics and Chemistry of TMC-1. *Astrophys. J*, 486:862 (1997). doi:10.1086/304553. 71, 74

Przygodda, F., van Boekel, R., Àbrahàm, P., et al. Evidence for grain growth in T Tauri disks. *Astron. Astrophys*, 412:L43–L46 (2003). doi:10.1051/0004-6361:20034606. 93

Qi, C., Kessler, J. E., Koerner, D. W., et al. Continuum and CO/HCO^+ Emission from the Disk Around the T Tauri Star LkCa 15. *Astrophys. J*, 597:986–997 (2003). doi:10.1086/378494. 9

Qi, C., Wilner, D. J., Blake, G. A., et al. Chemistry in the disk around TW Hya. In D. C. Lis, G. A. Blake, and E. Herbst, editors, *IAU Symposium*, pages 188–192 (2005). 9

Roberge, W. G., Jones, D., Lepp, S., et al. Interstellar photodissociation and photoionization rates. *Astrophys. J., Suppl. Ser*, 77:287–297 (1991). doi:10.1086/191604. 39, 40

Roberts, H., Herbst, E., and Millar, T. J. The chemistry of multiply deuterated species in cold, dense interstellar cores. *Astron. Astrophys*, 424:905–917 (2004). doi:10.1051/0004-6361:20040441. 50, 79

Rodmann, J., Henning, T., Chandler, C. J., et al. Large dust particles in disks around T Tauri stars. *Astron. Astrophys*, 446:211–221 (2006). doi:10.1051/0004-6361:20054038. 4, 96

Ruffle, D. P. and Herbst, E. New models of interstellar gas-grain chemistry - I. Surface diffusion rates. *Mon. Not. R. Astron. Soc*, 319:837–850 (2000). 56

Salyk, C., Blake, G. A., Boogert, A. C. A., et al. Molecular Gas in the Inner 1 AU of the TW Hya and GM Aur Transitional Disks. *Astrophys. J., Lett*, 655:L105–L108 (2007). doi:10.1086/512012. 4

Salyk, C., Blake, G. A., Boogert, A. C. A., et al. High-resolution 5 μm Spectroscopy of Transitional Disks. *Astrophys. J*, 699:330–347 (2009). doi:10.1088/0004-637X/699/1/330. 96

Schilke, P., Keene, J., Le Bourlot, J., et al. Atomic carbon in a dark cloud: TMC-1. *Astron. Astrophys*, 294:L17–L20 (1995). 74

Semaniak, J., Minaev, B. F., Derkatch, A. M., et al. Dissociative Recombination of HCNH$^+$: Absolute Cross-Sections and Branching Ratios. *Astrophys. J., Suppl. Ser*, 135:275–283 (2001). 10, 43

Semenov, D., Henning, T., Helling, C., et al. Rosseland and Planck mean opacities for protoplanetary discs. *Astron. Astrophys*, 410:611–621 (2003). doi:10.1051/0004-6361:20031279. 13, 51

Semenov, D., Pavlyuchenkov, Y., Schreyer, K., et al. Millimeter Observations and Modeling of the AB Aurigae System. *Astrophys. J*, 621:853–874 (2005). doi:10.1086/427725. 4, 10, 13, 114

Semenov, D., Wiebe, D., and Henning, T. Reduction of chemical networks. II. Analysis of the fractional ionisation in protoplanetary discs. *Astron. Astrophys*, 417:93–106 (2004). doi:10.1051/0004-6361:20034128. 38, 50, 71, 72, 79, 88

Setiawan, J., Henning, T., Launhardt, R., et al. A young massive planet in a star-disk system. *Nature*, 451:38–41 (2008). doi:10.1038/nature06426. 4

Shakura, N. I. and Sunyaev, R. A. Black holes in binary systems. Observational appearance. *Astron. Astrophys*, 24:337–355 (1973). 98

Shalabiea, O. M., Caselli, P., and Herbst, E. Grain Surface Chemistry: Modified Models. *Astrophys. J*, 502:652–+ (1998). doi:10.1086/305942. 78

Shalabiea, O. M. and Greenberg, J. M. Bistability and dust/gas chemical modelling in dark interstellar clouds. *Astron. Astrophys*, 296:779 (1995). 11, 46

Sicilia-Aguilar, A., Bouwman, J., Juhasz, A., et al. The Long-Lived Disks in the Eta Chamaeleontis Cluster. *ArXiv e-prints* (2009). 96

Sicilia-Aguilar, A., Hartmann, L., Calvet, N., et al. Disk Evolution in Cep OB2: Results from the Spitzer Space Telescope. *Astrophys. J*, 638:897–919 (2006). doi:10.1086/498085. 4, 96

Simon, M., Dutrey, A., and Guilloteau, S. Dynamical Masses of T Tauri Stars and Calibration of Pre-Main-Sequence Evolution. *Astrophys. J*, 545:1034–1043 (2000). doi:10.1086/317838. 9, 12

Sims, I. R., Queffelec, J.-L., Defrance, A., et al. Ultralow temperature kinetics of neutral-neutral reactions. The technique and results for the reactions $CN+O_2$ down to 13 K and $CN+NH_3$ down to 25 K. *J. Chem. Phys*, 100:4229–4241 (1994a). 40

Sims, I. R., Queffelec, J.-L., Travers, D., et al. Rate constants for the reactions of CN with hydrocarbons at low and ultra-low temperatures. *Chemical Physics Letters*, 211:461–468 (1993). 40

Sims, I. R., Smith, I. W. M., Clary, D. C., et al. Ultra-low temperature kinetics of neutral-neutral reactions: New experimental and theoretical results for OH+HBr between 295 and 23 K. *J. Chem. Phys*, 101:1748–1751 (1994b). 40

Singh, P. D. and Andreazza, C. M. The Formation of CN and CN^+ by Direct Radiative Association. *Astrophys. J*, 537:261–263 (2000). doi:10.1086/309023. 37

Smith, I. W. M. Experimental Measurements of the Rate Constants for Neutral-Neutral Reactions. In T. J. Millar and D. A. Williams, editors, *ASSL Vol. 146: Rate Coefficients in Astrochemistry*, pages 106–116. Kluwer Academic Publishers, Dordrecht (1988). 40

Smith, I. W. M. Effects of quantum mechanical tunneling on rates of radiative association. *Astrophys. J*, 347:282–288 (1989). doi:10.1086/168116. 36

Smith, I. W. M., Herbst, E., and Chang, Q. Rapid neutral-neutral reactions at low temperatures: a new network and first results for TMC-1. *Mon. Not. R. Astron. Soc*, 350:323–330 (2004). doi:10.1111/j.1365-2966.2004.07656.x. 10, 36, 37, 40, 41, 42, 74

Snow, T. P. and McCall, B. J. Diffuse Atomic and Molecular Clouds. *Ann. Rev. Astron. Astrophys*, 44:367–414 (2006). doi:10.1146/annurev.astro.43.072103.150624PDF: http://arjournals.annualreviews.org/doi/pdf/10.1146/annurev.astro.43.072103. 150624. 50, 79

Snyder, L. E., Buhl, D., Schwartz, P. R., et al. Radio Detection of Interstellar Dimethyl Ether. *Astrophys. J., Lett*, 191:L79+ (1974). 9

Solomon, P. M. and Werner, M. W. Low-Energy Cosmic Rays and the Abundance of Atomic Hydrogen in Dark Clouds. *Astrophys. J*, 165:41 (1971). 38

Spitzer, L. *Physical processes in the interstellar medium.* New York Wiley-Interscience, 333 p. (1978). 39

Spitzer, L. J. and Tomasko, M. G. Heating of H i Regions by Energetic Particles. *Astrophys. J*, 152:971 (1968). 38, 50

Stantcheva, T., Caselli, P., and Herbst, E. Modified rate equations revisited. A corrected treatment for diffusive reactions on grain surfaces. *Astron. Astrophys*, 375:673–679 (2001). doi:10.1051/0004-6361:20010859. 46, 78

Stantcheva, T. and Herbst, E. Deuterium fractionation on interstellar grains studied with the direct master equation approach. *Mon. Not. R. Astron. Soc*, 340:983–988 (2003). doi:10.1046/j.1365-8711.2003.06368.x. 47, 56

Stantcheva, T. and Herbst, E. Models of gas-grain chemistry in interstellar cloud cores with a stochastic approach to surface chemistry. *Astron. Astrophys*, 423:241–251 (2004). doi:10.1051/0004-6361:20040433. 45, 47, 54, 56

Stantcheva, T., Shematovich, V. I., and Herbst, E. On the master equation approach to diffusive grain-surface chemistry: The H, O, CO system. *Astron. Astrophys*, 391:1069–1080 (2002). doi:10.1051/0004-6361:20020838. 47, 56

Stäuber, P., Doty, S. D., van Dishoeck, E. F., et al. X-ray chemistry in the envelopes around young stellar objects. *Astron. Astrophys*, 440:949–966 (2005). doi:10.1051/0004-6361:20052889. 38

Thi, W.-F., van Zadelhoff, G.-J., and van Dishoeck, E. F. Organic molecules in proto-planetary disks around T Tauri and Herbig Ae stars. *Astron. Astrophys*, 425:955–972 (2004). doi:10.1051/0004-6361:200400026. 9

Thrane, K., Bizzarro, M., and Baker, J. A. Extremely Brief Formation Interval for Refractory Inclusions and Uniform Distribution of ^{26}Al in the Early Solar System. *Astrophys. J., Lett*, 646:L159–L162 (2006). doi:10.1086/506910. 96

Tielens, A. G. G. M. and Hagen, W. Model calculations of the molecular composition of interstellar grain mantles. *Astron. Astrophys*, 114:245–260 (1982). 5, 45, 46, 78

Tscharnuter, W. M. and Gail, H.-P. 2-D preplanetary accretion disks. I. Hydrody-namics, chemistry, and mixing processes. *Astron. Astrophys*, 463:369–392 (2007). doi:10.1051/0004-6361:20065794. 10, 42

Turanyi, T. Applications of sensitivity analysis to combustion chemistry. *Reliability Engineering and System Safety*, 57:41–47 (1997). 30

Turner, B. E., Herbst, E., and Terzieva, R. The Physics and Chemistry of Small Translucent Molecular Clouds. XIII. The Basic Hydrocarbon Chemistry. *Astrophys. J., Suppl. Ser*, 126:427–460 (2000). doi:10.1086/313301. 74

Udry, S. and Santos, N. C. Statistical Properties of Exoplanets. *Ann. Rev. Astron. Astrophys*, 45:397–439 (2007). doi:10.1146/annurev.astro.45.051806.110529. 95

van Boekel, R., Min, M., Leinert, C., et al. The building blocks of planets within the 'terrestrial' region of protoplanetary disks. *Nature*, 432:479–482 (2004). doi:10.1038/nature03088. 4, 95

van Boekel, R., Min, M., Waters, L. B. F. M., et al. A 10 μm spectroscopic survey of Herbig Ae star disks: Grain growth and crystallization. *Astron. Astrophys*, 437:189–208 (2005). doi:10.1051/0004-6361:20042339. 4, 93

van Dishoeck, E. F. Photodissociation Processes of Astrophysical Molecules. In M. S. Vardya and S. P. Tarafdar, editors, *IAU Symp. 120: Astrochemistry*, pages 51–63 (1987). 40

van Dishoeck, E. F. Photodissociation and Photoionization Processes. In T. J. Millar and D. A. Williams, editors, *ASSL Vol. 146: Rate Coefficients in Astrochemistry*, pages 49–82 (1988). 13, 14, 16, 24, 39

van Dishoeck, E. F. Photochemistry and the Interstellar Radiation Field. In R. Cutri and W. Latter, editors, *ASP Conf. Ser. 58: The First Symposium on the Infrared Cirrus and Diffuse Interstellar Clouds*, pages 319–331. Astr. Soc. Pacific (1994). 39

van Dishoeck, E. F. and Blake, G. A. Chemical Evolution of Star-Forming Regions. *Ann. Rev. Astron. Astrophys*, 36:317–368 (1998). doi:10.1146/annurev.astro.36.1.317. 4, 36

van Dishoeck, E. F., Jonkheid, B., and van Hemert, M. C. Photoprocesses in protoplanetary disks. In I. R. Sims and D. A. Williams, editors, *Faraday Discussions 133: Chemical Evolution of the Universe*, pages 231–243 (2006a). 16, 39

van Dishoeck, E. F., Jonkheid, B., and van Hemert, M. C. Photoprocesses in protoplanetary disks. In I. R. Sims and D. A. Williams, editors, *Faraday Discussions 133: Chemical Evolution of the Universe*, pages 231–243 (2006b). 50, 79

van Zadelhoff, G.-J., Aikawa, Y., Hogerheijde, M. R., et al. Axi-symmetric models of ultraviolet radiative transfer with applications to circumstellar disk chemistry. *Astron. Astrophys*, 397:789–802 (2003a). doi:10.1051/0004-6361:20021592. 4, 10, 14, 26, 39, 109

van Zadelhoff, G.-J., Aikawa, Y., Hogerheijde, M. R., et al. Axi-symmetric models of ultraviolet radiative transfer with applications to circumstellar disk chemistry. *Astron. Astrophys*, 397:789–802 (2003b). doi:10.1051/0004-6361:20021592. 50

van Zadelhoff, G.-J., van Dishoeck, E. F., Thi, W.-F., et al. Submillimeter lines from circumstellar disks around pre-main sequence stars. *Astron. Astrophys*, 377:566–580 (2001). doi:10.1051/0004-6361:20011137. 9

BIBLIOGRAPHY

Vasyunin, A. I., Semenov, D., Henning, T., et al. Chemistry in Protoplanetary Disks: A Sensitivity Analysis. *Astrophys. J*, 672:629–641 (2008). doi:10.1086/523887. 50, 79, 88, 93, 104, 114

Vasyunin, A. I., Semenov, D. A., Wiebe, D. S., et al. A Unified Monte Carlo Treatment of Gas-Grain Chemistry for Large Reaction Networks. I. Testing Validity of Rate Equations in Molecular Clouds. *Astrophys. J*, 691:1459–1469 (2009). doi:10.1088/0004-637X/691/2/1459. 78, 79, 80, 85

Vasyunin, A. I., Sobolev, A. M., Wiebe, D. S., et al. Influence of Uncertainties in the Rate Constants of Chemical Reactions on Astrochemical Modeling Results. *Astronomy Letters*, 30:566–576 (2004). doi:10.1134/1.1784498. 10, 11, 25, 71

Vikor, L., Al-Khalili, A., Danared, H., et al. Branching fractions in the dissociative recombination of NH_4^+ and NH_2^+ molecular ions. *Astron. Astrophys*, 344:1027–1033 (1999). 43

Wakelam, V., Herbst, E., and Selsis, F. The effect of uncertainties on chemical models of dark clouds. *Astron. Astrophys*, 451:551–562 (2006a). doi:10.1051/0004-6361:20054682. 11, 25, 71

Wakelam, V., Herbst, E., Selsis, F., et al. Chemical sensitivity to the ratio of the cosmic-ray ionization rates of He and H2 in dense clouds. *Astron. Astrophys*, 459:813–820 (2006b). doi:10.1051/0004-6361:20065472. 11, 14, 18, 26, 38, 39

Wakelam, V., Selsis, F., Herbst, E., et al. Estimation and reduction of the uncertainties in chemical models: application to hot core chemistry. *Astron. Astrophys*, 444:883–891 (2005). doi:10.1051/0004-6361:20053673. 11, 16, 17

Wasson, J. T. and Kallemeyn, G. W. Compositions of chondrites. *Royal Society of London Philosophical Transactions Series A*, 325:535–544 (1988). 96

Weidenschilling, S. J. The distribution of mass in the planetary system and solar nebula. *Astrophys. Space. Sci*, 51:153–158 (1977). doi:10.1007/BF00642464. 104

Weidenschilling, S. J. The Origin of Comets in the Solar Nebula: A Unified Model. *Icarus*, 127:290–306 (1997). doi:10.1006/icar.1997.5712. 96, 100

Westley, M. S., Baragiola, R. A., Johnson, R. E., et al. Photodesorption from low-temperature water ice in interstellar and circumsolar grains. *Nature*, 373:405–407 (1995). doi:10.1038/373405a0. 109

Wiebe, D., Semenov, D., and Henning, T. Reduction of chemical networks. I. The case of molecular clouds. *Astron. Astrophys*, 399:197–210 (2003). doi:10.1051/0004-6361:20021773. 20

Willacy, K., Klahr, H. H., Millar, T. J., et al. Gas and grain chemistry in a protoplanetary disk. *Astron. Astrophys*, 338:995–1005 (1998). 14

Willacy, K., Langer, W., Allen, M., et al. Turbulence-driven Diffusion in Protoplanetary Disks: Chemical Effects in the Outer Regions. *Astrophys. J*, 644:1202–1213 (2006). doi:10.1086/503702. 22

Willacy, K. and Langer, W. D. The Importance of Photoprocessing in Protoplanetary Disks. *Astrophys. J*, 544:903–920 (2000). doi:10.1086/317236. 10, 22

Williams, D. A. Association Reactions. *Astrophys. Lett. Commun*, 10:L17–L21 (1972). 10, 36

Wilner, D. J., D'Alessio, P., Calvet, N., et al. Toward Planetesimals in the Disk around TW Hydrae: 3.5 Centimeter Dust Emission. *Astrophys. J., Lett*, 626:L109–L112 (2005). doi:10.1086/431757. 96

Woodall, J., Agúndez, M., Markwick-Kemper, A. J., et al. The UMIST database for astrochemistry 2006. *Astron. Astrophys*, 466:1197–1204 (2007). doi:10.1051/0004-6361:20064981. 10, 14, 16, 36, 37, 38, 41, 42, 50, 79

Zsom, A. and Dullemond, C. P. A representative particle approach to coagulation and fragmentation of dust aggregates and fluid droplets. *Astron. Astrophys*, 489:931–941 (2008). doi:10.1051/0004-6361:200809921. 100

Declaration

I herewith declare that I have produced this paper without the prohibited assistance of third parties and without making use of aids other than those specified; notions taken over directly or indirectly from other sources have been identified as such. This paper has not previously been presented in identical or similar form to any other German or foreign examination board.

The thesis work was conducted from 2006 to 2009 under the supervision of Dr. Prof. Thomas Henning and Dr. Dmitry Semenov at Max-Planck-Institute for Astronomy (MPIA).

Heidelberg, September 21, 2009.